Πανεπιστήμιο Κύπρου
University of Cyprus

THE CYPRUS INSTITUTE OF NEUROLOGY & GENETICS

DEPARTMENT OF BIOLOGICAL SCIENCES

Transgenic Replacement of Cx32 in Gap Junction-Deficient Oligodendrocytes Rescues the Phenotype of a Hypomyelinating Leukodystrophy Model

Natasa Schiza

DOCTOR OF PHILOSOPHY DISSERTATION

May, 2015

The Cyprus Institute of Neurology and Genetics,
Neuroscience Laboratory

Πανεπιστήμιο Κύπρου
University of Cyprus

THE CYPRUS INSTITUTE OF NEUROLOGY & GENETICS

DEPARTMENT OF BIOLOGICAL SCIENCES

Transgenic Replacement of Cx32 in Gap Junction-Deficient Oligodendrocytes Rescues the Phenotype of a Hypomyelinating Leukodystrophy Model

by

Natasa Schiza

A dissertation submitted to the University of Cyprus in partial fulfilment

of the requirements for the degree of Doctor of Philosophy

May, 2015

The Cyprus Institute of Neurology and Genetics,
Neuroscience Laboratory

VALIDATION PAGE

Doctoral Candidate: Natasa C. Schiza

Doctoral Thesis Title: Transgenic Replacement of Cx32 in Gap Junction Deficient Oligodendrocytes Rescues the Phenotype of a Hypomyelinating Leukodystrophy Model

The present Doctoral Dissertation was submitted in partial fulfillment of the requirements for the Degree of Doctor of Philosophy at the Department of Biological Sciences and was approved on the 20th May 2015 by the members of the Examination Committee.

Examination Committee:

Research Supervisor: Kleopas A. Kleopa, MD, PhD, Professor

Signature:……

Committee Member: Pantelis Georgiades, Associate Professor

Signature:……

Committee Member: Kyproula Christodoulou, Professor

Committee Member: Nikolaos Grigoriadis, MD, PhD

Committee Member: Domna Karagogeos, Professor

DECLARATION OF DOCTORAL CANDIDATE

The present doctoral dissertation was submitted in partial fulfilment of the requirements for the degree of Doctor of Philosophy of the University of Cyprus. It is a product of original work of my own, unless otherwise mentioned through references, notes, or any other statements.

Natasa C. Schiza

ABSTRACT

Oligodendrocytes are coupled by gap junctions (GJs) formed mainly by connexin47 (Cx47) and connexin32 (Cx32). Recessive *GJC2*/Cx47 mutations cause Pelizaeus–Merzbacher-like disease, a hypomyelinating leukodystrophy, while *GJB1*/Cx32 mutations cause peripheral neuropathy and chronic or acute-transient encephalopathy syndromes. Cx32/Cx47 double knockout (Cx32/Cx47dKO) mice develop severe CNS demyelination beginning at 1 month of age leading to death within weeks, offering a relevant model to study disease mechanisms. In order to clarify whether the loss of oligodendrocyte connexins has cell autonomous effects, we generated transgenic mice expressing the wild-type human Cx32 under the control of the mouse proteolipid protein promoter (Plp), obtaining exogenous hCx32 expression in oligodendrocytes. By crossing these mice with Cx32KO mice, we obtained expression of hCx32 on Cx32KO background. Immunohistochemical and immunoblot analysis confirmed strong CNS expression of hCx32 specifically in oligodendrocytes and correct localization forming GJs at cell bodies and along the myelin sheath. TG^{+}Cx32/Cx47dKO mice were generated by further crossing with Cx47KO mice. Transgenic expression of hCx32 rescued the severe early phenotype of CNS demyelination in Cx32/Cx47dKO mice, resulting in marked improvement of behavioral abnormalities at 1 month of age, and prevented the early mortality. Furthermore, TG^{+}Cx32/Cx47dKO mice showed significant improvement of myelination compared with Cx32/Cx47dKO CNS at 1 month of age, while the inflammatory and astrogliotic changes were fully reversed. Our study confirms that loss of oligodendrocyte GJs has cell autonomous effects and that re-establishment of GJ connectivity by replacement of at least one GJ protein provides correction of the leukodystrophy phenotype.

ΠΕΡΙΛΗΨΗ

Οι χασμοσυνδέσμοι στα ολιγοδενδροκύτταρα σχηματίζονται κυρίως από την κοννεξίνη 47 (Cx47) και κοννεξίνη 32 (Cx32). Υπολειπόμενες μεταλλάξεις στο γονίδιο *GJC2*, της Cx47 προκαλούν την ασθένεια Pelizaeus-Merzbacher, η οποία υπάγεται στην κατηγορία των υπομυελινωτικών λευκοδυστροφιών, ενώ μεταλλάξεις στο γονίδιο *GJB1*, της Cx32 προκαλούν περιφερική νευροπάθεια, χρόνια ή οξεία παροδική εγκεφαλοπάθεια. Τα ποντίκια στα οποία λείπουν και τα δύο γονίδια της Cx32 και Cx47 (Cx32/Cx47dKO) αναπτύσσουν σοβαρή απομυελίνωση του κεντρικού νευρικού συστήματος (ΚΝΣ) που αρχίζει σε ηλικία ενός μηνός και οδηγεί στο θάνατο μέσα σε λίγες εβδομάδες. Αυτό το μοντέλο λευκοδυστροφίας προσφέρεται για μελέτη των μηχανισμών αυτή της νόσου. Προκειμένου να διευκρινιστεί αν η απώλεια των χασμοσυνδέσμων στα ολιγοδενδροκυττάρα έχει αυτόνομες κυτταρικές επιδράσεις, δημιουργήσαμε διαγονιδιακά ποντίκια που εκφράζουν την άγριου-τύπου ανθρώπινη Cx32 υπό τον έλεγχο του υποκινητή της πρωτεολιπιδικής πρωτεΐνης ποντικού για την απόκτηση εξωγενούς έκφρασης hCx32 σε ολιγοδενδροκύτταρα. Με την αναπαραγωγή των ιδρυτών με Cx32KO ποντίκια, πήραμε την έκφραση της hCx32 σε Cx32KO ποντίκια, που επιβεβαιώθηκε με ανοσοϊστοχημεία και ανοσοαποτύπωση. Παρατηρήσαμε έντονη έκφραση της στα ολιγοδενδροκύτταρα του ΚΝΣ στα TG^{+}Cx32KO ποντίκια όπως επίσης εντοπισμό και σχηματισμό χασμοσυνδέσμων σε αυτά κατά μήκος της μυελίνης. Με περαιτέρω διασταύρωση αυτών των ποντικιών με Cx47KO ποντίκια δημιουργηθήκαν τα TG^{+}Cx32/Cx47dKO τα οποία έδειξαν ότι η διαγονιδιακή έκφραση της hCx32 έσωσε τη σοβαρή απομυελίνωση του ΚΝΣ σε ποντίκια Cx32/Cx47dKO, με αποτέλεσμα την σημαντική βελτίωση των ανωμαλιών συμπεριφοράς από τον 1ο μήνα της ηλικίας τους, και την πρόληψη της πρόωρης θνησιμότητας. Επιπλέον, οι TG^{+}Cx32/Cx47dKO ποντικοί έδειξαν σημαντική βελτίωση της απομυελίνωσης ενώ οι φλεγμονές και οι αστρογλιοτικές αλλαγές αντιστράφηκαν πλήρως σε σύγκριση με τους Cx32/Cx47dKO στον 1 μήνα ηλικίας. Η μελέτη μας επιβεβαιώνει ότι η απώλεια των χασμοσυνδέσμων στα ολιγοδενδροκυττάρα έχει αυτόνομες επιδράσεις και με την αντικατάσταση τουλάχιστον μιας κοννεξίνης επιτυγχάνεται η διόρθωση του φαινοτύπου της λευκοδυστροφίας και επανασύνδεση των χασμοδυνδέσμων.

AKNOWLEDGEMENTS

I could not find the best words for conveying my deep gratitude and respect to my research advisor, Professor Kleopas Kleopa, MD. I would like to thank him for giving me the opportunity and trusted me to do my PhD thesis in his laboratory. He has inspired me to become an independent researcher and helped me realize the power of critical reasoning. He demonstrated what a hard-working scientist can accomplish. I appreciate all his endless time, ideas, and funding to make my trip towards my Ph.D. productive and stimulating. The joy and enthusiasm he has for his research was contagious and motivational, even during tough times. He quickly spotted my weaknesses and helped me through hard work to overcome them.

I would also like to thank my academic advisor Professor Constantinos Deltas for his constant support and encouragement during the regular meetings we had at the University to discuss any problems on the project.

I cannot forget friends, my academic family and the hard times we had together; they cheered me up, created a pleasant atmosphere in the lab and celebrated each accomplishment together: Dr. Irene Sargiannidou, Dr. Alexia Kagiava, Margarita Olympiou, Styliana Kyriakoudes, Dr. Elena Georgiou, and Dr. Christos Papaneofitou, Dr. Elena Panagiotou, Rebecca Papacharalambous, thank you.

I would also like to thank the team of the transgenic mouse facility at the Cyprus Institute of Neurology and Genetics, Christos Karaiskos and Dr. George Lapathitis for the pronuclear injections procedure and for all their support and assistance with the mice.

She has always been ready to help me and took care of all non-scientific works during these years; she is our secretary Elena Polycarpou and I sincerely thank her.

I can’t imagine me without the love, support and encouragement from my dad, mom and my sister during these years. I thank my hard working parents, Christos and Elena, for their efforts to provide me all the necessities for a good education, and for becoming a potential contributor to the wellbeing of the society. My younger sister Eirini has always been my best friend and I thank her for all her advices, support and caring.

Last but not least, I would like to thank my grandmother for her endless love, and I believe that her prayers for me were what sustained me thus far.

An inspiring personality came unexpectedly in my life at the climax of the writing up of this Thesis, few months ago. His presence in my life at that moment scared me as a potential obstacle in my writing up that came to cause delays. I took the challenge however, and it turned out eventually that this relationship gave me the necessary muscle for boosting my efforts for finishing up the writing of the Thesis, right on time. Thank you Andreas for being there.

Natasa C. Schiza

May 2015

Ο άνθρωπος οφείλει να φυτέψει τουλάχιστον ένα δέντρο. Να γεννήσει τουλάχιστον ένα παιδί. Να γράψει τουλάχιστον ένα βιβλίο.

Έλλη Αλεξίου, 1894-1988, Ελληνίδα πεζογράφος

This thesis is dedicated to Christos, Elena and Irene…

TABLE OF CONTENTS

LIST OF FIGURES

Chapter 1 - Introduction

Chapter 2 – Materials & Methods

Chapter 3 - Results

LIST OF TABLES

Chapter 3 - Results

Appendix

LIST OF ABBREVIATIONS

GJ- Gap Junction
CMT1X- Charcot Marie Tooth
NCV- Nerve Conduction Velocity
CNS- Central Nervous System
PNS- Peripheral Nervous System
PMD- Pelizaeus Merzbacher Disease
PMLD- Pelizaeus Merzbacher-Like-Disease
HSP- Hereditary Spastic Paraplegia
PLP1- Proteolipid Protein
MRI- Magnetic Resonance Imaging
MRS- Magnetic Resonance Spectroscopy
Cx- Connexin
KO- Knocked out
WT- Wild type
SRP- Signal Recognition Particle
ORF- Open Reading Frame
PCR- Polymerase Chain Reaction
MBP- Myelin Basic Protein
EGFP- Enhanced Green Fluorescent Protein
IRES- Internal Ribosomal Entry Site
F1- First Generation
TG^{+}- Transgenic
RT- Reverse Transcription
cDNA- Complimentary DNA
GFAP- Glial fibrillary acidic protein
CC- Corpus Callosum
WM- White Matter
GM- Gray Matter
BR- Brain
SC- Spinal Cord
BSC- Brain Stem Cerebellum
LV- Liver
fs- Frameshift
X- Stop

Chapter 1:
INTRODUCTION

INTRODUCTION

1.1 Gap junctions

Communication and cellular interaction between cells is essential for proper function and organisation. The ability to send and receive signals is essential for the survival of the cell. Cells communicate via different mechanisms such as ligands and their receptors, second messengers, tight junctions, anchoring junctions, gap junctions (GJ), etc. GJ are found in most tissues and connect cells to other cells or bind different layers of the same cell, for example the myelin sheath that wraps around nerve axons (Bruzzone et al., 1996, White and Paul, 1999). Intercellular communication through GJs is involved in electrical connectivity, metabolic cooperation, growth control, cellular differentiation, and pattern formation during development.

1.1.1 Structure of a connexin molecule to gap junction channel formation

GJ channels are composed of two apposed hemichannels (or connexons) that provide a contiguous pathway between adjacent cells or cell compartments. Each connexon is composed of a hexamer of connexin molecules arranged around a central pore (***Fig.1.1***). Channel diameter is about 1.2 nm and only allows transfer of small molecules (<1000 Da), including ions and second messengers.

Connexins belong to a multigene family of over 20 GJ proteins (Willecke et al., 2002). They show a high degree of homology, indicating that their structure and function were conserved as they evolved from a common ancestral gene. Each connexin protein is named according to its predicted molecular mass (in kDa). Connexins have the same structure that consists of a cytoplasmic amino terminus, four transmembrane domains with alpha helix structure, one intracellular loop, two extracellular loops and a carboxy terminus (Bruzzone et al., 1996, Unger et al., 1999, White and Paul, 1999).

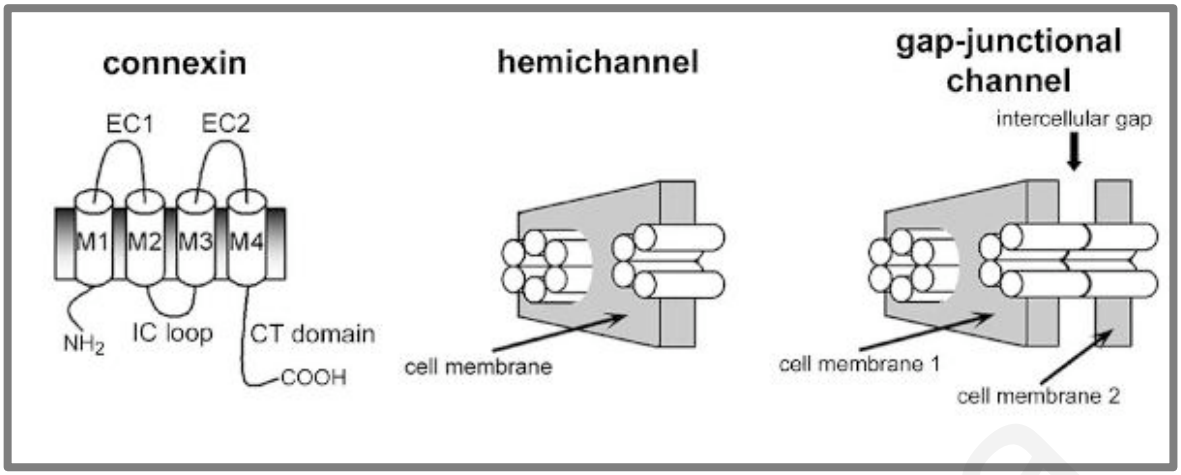

Figure 1.1: Structure of a connexin molecule.
Each molecule consists of four transmembrane domains, the cytoplasmic amino terminus, the carboxy terminus, one intracellular loop and two extracellular loops. A connexon (hemichannel) is formed by six connexin molecules of the same connexin isoform. A gap junction channel contains either two identical connexons (homotypic) or two different isoforms of connexons (heterotypic) Modified from (Fiori et al., 2014).

The third transmembrane domain probably forms the central pore, with polar residues lining the wall of the pore. The intracellular loop and C-terminal domain are the most divergent parts of the connexins and differences in their sizes account for the different molecular masses of the connexins (Willecke et al., 2002). The two extracellular loops regulate the connexon-connexon interactions, including heterotypic channel formation. Each loop contains three cysteine residues that are conserved among all connexins and join the two loops via disulfide bonds.

1.1.2 Gap junction synthesis and assembly

In a eukaryotic cell, a fundamental process, trafficking in the correct direction, assembly of membrane proteins and finally degradation are necessary for GJ synthesis. Connexins have a relatively short half-life of approximately 1 to 5 hours in-vivo (Laird, 2006), so they are rapidly synthesised and degraded. Once connexin mRNA is outside the nucleus, it is detected by a signal recognition particle (SRP). This particle binds to mRNA and forms a ribosome/polypeptide/SRP/mRNA complex (Segretain and Falk, 2004). Connexin molecules are folded in the endoplasmic reticulum (ER) and proteins are released sequentially into the ER lumen. Folded proteins pass through the ER-Golgi intermediate to enter Golgi. In the Golgi, connexin molecules oligomerise to

connexons (depending on the connexin type). After completion of connexin oligomerisation, connexons are packed into vesicles and delivered to the plasma membrane via actin or microtubule networks (Lauf et al., 2002, Segretain and Falk, 2004). Once in the plasma membrane connexons interact via their extracellular loops to form channels that aggregate in the cell membrane to form GJ plaques (***Fig.1.2***) (Duffy et al., 2002).

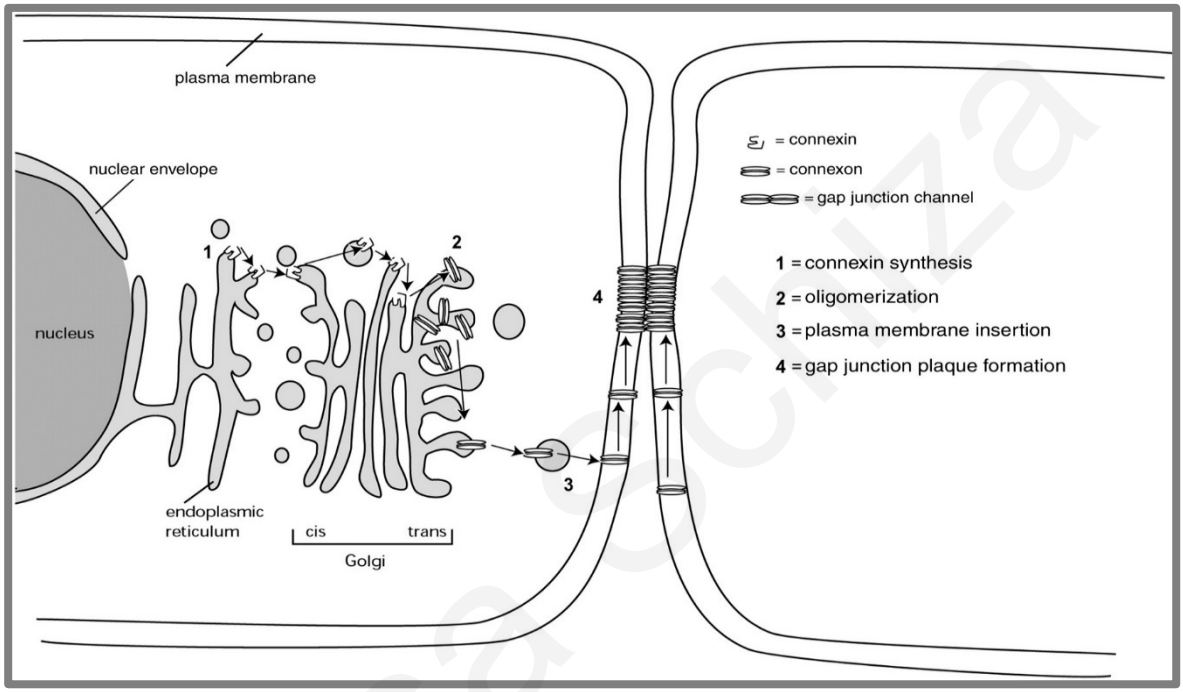

Figure 1.2: Synthesis and assembly of GJ channels.

(1) Synthesis of the polypeptide at ER membrane, (2) Oligomerisation of connexins to connexons (hemichannels) in the Golgi, (3) Diffusion of connexons in the plasma membrane, (4) Aggregation of connexons in the plasma membrane to form gap junction plaques (Yeager et al., 1998).

1.2 Disorders associated with gap junction dysfunction in myelinating cells

1.2.1 X-linked Charcot-Marie-Tooth disease is caused by mutations in the gene encoding connexin 32 (Cx32)

CMT1X is an X-linked dominant disease with onset in affected males between 5 and 20 years of age (Hahn et al., 1990, Nicholson and Nash, 1993, Birouk et al., 1998, Hahn et al., 2000). Initial symptoms include difficulty in running and frequently sprained ankles; foot drop and sensory loss in the legs develop later. Depending on the severity of the disease, the distal weakness may progress to involve the leg muscles and assistive devices may be required for ambulation. Weakness, atrophy, and sensory loss also develop in the hands, particularly in thenar muscles (***Fig.1.3***).

On examination, patients may exhibit distal muscle weakness and atrophy, diminished to absent reflexes, and sensory impairment, all of which are length-dependent and worsen insidiously over time to varying degrees. Affected women may be asymptomatic or they may have a later onset than men, after the age of twenty years, and a milder version of the same phenotype. This is probably due to random X-chromosome inactivation that leads to only a fraction of their myelinating Schwann cells expressing the mutant *GJB1* allele (Scherer et al., 1998).

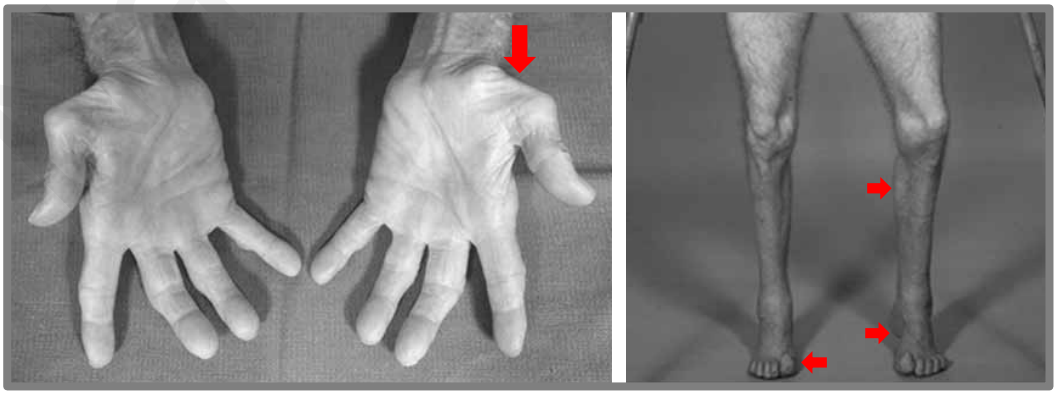

Figure 1.3: Characteristic clinical findings in a CMT1X patient.
Atrophy develops in the hands especially in the thenar muscles (red arrow). In the legs, there is weakness particularly in the gastrocnemius and soleus muscles, as well as deformed claw toes and high arches (modified from (Kleopa and Scherer, 2006a)).

Electrophysiologically, patients with CMT1X have “intermediate” slowing of nerve conduction velocities (NCV), and mildly prolonged distal motor and F-wave latencies. Forearm median or ulnar motor NCV are in the range of 30-40 m/s in affected males, and 30-50 m/s in affected females (Rozear et al., 1987, Hahn et al., 1990, Nicholson and Nash, 1993, Rouger et al., 1997, Birouk et al., 1998, Hahn et al., 1999, Senderek et al., 1999, Tabaraud et al., 1999, Gutierrez et al., 2000, Hattori et al., 2003). There is also evidence of axonal loss that is more severe distally and increases with age, whereas slowing of NCV may be evident even in presymptomatic affected male children (Kuntzer et al., 2003, Vondracek et al., 2005).

Nerve biopsies in patients with CMT1X show age-related loss of myelinated fibres, and at the same time increasing number of regenerated axon clusters (Rozear et al., 1987, Hahn et al., 1990, Nicholson and Nash, 1993, Birouk et al., 1998, Sander et al., 1998, Senderek et al., 1998, Hahn et al., 1999, Senderek et al., 1999, Tabaraud et al., 1999, Gutierrez et al., 2000, Vital et al., 2001, Kleopa et al., 2006a). Many myelin sheaths are too thin for the axonal diameter, a sign of chronic and on-going segmental demyelination and remyelination, or remyelination after axonal regeneration (Sander et al., 1998, Hahn et al., 2001, Vital et al., 2001, Hattori et al., 2003). Electron microscopy studies have shown enlargement and widening of the adaxonal Schwann cell cytoplasm (Senderek et al., 1999, Hahn et al., 2001, Kuntzer et al., 2003) and increased packing density of neurofilaments (Hahn et al., 2001). These features also occur in *Gjb1*-null mice (Anzini et al., 1997, Scherer et al., 1998). There are structural alterations in Schmidt-Lanterman incisures (Senderek et al., 1999), where Cx32 is normally localised (Scherer et al., 1995), as well as myelin discompaction and vesicle formation between its degenerating innermost layers (***Fig.1.4***) (Kleopa and Scherer, 2006b).

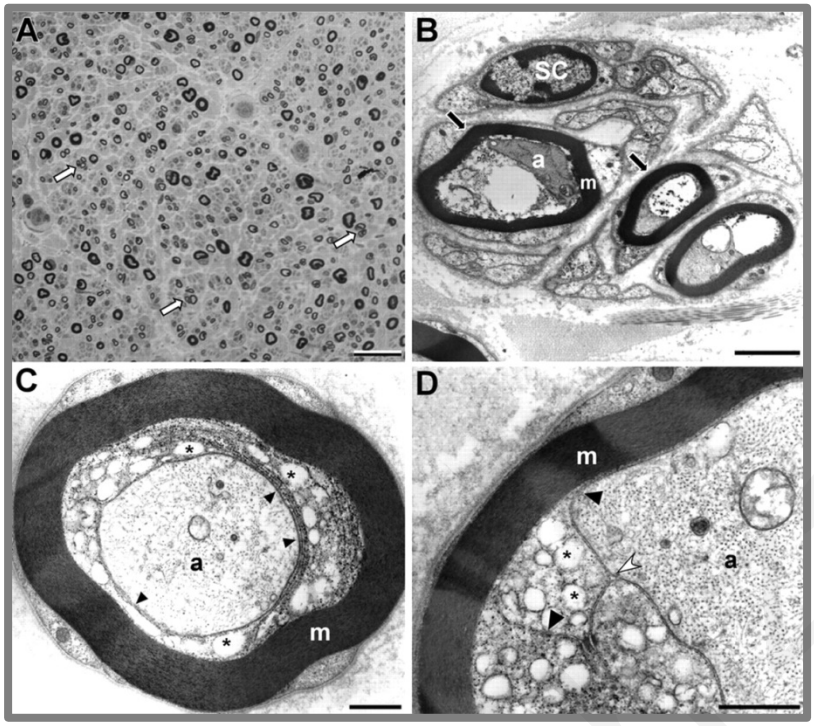

Figure 1.4: Nerve biopsy of CMT1X patient.
(A) Semi thin section from biopsied sural nerve from a CMT1X patient with V140E mutations. White arrows indicate partially demyelinated axons. (B-D) Ultrathin sections from the same biopsy (black arrows pointing to abnormally myelinated fibres). The myelin sheath is altered with discompaction of the inner layers and vacuole formation (black arrow heads), which leads to de-myelination and re-myelination of axons (Kleopa et al., 2006b).

In addition to the peripheral manifestations, CMT1X patients often have asymptomatic evidence of Central Nervous System (CNS) involvement, such as abnormal brainstem auditory evoked potentials (Nicholson and Corbett, 1996, Nicholson et al., 1998). Moreover, numerous CMT1X mutations have been increasingly associated with clinical CNS phenotypes (Kleopa et al., 2002). Signs of chronic corticospinal tract dysfunction, such as spasticity, extensor plantar responses and hyperactive reflexes have been reported in patients with the A39V (Marques et al., 1999), T55I (Panas et al., 1998), M93V (Bell et al., 1996), R164Q (Panas et al., 1998), R183H (Bort et al., 1997), T191 frameshift (Lee et al., 2002) and L143P (Kleopa et al., 2006a) Cx32 mutations. An insertion mutation at position 55 results in the duplication of amino acids 55-61 that causes progressive cerebellar ataxia, dysarthria and delayed central somatosensory responses (Kawakami et al., 2002). In addition, acute transient encephalopathy syndromes associated with magnetic resonance imaging (MRI) changes suggesting central myelin dysfunction have been described in CMT1X patients with the T55I, R75W, E102del, R142W, R164W and C168Y mutations (Panas et al., 2001, Paulson et

al., 2002, Schelhaas et al., 2002, Hanemann et al., 2003, Taylor et al., 2003). In most patients, encephalopathy developed under conditions of metabolic stress caused by travel to high altitudes (Paulson et al., 2002), febrile illness (Schelhaas et al., 2002, Hanemann et al., 2003), hyperventilation (Srinivasan et al., 2008), or concussion (Halbrich et al., 2008). Thus, CMT1X affects both the Peripheral Nervous System (PNS) and CNS, reflecting the expression of Cx32.

1.2.2 Pelizaeus-Merzbacher disease (PMD)/ Pelizaeus-Merzbacher-like disease (PMLD) and hereditary spastic paraplegia (HSP)

Pelizaeus-Merzbacher disease (PMD) is an X-linked disorder caused by mutations in *PLP1*, the gene encoding proteolipid protein, the main protein in CNS myelin. Classic PMD affects boys and is characterised by nystagmus and impaired psychomotor development within the first year of life, followed by progressive spasticity, ataxia, choreoathetosis and diffuse white matter changes on MRI (Nave and Boespflug-Tanguy, 1996, Hudson et al., 2004, Inoue, 2005).
Proteolipid protein-1 (*PLP1*) mutations may also cause a more severe 'connatal' PMD phenotype, as well as a milder disease, hereditary spastic paraplegia (HSP) type 2. (Garbern et al., 1999, Hudson et al., 2004, Garbern, 2007).

Pelizaeus-Merzbacher-like disease (PMLD) is clinically and neuroradiologically similar to classic PMD, but is not associated with *PLP1* mutations. The PMLD patients described to date have similar phenotypes, including nystagmus by 7 weeks of age, impaired motor development and ataxia by 15 months, evidence of hypomyelination on MRI, and later development of spasticity.

Different homozygous and compound heterozygous *GJA12*/*GJC2* mutations affecting the GJ protein connexin47 (Cx47) were identified in consanguineous and non-consanguineous PMLD families with autosomal recessive inheritance (Uhlenberg et al., 2004, Bugiani et al., 2006). Homozygous deletions leading to frameshift in the *GJA12*/*GJC2* gene were also reported to cause a similar phenotype (Wolf et al., 2007, Salviati et al., 2007), suggesting loss-of-function effect. However, subsequent studies revealed that only 7.7% of a large cohort of PMLD families harbour *GJA12/GJC2* mutations (Henneke et al., 2008), which are therefore not a common cause of PMLD.

Compared to “classical” PMD with *PLP1* mutations, PMLD patients with *GJA12/GJC2* mutations initially have a milder phenotype with higher achieved cognitive levels and speech capacity. However, neurologic deterioration starts earlier and progresses faster with shorter interval to loss of speech capacity as well as loss of ambulation, leading to wheelchair dependency (Henneke et al., 2008). One hypothesis to account for this clinical difference is that loss of Cx47-containing GJs leads to more rapid axonal degeneration than loss of PLP (Cailloux et al., 2000). Axonal degeneration likely correlates with the severity of the phenotype in PMLD similar to other CNS white matter disorders including PMD (Inoue, 2005, Garbern, 2007) and multiple sclerosis (Bjartmar et al., 2000).

Most recently, the phenotypic spectrum of *GJA12/GJC2* mutations has been expanded to include the complicated HSP presentation, caused by a novel recessively inherited mutation affecting Cx47, I33M. These patients exhibited a late-onset, slowly progressive, complicated spastic paraplegia, with normal or near-normal psychomotor development, preserved walking capability through adulthood, and no nystagmus. MRI and magnetic resonance spectroscopy (MRS) imaging were consistent with a hypomyelinating leukoencephalopathy (Orthmann-Murphy JL et al., 2009). Thus, *GJA12*/*GJC2* mutations, like *PLP1* mutations, can result in a milder phenotype than PMLD. Furthermore, distinct *GJC2* mutations were recently identified in several families with primary lymphedema (Ferrell et al., 2010), a peripheral disorder. The exact role of Cx47 in lymphatic tissue and the manner in which their cellular mechanisms differ from the mutations causing CNS disease remain to be determined.

1.3 Expression pattern of connexins in glia cells

1.3.1 Cx32 expression in myelinating Schwann cells

Cx32 was the first connexin to be cloned. It is highly conserved across mammalian species; the amino acid sequence of human Cx32 protein is 98% identical to those of the mouse and rat. Although Cx32 is most abundant in liver, it is also expressed by many cell types including oligodendrocytes and perhaps some neurons, as well as by myelinating Schwann cells (Scherer et al., 1995, Chandross et al., 1996, Söhl et al., 1996, Ressot and Bruzzone, 2000).

Despite this broad expression pattern, peripheral neuropathy and sometimes mild CNS phenotypes are usually the sole clinical manifestations of *GJB1* mutations. The reason the tissues, other than peripheral and central nervous system are not affected is unclear. One reason may be the co-expression of one or more other connexins, which could “protect” against the loss of Cx32. Myelinating Schwann cells in rodents express connexin29 (Cx29) (Söhl et al., 2001, Altevogt et al., 2002), but this does not appear to form functional gap junctions, at least *in vitro* (Altevogt et al., 2002), and may instead form hemichannels (Ahn et al., 2008, Sargiannidou et al., 2008) (***Fig.1.5***). Furthermore, it does not prevent the development of demyelinating neuropathy in *cx32*-null mice (Anzini et al., 1997, Scherer et al., 1998) or in CMT1X mutant mice (Jeng et al., 2006, Sargiannidou et al., 2009a).

GJ-like structures were first observed by freeze-fracture electron microscopy at the incisures and paranodes of myelin (Schnapp and Mugnaini, 1978, Sandri et al., 1982, Tetzlaff, 1982) and this localisation was recently confirmed by freeze-fracture replica immunogold labelling (Meier et al., 2004). The localisation of Cx32 in the same areas suggested that Cx32 forms these GJ between the layers of the Schwann cell myelin sheath (Bergoffen et al., 1993). A radial pathway formed by gap junctions at these locations would be up to a 1000-fold shorter than the circumferential pathway within the Schwann cell cytoplasm (Scherer et al., 1995). Diffusion of low molecular mass fluorescent dyes has been documented by fluorescence microscopy across the myelin sheath following injection in the perinuclear region of living myelinating Schwann cells (Balice-Gordon et al., 1998). Impairment of this radial pathway may damage myelinating Schwann cells and

their axons, causing neuropathy. The same fluorescent dye diffuses across the myelin sheath in *Gjb1/cx32*-null mice (Balice-Gordon et al., 1998) indicating that another gap junction protein is present in the Schwann cell myelin sheath, most likely Cx29, which is also localised in incisures (Altevogt et al., 2002).

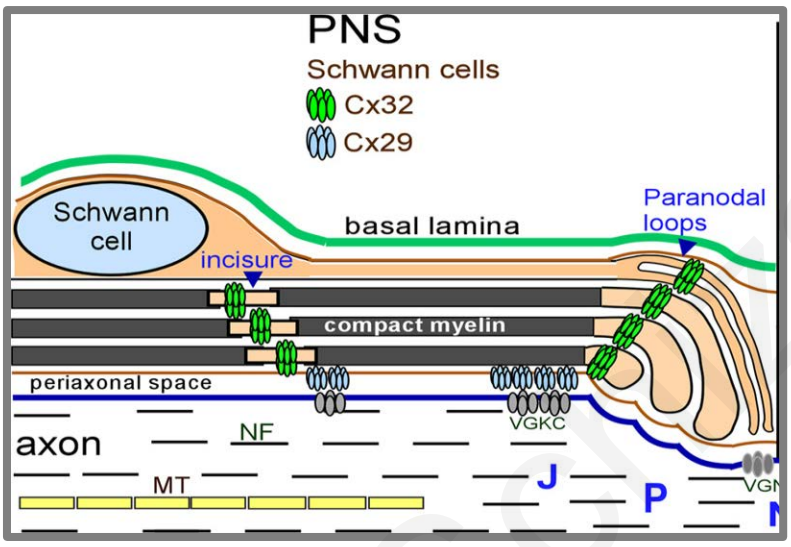

Figure 1.5: Expression of Cx32 and Cx29 in the PNS.
Diagram shows Cx32 forming gap junctions in non-compact myelin areas including paranodal loops and Schmidt-Lantermann incisures in Schwann cells. Cx29 forms hemichannels adjacent to the axonal membrane opposite voltage gated potassium channels (VGKC). NF-neurofilaments; MT-microtubule ; N-node ; P-paranode ; J-juxtaparanode (Kleopa, 2011).

1.3.2 Cx32 and Cx47 expression in oligodendrocytes

There is extensive gap junctional connectivity in the CNS suggesting a syncytium-like organisation of glial compartments (Nagy and Rash, 2000). Oligodendrocytes express at least 3 different gap junction proteins, Cx32, Cx47, and Cx29, in a highly specialized pattern (Altevogt et al., 2002, Kleopa et al., 2004) (***Fig.1.6***) and form GJ mostly with astrocytes (Rash et al., 2001, Altevogt and Paul, 2004).

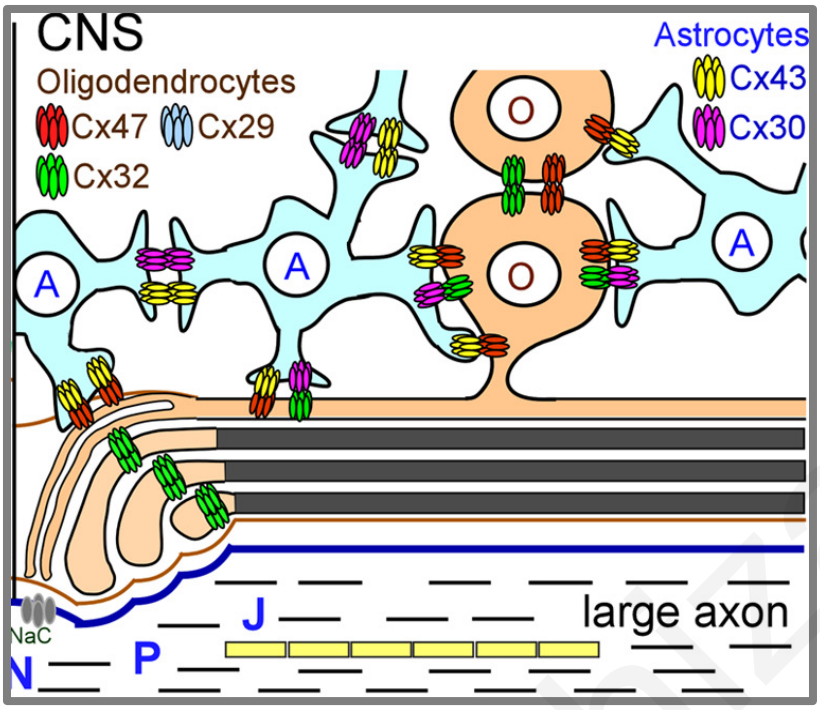

Figure 1.6: Expression of Cx32 and Cx47 in CNS large myelinating fibres.
In the CNS all oligodendrocytes (O) express Cx32 and Cx47 in the cell bodies and proximal processes. Cx32 and mainly Cx47 form O:O GJ while most O:A GJs are formed by Cx47 and Cx43 as astrocytic partner, and to a lesser degree by Cx32 and astrocytic Cx30 (Kleopa, 2011).

The subcellular distribution of oligodendrocytic GJ proteins is highly complex: Cx29 (Altevogt et al., 2002, Kleopa et al., 2004) and its human ortholog connexin31.3 (Cx31.3) (Sargiannidou et al., 2008) appear to form hemichannels within the myelin sheath of small fibres in some white matter tracts and cortex and rarely colocalise with any of the other glial connexins (Altevogt and Paul, 2004), suggesting that they do not form intercellular channels. Cx47 is prominent in oligodendrocyte somata (Menichella et al., 2003, Odermatt et al., 2003, Kleopa et al., 2004), forming gap junctions with astrocytic processes. Its astrocytic partner is mainly connexin43 (Cx43) and less frequently connexin30 (Cx30) (Altevogt and Paul, 2004, Kamasawa et al., 2005). Cx32 is mainly expressed along the large myelinated fibres of the white matter in Schmidt-Lantermann incisures (Altevogt et al., 2002, Kleopa et al., 2004) and paranodes bordering nodes of Ranvier, forming both intracellular GJ (Kamasawa et al., 2005) and intercellular ones with astrocytic connexin26 (Cx26) and Cx30 (Nagy et al., 2003a, b, Altevogt and Paul, 2004). Cx32 also forms most autologous GJs within the myelin sheath (Rash et al., 2001, Nagy et al., 2003b, Altevogt and Paul, 2004, Kamasawa et al., 2005). Oligodendrocytes form GJ with astrocytes (Rash et al., 2001, Altevogt and Paul,

2004) as well as with other oligodendrocytes (Maglione et al., 2010, Wasseff and Scherer, 2011).

1.3.3 Cellular and molecular effects of Cx32 mutants

Numerous Cx32 mutants that cause CMT1X have been studied in heterologous cells (Abrams et al., 2000). When expressed in *Xenopus* oocytes, many mutants do not form functional channels, and some of these also exert dominant-negative effects on the WT Cx32 (Bruzzone et al., 1994), indicating the potential for such interactions with co-expressed connexins in CMT1X. Other mutants form functional channels with altered biophysical characteristics, such as reduced pore diameter, that may prevent the diffusion of second messengers like IP3, cAMP, and Ca^{2+} (Oh et al., 1997). The position of the Cx32 mutation alone does not necessarily predict molecular and functional consequences (Abrams et al., 2001). Mutants in the C-terminal domain form functional GJ (Rabadan-Diehl et al., 1994, Castro et al., 1999), although they may be less stable or may have abnormal electrophysiological characteristics and cause leaky hemichannels, resulting in abnormal gain of function (Liang et al., 2005).

Expression of Cx32 mutants in cultured mammalian cells with more stringent requirements for protein trafficking revealed that they often have abnormal localisation (Omori et al., 1996, Yoshimura et al., 1998, Yum et al., 2002); either no Cx32 is detected, even though its mRNA is expressed, or Cx32 appears to be retained in the ER and/or Golgi (Deschênes et al., 1996, Deschênes et al., 1997, Oh et al., 1997, Martin et al., 2000, Matsuyama et al., 2001, Kleopa et al., 2002, Yum et al., 2002, Kleopa et al., 2006a), and degraded via endosomal and proteasomal pathways (VanSlyke et al., 2000, Kleopa et al., 2002). Some mutants form rare GJ-like plaques but mostly retained in the Golgi, while many mutants that reach the cell membrane typically form increased cytoplasmic granules. Several mutants, the majority of which occur in the C-terminal domain, are mainly localised on the cell membrane and show no significant difference to WT protein (Kleopa et al., 2002, Yum et al., 2002), but may have abnormal properties (Abrams et al., 2000).

Expression studies of Cx32 mutants *in vitro* allow tentative structure-function correlations (Abrams et al., 2000). N-terminal mutations have altered

biophysical properties and may cause reversal of gating polarity by negative charge substitutions, in keeping with the role of this protein domain in the insertion of the nascent polypeptide chain into the ER, and along with the first transmembrane domain in the regulation of voltage gating. Shifted voltage gating and abnormally increased opening has been shown for several mutants affecting the first and second transmembrane domain, which cause conformational changes (Abrams et al., 2002). Mutations affecting the cysteine in the two extracellular loops, which participate in interactions between apposed connexons, leads to a loss of functional channels. Mutations of the intracellular loop and C-terminal domain may affect pH gating (Castro et al., 1999). Two mutations that affect a consensus prenylation motif of Cx32 (C280G and S281X) abolish prenylation, a lipid modification (Huang et al., 2005).

In the past 10 years *in vivo* studies have provided further insights into CMT1X pathogenesis. Mice with targeted deletion of the *Gjb1/cx32* gene develop a progressive, demyelinating peripheral neuropathy beginning at about three months of age (Anzini et al., 1997, Scherer et al., 1998) as well as mild CNS pathology (Sutor et al., 2000). Motor fibers are much more affected than sensory fibers. Heterozygous females have less demyelinated and remyelinated axons than age-matched *Gjb1/cx32*-null females or males (Scherer et al., 1998), in keeping with the clinical phenotype of affected women who are obligate carriers of CMT1X. Expression of wild type human Cx32 protein largely prevents peripheral demyelination in Cx32 knocked-out (Cx32KO) mice (Scherer et al., 2005), confirming that the loss of Schwann cell autonomous expression of Cx32 is sufficient to account for demyelination in CMT1X.

Transgenic mice expressing the 175frameshift (fs), R142W, C280G, and S281stop (X) Cx32 mutations have also been generated. No Cx32 protein could be detected and no peripheral neuropathy was noted in 26 lines of mice expressing the 175fs transgene, even though transgenic/human mRNA was highly expressed in some lines (Abel et al., 1999). In contrast, mice expressing the R142W mutation developed a mild demyelinating neuropathy (Scherer et al., 1999). The mutant protein was retained in the perinuclear region and did not reach the incisures or paranodes, where Cx32 is normally localized. Moreover, the presence of the mutant Cx32 reduced the level of the endogenous/mouse Cx32,

indicating that R142W may have dominant-negative interactions with endogenous Cx32. However, it did not affect the coexpressed Cx29 (Jeng et al., 2006). In mice expressing the C280G or S281X mutations, the Cx32 mutants were properly localized to incisures and paranodes, and appeared to prevent demyelination in Cx32KO mice, indicating that these mutants may form functional channels in the myelin sheath (Huang et al., 2005).

Two further Cx32 mutations, T55I and R75W have been generated in our lab (Sargiannidou et al., 2009a). These mutants were expressed in Schwann cells and for the first time also in oligodendrocytes of the CNS, driven by the CNP promoter, in order to explore the possibility that they have gain-of-function effects. The mutants were expressed in almost all Schwann cells and oligodendrocytes. In both cell types these mutants failed to form GJ plaques (***Fig.1.7***) and as in cultured cells they were instead retained in the perinuclear cytoplasm, colocalizing with markers of the ER (T55I) or Golgi (R75W). On a *Cx32*-null background they caused a progressive demyelinating neuropathy as well as mild CNS myelination defects. In myelinating Schwann cells, R75W had dominant effects on endogenous Cx32 resulting in a mild demyelination also in a WT background and a more severe demyelinating neuropathy in a KO background.

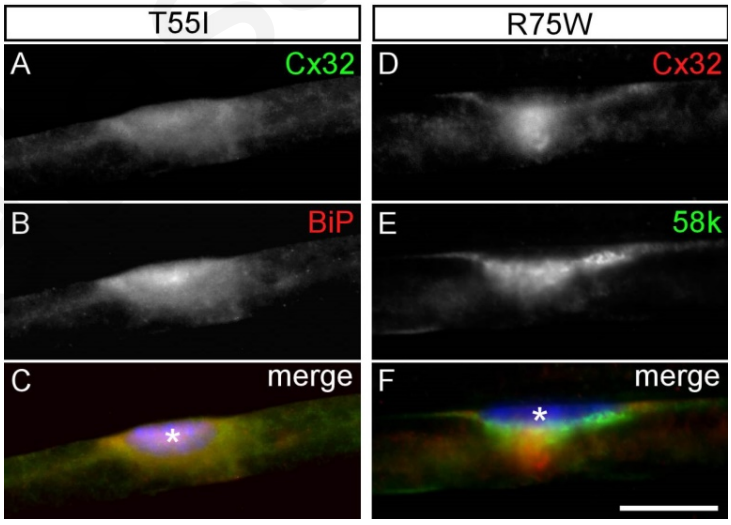

Figure 1.7: Abnormal retention of Cx32 mutants expressed in PNS myelinating cells.
Teased fibres from transgenic mice expressing the T55I (A-C) or R75W (D-F) mutations were double stained with antibodies to Cx32 and markers of the ER (BiP) or Golgi (58k). The T55I mutant colocalizes with BiP in the ER, while the R75W mutant colocalizes with 58k in the Golgi. Scale bar: 10 μm (unpublished results of (Sargiannidou et al., 2009a)).

In oligodendrocytes, the R75W but not the T55I mutant had subtle effects on CNS myelin in WT background, and both mutants had no additional effects in a KO background. Like a null allele of *Gjb1*, neither the T55I nor the R75W mutant appeared to affect Cx29 expression in Schwann cells, or Cx29 and Cx47 expression in oligodendrocytes (***Fig.1.8***). Since the partial dominant effect of the R75W mutant on the wild type protein is not relevant for the X-linked human disease, the loss of Cx32 function appears to be the main effect of the T55I and R75W mutants, both in the PNS and CNS (Sargiannidou et al., 2009a).

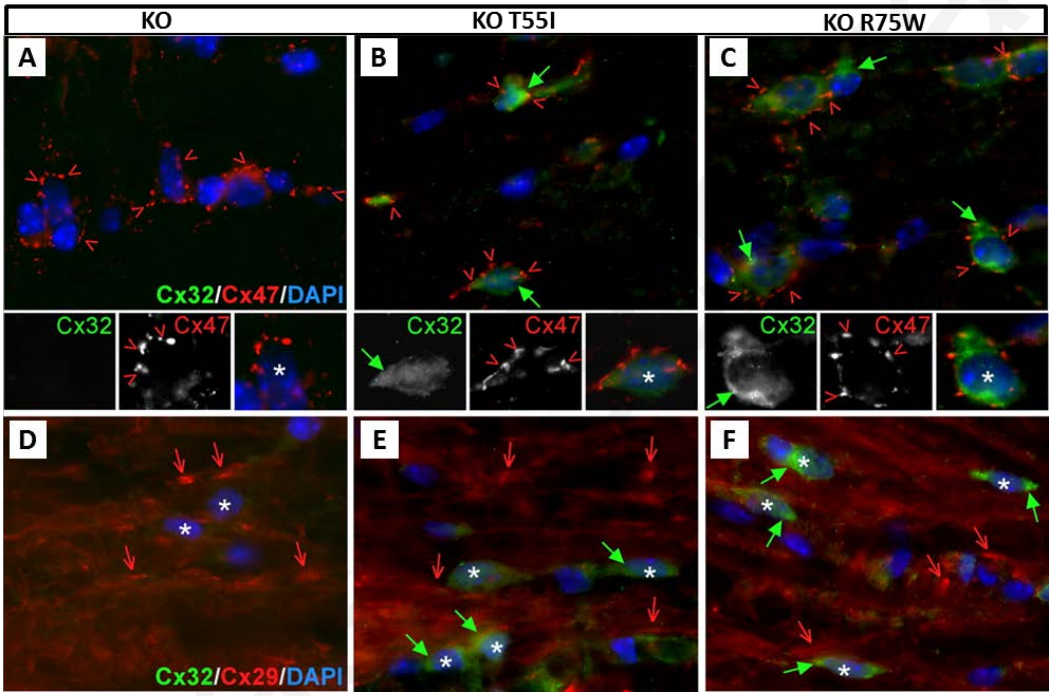

Figure 1.8: Abnormal retention of Cx32 mutants in the CNS.
Images from longitudinal sections of white matter spinal cord from Cx32KO (A-B) as well as T55I (C-D) and R75W (E-F) mutant mice. Sections were double labelled with Cx32 (green) and Cx47 (A, C, D) and Cx29 (B, D, E). Nuclei are stained blue. Cx32 is absent from Cx32KO mice (A) and mutant Cx32 is localized in the cytoplasm of oligodendrocytes in both T55I and R75W lines (C,E). Cx47 appears normal forming GJ plaques (A, C, E). Cx29 is also normally localized along the thin myelinated fibers (red arrows) in the mutant and Cx32KO mice. Scale bars: 10μm (Sargiannidou et al., 2009a).

1.3.4 Cellular and molecular effects of Cx47 mutants

Patients with PMLD have similar phenotypes although they have different missense mutations on the same gene, as described above. Mutated genotypes such as 128fs, M283T, G233S, or L278fs, P87S/P327fs or Y269D/R237X mutations – cause the same phenotype, including alleles that would be predicted

to disrupt the protein (P128fs, R237X, L278fs, and P327fs), as well as ones that may not (P87S, G233S, Y269D, and M283T) (Uhlenberg et al., 2004, Bugiani et al., 2006).

PMLD missense mutations affecting Cx47 (P87S, Y269D, M283T) result in loss-of-function of the protein when expressed in HeLa and Neuro2A cell lines (Orthmann-Murphy et al., 2007a). In all three mutants Cx47 was partially retained in the ER and failed to form functional homotypic channels, suggesting loss-of-function. M283T mutation seems to be an exception, as some puncta appeared around oligodendrocyte cell bodies which may be GJ plaques. These puncta were also visualised in the optic nerve of rhesus monkeys and when double labelled with Cx43 colocalisation was present, indicating the formation of O/A gap junctions in the primate brain (Orthmann-Murphy et al., 2007a).

Cx47 mutants most likely cause the PMLD phenotype by interfering with the normal function of Cx47/Cx43 and Cx47/Cx47 channels. Indeed, all three missense mutants fail to form functional Cx47/Cx43 channels (Orthmann-Murphy et al., 2007b).

The I33M Cx47 mutation causes HSP, a milder phenotype than PMLD. I33M forms GJ plaques similar to WT Cx47 in transfected cells, but fails to form functional homotypic channels in scrape-loading and dual whole-cell patch clamp assays. Furthermore, I33M/Cx43 channels open only when a large voltage difference is applied to paired cells; consequently, these channels probably do not function under physiological conditions. This suggests that in HSP, Cx47/Cx43 channels between astrocytes and oligodendrocytes are disrupted, similar to the PMLD mutants (Orthmann-Murphy et al., 2009). Whether the spastic paraplegia mutant retains a function of Cx47 not directly related to forming functional GJ channels remains to be determined.

Similar to *Gjb1/Cx32*-null mice, *Gjc2/Cx47*-null mice are long lived, but develop mild CNS pathology consisting of vacuolation of nerve fibres, especially in the proximal optic nerve where myelination begins.

Cx47 mutations associated with PMLD or with HSP appear to cause loss of function and are recessively inherited. Cx47 plays a paramount role in both O/O and O/A gap junctional connectivity, and loss of all or some of its functions may cause a spectrum of phenotypes caused by disturbed oligodendrocyte homeostasis and secondary axonal injury.

1.3.5 Cellular and molecular effects of Cx32 and Cx47 mutants in the CNS

Cx32 and Cx47 seem to have partially overlapping functions in oligodendrocytes, because mice deficient for either Cx32 or Cx47 alone develop minimal CNS pathology, whereas double knockout mice (dKO) develop severe CNS demyelination (Scherer et al., 1998; Menichella et al., 2003; Odermatt et al., 2003). In contrast to the mild phenotypes of single knockout mice, Cx32 and Cx47 dKO mice present with a coarse action tremor during the third postnatal week that is accentuated on movement and whose severity worsens over time. Tonic seizures begin during the fourth to fifth postnatal week and are characterized by limb extension and loss of consciousness. The seizures increase in frequency and severity until the animals die, typically during the sixth postnatal week (Menichella et al., 2003; Odermatt et al., 2003). At 1 month of age, these dKO mice show extensive pathology in the CNS including severe demyelination, axonal degeneration and apoptosis of oligodendrocytes in the spinal cord funiculi and in the optic nerve (Menichella et al., 2003; Odermatt et al., 2003). Vacuoles are present in the periaxonal space, as well as thinner myelin sheaths than age matched littermates and edematous extracellular spaces separating degenerating axons from their myelin sheath (Menichella et al., 2003, Odermatt et al., 2003).

This glial network of GJs in the CNS may serve the spatial buffering of K+ elaborated during the propagation of action potentials (Kamasawa et al., 2005; Menichella et al., 2006). The importance of this network in humans is supported by the discovery of Cx47 mutations in patients with PMLD, a severe demyelinating disorder of the CNS (Uhlenberg et al., 2004; Bugiani et al., 2006; Orthmann-Murphy et al., 2007).

1.4 Aim of the study

Based on the available evidence, transgenic replacement therapy is a promising approach to the treatment of patients suffering from this or similar disorders. Therefore, we consider that it is justified and timely to study the feasibility of transgenic replacement therapy to repair oligodendrocyte gap junctional connectivity in relevant disease models.

Animal models of CMT1X have been generated, which express Cx32 mutations in the PNS and CNS that develop progressive demyelinating peripheral neuropathy with early axonal pathology combined with CNS myelination defects (Sargiannidou et al., 2009b). These models provide a valuable tool to investigate further possible therapeutic approaches for these currently incurable diseases. Transgenic replacement of Cx32 expression in Schwann cells of Cx32KO mice resulted in full rescue of the peripheral neuropathy, confirming the cell autonomous mechanisms in CMT1X (Scherer et al., 2005). However, such cell autonomous effect needs also to be shown for CNS pathology resulting from connexin mutations, given the more complex cell–cell interactions and restricted compatibilities between glial connexins (Altevogt and Paul, 2004, Orthmann-Murphy et al., 2007b, Orthmann-Murphy JL et al., 2009).

It appears highly relevant to test first whether the introduction of the wild type human Cx32 in mice lacking the *GJB1* gene and cell-autonomous expression in oligodendrocytes would be sufficient to rescue the demyelinating CNS phenotype in mice with combined deficiency of Cx32 and Cx47. The originality of this project is to generate a transgenic construct with an oligodendrocyte-specific promoter, Plp, followed by our gene of interest Cx32. The Plp promoter has been previously used successfully to generate transgenic mice (Savvaki et al., 2010, Fuss et al., 2000, Wight et al., 1993, Michalski et al., 2011a). The goal of this project is to rescue the CNS and PNS clinical and pathological phenotype of Cx32/Cx47dKO mice as a model for PMLD.

Chapter 2

MATERIALS AND METHODS

MATERIALS AND METHODS

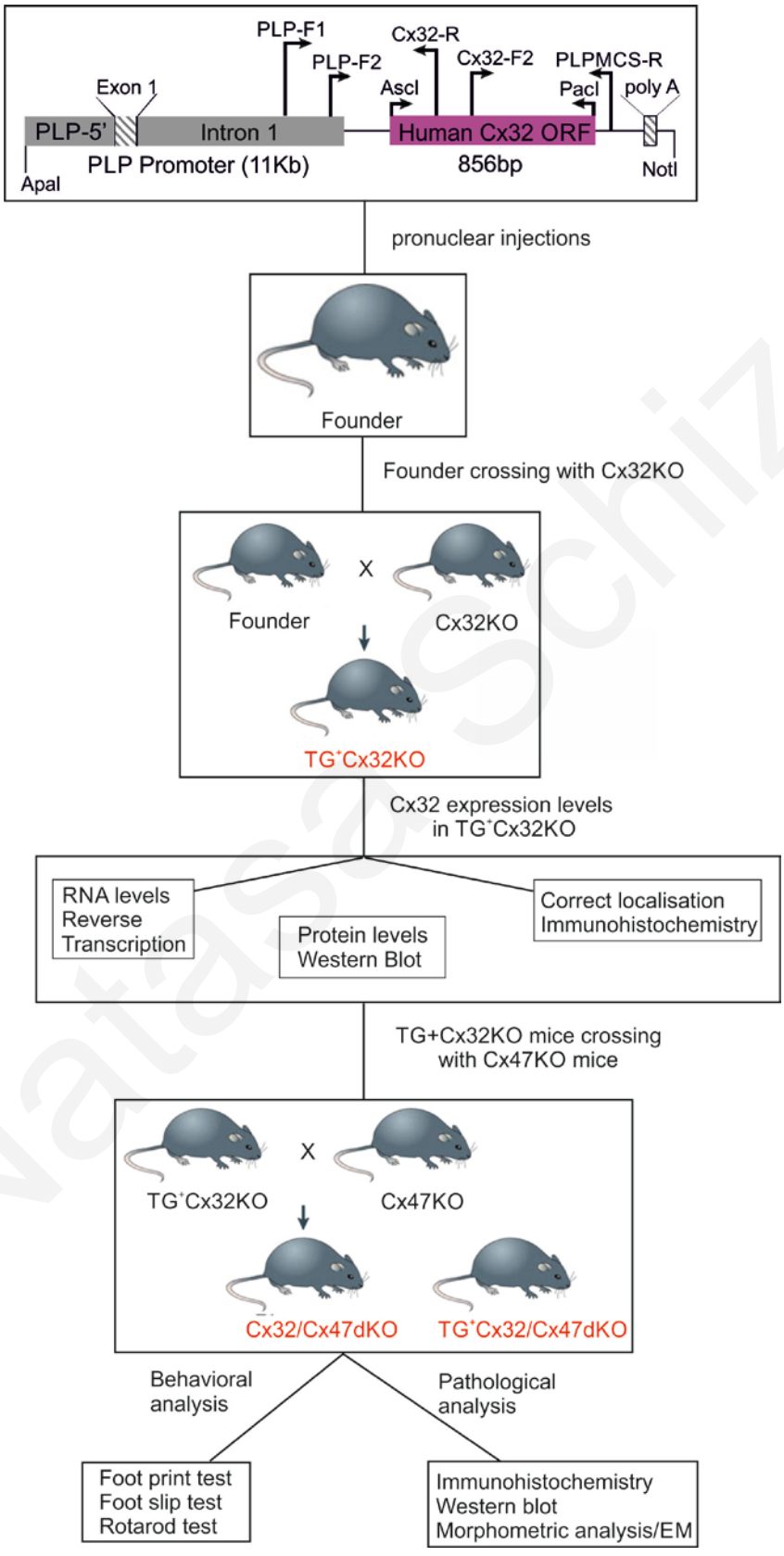

Figure 2.1: Flow Chart.

2.1 Cloning of the transgenic construct

The transgenic construct consists of the Plp promoter followed downstream by the human Cx32 gene, *GJB1*. The ~11Kb mouse Plp promoter was cloned in pBluescript SK+ vector (a gift from Prof. Karagogeos lab, University of Crete) previously used successfully to generate transgenic mice driving expression specifically in oligodendrocytes (Wight et al., 1993, Fuss et al., 2000, Savvaki et al., 2010, Michalski et al., 2011b). The human *GJB1*/Cx32 open reading frame (ORF) was already cloned in pSLN1180 vector in our lab (Sargiannidou et al., 2009a). In order to have compatible sites, two new restriction sites, AscI and PacI, were introduced in the pSLN1180 vector by PCR amplification using the following primers: AscI-F1 (see appendix) and PacI-R (see appendix). The hCx32 ORF was isolated from the pSLN1180 vector using AscI and PacI restriction enzymes. The fragment of interest was then purified using Centricon (Millipore, 4212) and ligated overnight at 20^{o}C in the MCS of pBluescript SK+. Purified Plp promoter-hCx32 construct was heat shock transformed into XL1-blue bacterial cells (see appendix). 1μl of the extracted DNA was added to 100μl aliquote of XL1-blue cells and left to stand for 30 minutes on ice. The DNA with the bacterial cells were then incubated in a 42^{o}C waterbath for 45 seconds and then chilled on ice for 2 minutes. 900μl of SOC medium (see appendix) were added to the 110μl DNA/XL1, transferred to a falcon tube and incubated for 1 hour at 37^{o}C by continuously shaking at 250rpm. Using a sterile pipette 100μl of the transformed cells were spread with a sterile inoculator on agar plates until bacterial cells were absorbed. Agar plates (see appendix) with the selected antibiotic, ampicillin were incubated at 37^{o}C overnight in an upside down position. The next day ampicillin resistant colonies were grown on the plates; some colonies were randomly picked up with sterile toothpicks. Each colony was grown in 500μl of L-Broth (see appendix) for 2 hours with rapid shaking. Each mini culture was screened by PCR using two primer sets: Plp-F1 (see appendix) and Cx32-R (see appendix) resulting in an 824 bp PCR product (94^{o}C for 5 min 40 cycles of 94^{o}C x 30 sec, 60^{o}C x 30 sec, 72^{o}C x 30 sec and then 72^{o}C for 7 min), as well as with Plp-F2 (see appendix) and Cx32-R resulting in a 528 bp product. 100μl of a selected mini culture was further grown in a 500mL flask with 200μl of L-Broth and ampicillin at 37^{o}C for 16-18 hours with vigorous shaking at 250rpm. Using the endofree plasmid maxi kit (Qiagen, 12362), following the manufacturer's protocol, the transgenic construct was isolated with high purity and concentration.

The purified transgenic cassette which contains the hCx32 downstream of the Plp promoter was released from pBluescript SK+ by double digestion with ApaI and NotI (***Fig.3.1***). The ~12Kb band was further purified using a Gel extraction kit (Qiagen, 28704) and finally eluted in microinjection buffer (Millipore, MR-095-F). The orientation and the in-frame positioning of the transgenic construct was further confirmed by direct sequencing analysis, including the entire ORF.

For the alternative strategy we generated transgenic mice with the 2Kb MBP promoter, oligodendrocyte specific, that has been previously used (Gow et al., 1992). The 9Kb MBP promoter was already cloned in pBluescript vector and by restriction digest with AflII enzyme we minimized the size of the promoter to 6Kb and by further digestion with SacI we got the 2Kb fragment of the MBP followed by the IRES-EGFP.

2.2 Animal strains and procedures

For this study we used C57BL/6 mice (Harlan Laboratories) for generation of transgenic lines, as well as *Gjb1*-null/Cx32 knockout (KO) mice (C57BL/6_129) (Nelles et al., 1996) and *Gjc2*/Cx47 KO mice (C57BL/6;129P2/OlaHsd) (Odermatt et al., 2003), both obtained from the European Mouse Mutant Archive Monterotondo, Italy (originally generated by Prof. Klaus Willecke, University of Bonn). For all studies mice received anesthesia with intraperitoneal Avertin injection and then were either transcardially perfused and tissues were fixed for immunostaining analysis or electron microscopy, or tissues were removed unfixed for immunoblot and RNA analysis. All experimental procedures were conducted in accordance with the animal care protocols approved by the Cyprus Government's Chief Veterinary Officer according to EU guidelines (EC Directive 86/609/EEC).

2.3 Generation of transgenic mice expressing the wild type human Cx32

The purified fragment was microinjected into the male pronucleus of fertilized oocytes (***Fig.3.2***) obtained from C57BL/6 mice according to standard protocols at the Mouse Facility of the Cyprus Institute of Neurology and Genetics. After successful pregnancies and offspring delivery, founders were PCR screened by genomic tail DNA with specific primer sets for Plp promoter and Cx32 gene. Two primer sets were used for the promoter region (proximal ligation site) and one for the distal ligation site to the multiple cloning site: a) PlpF1 and Cx32-R (see appendix) b) PlpF2 and Cx32-R (see appendix) and c) PlpMCS-F (see appendix) and Cx32-F2 (see appendix) resulting a 600 bp product (***Fig.3.3***). Founders (TG^+) were bred with *Gjb1*-null/Cx32 KO mice in order to obtain mice expressing the transgene on a Cx32KO background (TG^+Cx32KO).

2.4 Generation of TG^+Cx32/Cx47dKO and Cx32/Cx47dKO mice

Cx47KO mice were crossed with transgenic mice on a Cx32KO background (TG^+Cx32KO). The mouse Cx47 coding region has been replaced with EGFP reporter gene in these mice. The mouse *Gjb1*/Cx32 gene is located on the X chromosome and *Gjc2*/Cx47 gene is autosomal. F1 offspring was then crossed again to obtain males TG^+Cx32KO/Cx47Het and Cx32KO/Cx47Het. Offspring of F2 generation were breed again to obtain TG^+Cx32KO/Cx47dKO and Cx32KO/Cx47dKO. Cx32 genotype was tested by PCR screening using primers mentioned above. Cx47 genotype was screened by multiplex-PCR using simultaneously 3 primers. One primer is Cx47 intron-specific (P1 -see appendix), the second is exon-specific (P3 - see appendix) and the last EGFP-specific (P4 - see appendix) under conditions 95^{o}C for 5 min 40 cycles of 94^{o}C x 45 sec, 64^{o}C x 45 sec, 72^{o}C x 1 min and then 72^{o}C for 7 min. A band at 530 bp represents the wild type (WT) allele and at 340bp the Cx47KO allele (Odermatt et al., 2003) (***Fig.3.3***).

2.5 Reverse transcription PCR

Snap-frozen brain and spinal cord tissue from TG^{+}Cx32KO, Cx32KO and WT mice were collected. RNA was isolated with the RNeasy Lipid Tissue Mini Kit (Qiagen, Cat.no. 74804) following manufacturer's protocol. DNase treatment was performed and RNA was quantified by spectrophotometry. 0.5µg of RNA was used to synthesize cDNA using Taqman Reverse transcription reagents (Applied Biosystems, N808-0234). cDNA was amplified using Cx32-F (see appendix) and Cx32-R (see appendix) primers. cDNA was then digested with MscI or HhaI as well as with both enzymes. MscI cuts the human cDNA into two fragments (280 and 273 bp); HhaI cuts the mouse cDNA product into two fragments (230 and 323 bp). Digestions were run on 1.5% agarose gel to estimate the relative levels of transgene/human and endogenous/mouse mRNAs (***Fig.3.4***).

2.6 Immunoblot analysis

Gel preparation

Two glass plates were assembled together in the gel electrophoresis (Bio-Rad) apparatus. A 12% polyacrylamide gel (see appendix) was prepared and poured in-between the glass plates. On top 1mL of 10% iso-propanol was added and left to polymerise at room temperature for 30 minutes. When polymerised, isopropanol was removed and a 4% stacking gel (see appendix) was prepared and poured on top of the polyacrylamide gel with a 10 well comb in top. The stacking gel was allowed to polymerise at room temperature for another 30 minutes. After polymerisation the comb was removed.

Sample preparation

Fresh mouse tissues were collected and lysed in ice cold Radio Immunoprecipitation Assay buffer (RIPA) (see appendix) containing a cocktail protease inhibitors (Roche, Basel, Switzerland). Tissues were sonicated and protein concentrations were measured on NanoDrop. 50µg of the denatured protein from each lysate and loading buffer (see appendix) was loaded into each well. Gel electrophoresis was performed in 1x Running buffer (see appendix) at a constant voltage of 120V for approximately 1-1$^{1/2}$ hours.

Transfer of proteins

The proteins were then transferred on Hybond-C extra membrane (GE Healthcare Bio-Sciences) under semi-dry conditions. A sandwich of whatman filter paper/gel/membrane/whatman filter paper are wetted in 1xTransfer buffer (see appendix) and placed on the transfer unit at a constant current of 10V for 45 minutes.

Blocking the membrane

To prevent non-specific background binding of the primary antibody the membrane was incubated with 5% non-fat milk in PBS-T by agitating for 1 hour at room temperature.

Incubation with the primary antibody

The primary antibody was then diluted at the suggested dilution by the manufacturer in 5% non-fat milk in PBS-T by agitating overnight at 4^{o}C.

Incubation with the secondary antibody

The membrane gets a room temperature and washed for 15 minutes (x3), to remove excess of the primary antibody, with PBS-T while agitating followed by incubation with anti-rabbit or anti-mouse horseradish peroxidase-conjugated secondary antiserum (Jackson ImmunoResearch Laboratories, 1:3000) in 5% milk-TBS-T, for 1 h.

Development method

After an hour the membrane was washed three times with PBS-T for 15 minutes each with agitation. The membrane was incubated with enhanced chemiluminescence labelling solution (ECL Plus, GE Healthcare Bio-Sciences, Amersham) for 5 minutes in dark conditions, then is placed in a cassette and exposed to UVP imaging system (Life Science). The protein of interest is visualised on the computer screen. GAPDH was used as a loading control. Band intensity was measured and quantified using TinaScan software version 2.07d.

2.7 Transcardial perfusion

The adult mouse is weighted to the nearest 0.1 gram. According to its weight the anaesthesia syringe is filled with Avertin and administered via intraperitoneal injection. Anaesthesia is assured by toe pinch. The anesthetized animal is placed lying on the back with face upwards. The ventral skin is wet with 100% ethanol and an incision through the skin is made along the thoracic midline. The peritoneal membrane is cut superficially and exposed to the diaphragm and visceral organs. The diaphragm is cut with gentle to avoid injury of any visceral organs in order to open the thoracic cavity. Continue with blunt dissection to carefully cut both lateral aspects of the rib cage. The ribcage is inverted to meet the ventral skin surface of the animal's neck area to expose the heart (***Fig.2.1***). The beating heart is secured with blunt forceps and the syringe filled with saline is inserted to the left ventricle. The right atrium is cut with scissors (first sign of blood flow) and the infusion of 5ml saline begins slowly until the fluid exiting the right atrium is clear. A clear colour of the liver is an indication of good saline perfusion. The saline is then switched to 4% paraformaldehyde (PFA) fixative (see appendix). When the mouse is stiff, tremoring due to muscle contraction is an indication that the fixative has passed through the circulatory system.

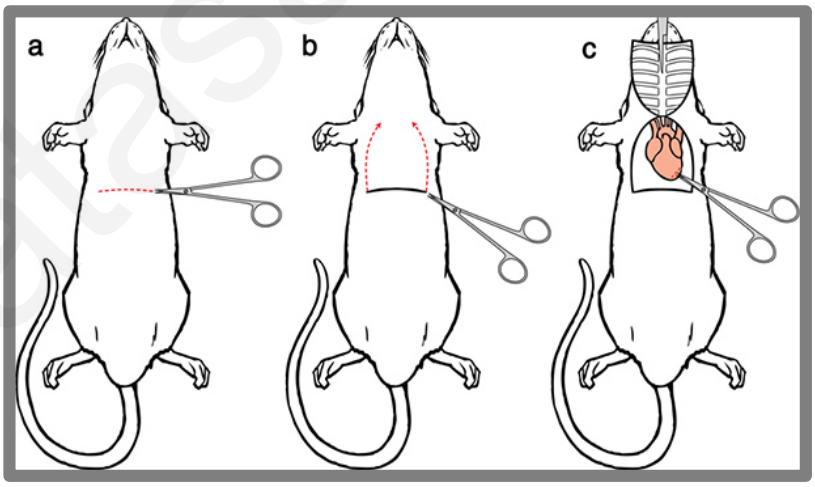

Figure 2.2: Transcardial perfusion (Gage et al., 2012).

2.8 Immunohistochemistry

Following transcardial perfusion with 4% PFA, brain, cerebellum, spinal cord, optic and sciatic nerves were dissected from the mouse body. 30 minute post fixation follows in the same fixative and then cryoprotected in 20% sucrose in 0.1M PB (see appendix) buffer overnight. Tissues were then embedded in OCT and placed in ice cold-acetone and stored in -80 ^{o}C degrees. 12 µm thick sections were thaw-mounted onto APES glass slides (see appendix). Tissues were permeabilized in cold acetone (-20^{o}C degrees) for 10 minutes. Slides were then washed three times 5minutes each in 1x PBS (see appendix) and then incubated at RT with blocking solution of 5% bovine serum albumin (BSA) containing 0.5% Triton-X100 (see appendix) for 1 h. Various combinations of primary antibodies (see appendix) are diluted in blocking solution followed by incubation overnight at 4°C. Slides were then washed three times 5 minutes each in 1x PBS and incubated with rhodamine (TRITC) conjugated Affinity Pure Goat Anti-rabbit IgG and Fluorescein (FITC) conjugated AffiniPure Goat Anti-Mouse IgG secondary antibodies (Jackson ImmunoResearch Laboratories, 1:500) for 1h at room temperature. Cell nuclei were visualized with 4',6'-diamidino-2-phenylindole (DAPI, Sigma-Aldrich). Slides were mounted in Fluorescent Mounting Medium (Dako). Images were photographed under a Zeiss fluorescence microscope with a digital camera using the Zeiss Axiovision software (Carl Zeiss MicroImaging) at magnifications x50, x100, x200, x400. Images with comparable exposure times were obtained to allow better comparison between different tissues. Selected images for GJ plaque counts were captured on a TCSL confocal microscope (Leica, Germany).

2.9 Quantitative analysis of pathology and GJ plaque formation

The fluorescent intensity of positive GFAP and Iba1 from microscope pictures was calculated using *ImageJ* software. For quantification of GJ formation by oligodendrocytes, we randomly captured at least 20 individual oligodendrocytes within an area of 20µm x 20µm from spinal cord gray matter from 3 different mice per genotype. Pictures from the three genotypes were captured at 400x magnification. The total number of Cx32, Cx30, and Cx43 GJ plaques in each image were counted using Adobe photoshop 6. In addition, we counted the

number of GJ plaques in which Cx32 colocalized with either Cx30 or with Cx43 immunoreactivity and the overlap ratio was calculated in Microsoft Excel.

2.10 Electron microscopy and morphometric analysis

For electron microscopy, 1-month-old litters of TG$^+$Cx32/Cx47dKO and Cx32/Cx47dKO mice (n=4 per genotype) were transcardially perfused with 2.5% glutaraldehyde in 0.1M PB. Brain, spinal cord, optic nerve and sciatic nerve were dissected and further fixed overnight at 4°C, then osmicated, dehydrated, and embedded in Araldite resin. Transverse semithin sections (1μm) were obtained and stained with alkaline toluidine blue. Ultrathin sections (80–100 nm) were counterstained with lead citrate and uranyl acetate before being examined in a JEOL JEM-1010 transmission electron microscope.

The CNS myelin fraction was calculated in semithin sections of the spinal cord dorsal and ventral funiculus and the optic nerve using a modified method to estimate the density of myelinated fibers and myelin sheaths (Tang and Nyengaard, 1997, Sutor et al., 2000, Vavlitou et al., 2010). Images of semithin sections captured at x630 final magnification following the same processing and microscopy settings were imported into Photoshop (Adobe Systems) and a transparent counting grid was placed on the image. All intersections of the grid lines hitting white matter, myelinated fibers and myelin sheaths were counted separately. The volume density of the myelinated fibers in the white matter was calculated by the total number of points hitting myelinated fibers in the white matter over the total number of points hitting white matter.

2.11 Behavioral analysis

2.11.1 Foot slip test

To explore the motor behavior of mice a modified method of Britt (Britt et al., 2010) was used, which is considered sensitive for CNS demyelination models. 1-month-old mice were placed in a 15x15x15 cm clear plexiglass box with a floor consisting of a metal wire grid with 1.25 cm spacing with a 1.25 cm grid suspended 1.25 cm above the floor. Mice were acclimated in the box for 1hr before each session. The trial consisted of 50 steps. If a misstep results in the hindlimb or forelimb falling through the grid but the limb is withdrawn prior to

touching the floor is scored 1; if the limb touches the floor it is scored 2. A video camera was used to film the mice to ensure accurate counts, and video recordings were evaluated in slow motion. TG^+ Cx32/Cx47dKO mice were compared to Cx32/Cx47dKO littermates using the student's T-test. Significance was defined as $p<0.05$ in all comparisons.

2.11.2 Rotarod test

This apparatus consists of a computer-controlled, motor-driven rotating spindle and 4 lanes for 4 mice. One-month old mice were habituated to the apparatus the first day for 180 sec sessions twice at constant speeds of 12 and 20rpm. On the second day mice exert 4 trials with accelerating speed from 4 to 40rpm. On the third day, mean latency to fall off the rotarod is calculated.

2.11.3 Foot print test

Footprints were obtained by painting the paws with nontoxic colored inks and the mouse was allowed to walk down a narrow, open-top runway covered with white paper. The runway length was 22 cm long 10 cm wide. Furthermore, the open-top runway was flanked by two walls at each side that were 11 cm high. The mice were acclimatized to the environment for at least 60 min, and were allowed two practice runs before coloring the paws. To facilitate subsequent analysis, forelimbs and hindlimbs were colored with different colors: blue for the front and red for the hindlimbs. Each mouse was subjected to a total of nine trials (three trials per day for 3 days). Once the footprints had dried, the following parameters were measured: overlap width, forelimb stride length, and hindlimb stride length for the left and right limbs separately.

2.11.4 Survival rate test

The Kaplan Maier survival curve was used to compare the survival rates of TG^+Cx32/Cx47dKO to those of Cx32/Cx47dKO littermates. Two groups of 10 mice were used for this analysis and followed until they became severely ill and preterminal, but before they died of seizures. A graph was blotted for the percentage of surviving animals over time in weeks.

Chapter 3

RESULTS

RESULTS

3.1 Generation of the transgenic construct expressing hCx32

To generate the transgenic construct we used the mouse Plp promoter and downstream the human *GJB1*/Cx32 open reading frame (ORF). The ~11Kb mouse Plp promoter was cloned in pBluescript SK+ vector which has been previously used successfully to generate transgenic mice driving expression specifically in oligodendrocytes (Wight et al., 1993, Fuss et al., 2000, Savvaki et al., 2010, Michalski et al., 2011a). hCx32 ORF was already cloned in pSLN1180 vector in our lab (Sargiannidou et al., 2009a). Two new restriction sites, AscI and PacI, were introduced by PCR amplification in pSLN1180 vector, followed by a double digestion so the Cx32 ORF was released. The 856bp ORF band was ligated into the multiple cloning site of the *Plp* promoter cassette in pBluescript vector. Then the ~12Kb transgenic cassette was released from pBluescript by double digestion with ApaI and NotI restriction enzymes (***Fig.3.1 A***). The fragment was then isolated and purified. The orientation and the in-frame positioning of the hCx32 ORF were confirmed by sequence analysis using specific primers within the ORF (see appendix).

As an alternative strategy we also used an oligodendrocyte specific promoter, Myelin basic protein (MBP). This promoter is 9Kb in size and is already cloned in the pBluescript vector in our lab. Downstream of the promoter the hCx32ORF-IRES-EGFP sequence is cloned. EGFP allows co expression of the green fluorescent protein in cells expressing the transgene. Previous studies (Foran and Peterson, 1992, Gow et al., 1992, Forghani et al., 2001) have shown that the last 1.9Kb fragment of the promoter is sufficient to drive expression in oligodendrocytes. The size of the promoter was minimised to 2Kb by two sequential digests. The full construct was first digested with AflII and two size bands were obtained, ~9Kb and ~6Kb. The ~6Kb band contained the hCx32ORF-IRES-EGFP with the promoter. We further digested with SacI restriction enzyme to minimise the promoter to ~2Kb (***Fig. 3.1 B***). The ~4Kb fragment was then purified and filtered in microinjection buffer. hCx32 ORF was sequenced using specific primers we have designed (see appendix) to ensure the construct was free of any mutations.

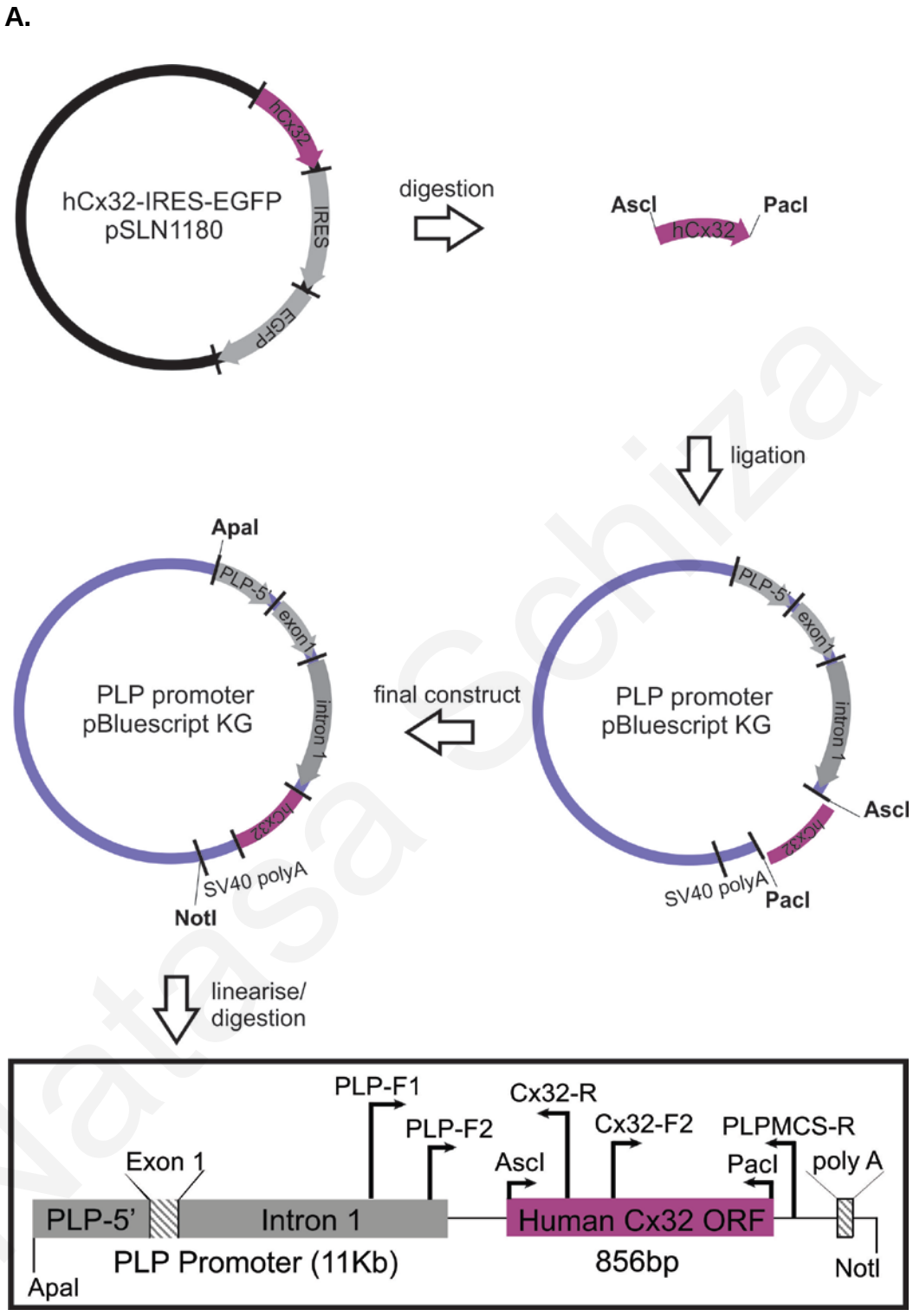

Figure 3.1: (A) Cloning of the Plp-hCx32 expression construct.
hCx32 ORF was isolated from pSLN1180 vector by digestion with AscI and PacI restriction enzymes and then ligated into pBluescript KS vector downstream of the Plp promoter. pBluescript KS was linearised with ApaI and NotI restriction enzymes.

B.

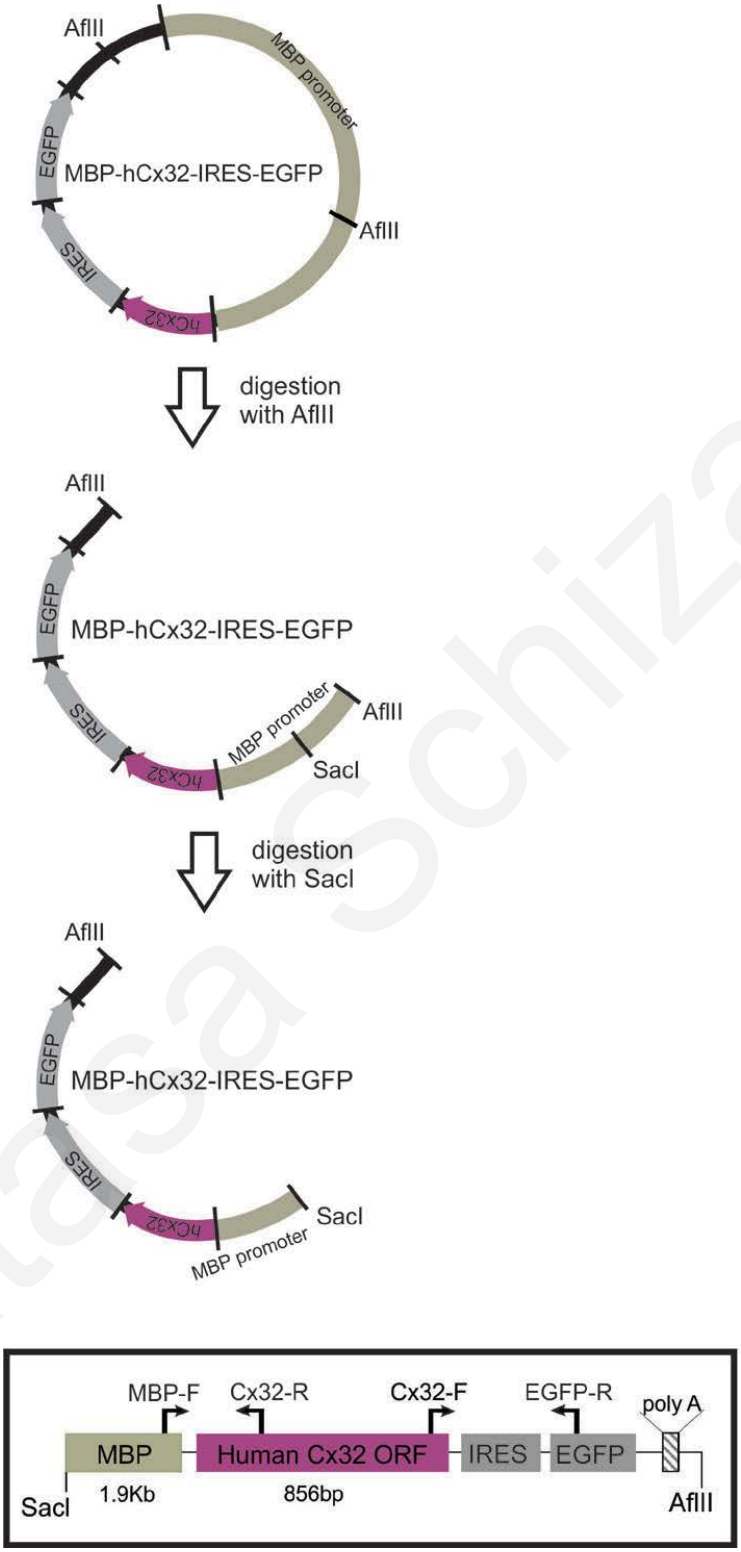

(B) Cloning of the MBP hCx32-IRES-EGFP expression construct.
The 9Kb MBP promoter followed by hCx32 ORF-IRES-EGFP were cloned in pBluescript vector. By restriction digest with AflII the promoter was minimised down to ~4Kb by further digestion with SacI the promoter was minimised to 1.9Kb.

3.2 Generation of Plp-hCx32TG^{+} and TG^{+}Cx32KO mice

MBP-hCx32-IRES-EGFP (~4Kb) and Plp-hCx32 (~12Kb) purified fragments were microinjected into the male pronucleus of the fertilised oocytes (***Fig.3.2***). Microinjection process was performed at the Mouse facility of the Cyprus Institute of Neurology and Genetics according to standard protocols. Multiple pronuclear injections of the MBP promoter construct MBP-hCx32-IRES-EGFP resulted in one positive founder which had no transmission to F1 generation. We therefore abandoned this strategy and all results described below relate to the Plp-hCx32 transgenic mice.

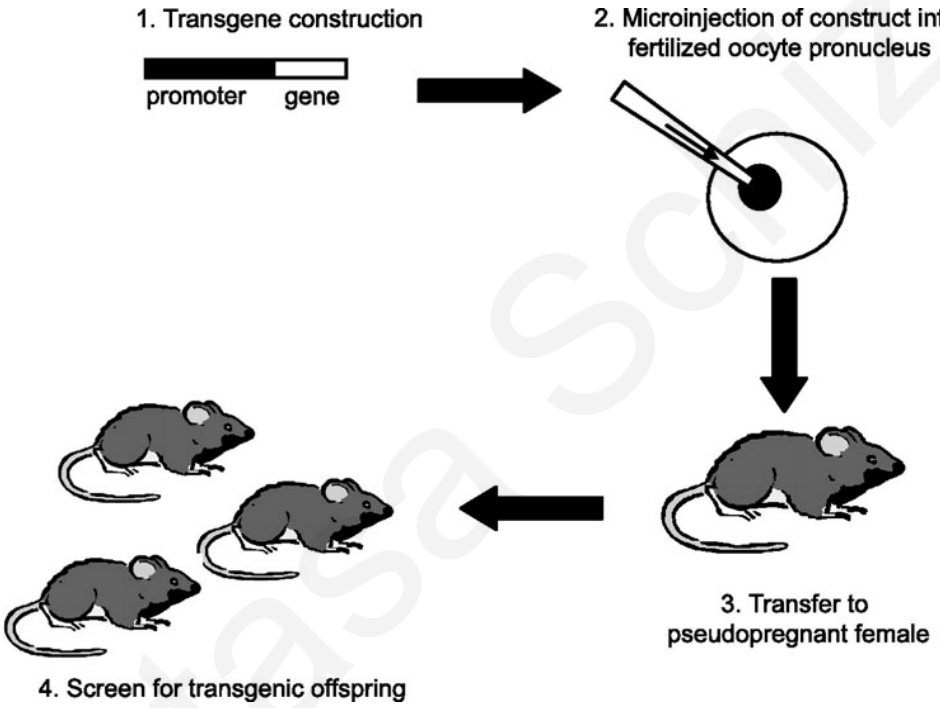

Figure 3.2: Pronuclear injection.
(1) Purified transgenic construct was (2) microinjected in the fertilised eggs from the female mouse. (3) The injected eggs were transferred in the uterus of the pseudopregnant female. (4) F1 pups were born and PCR screened for founders (Mullins et al., 2006).

After successful pregnancies, F1 offsprings were born and tailed at the age of P30. Tails were PCR screened using three different primer sets (see M&M section 2.3). Screening revealed 5 positive transgenic founders, 3 females and 2 males. These founders were further bred with Cx32KO male or female mice (the Cx32 gene is located on the X chromosome) accordingly to examine if the transgene is carried to the next generation and if so, the Cx32 expression levels in oligodendrocytes and Schwann cells.

Two of the founders showed stable transmission to the next generation and were crossed with Cx32KO mice and further genotyped (***Fig.3.3***). About 30% of the mice carried the transgene (TG^+). These mice were crucial for the assessment of the transgenic expression and exogenous Cx32 localization on a *Gjb1*-null/Cx32KO background. Therefore these two lines were further expanded on Cx32KO background and Cx32 expression levels were compared to select the best line (***Table1***).

Table 3.1: Summary of the Plp-hCx32 transgenic founders.
Three out of five positive founders had transmission to the next generation and two out of three had strong Cx32 expression in oligodendrocytes as well as in Schwann cells.

Line/Founders	*Transmission*	*Cx32 Expression*
Plp-1	Yes	Strong expression
Plp-2	No	----------
Plp-3	Yes	Strong expression
Plp-4	Yes	No expression
Plp-5	No	----------

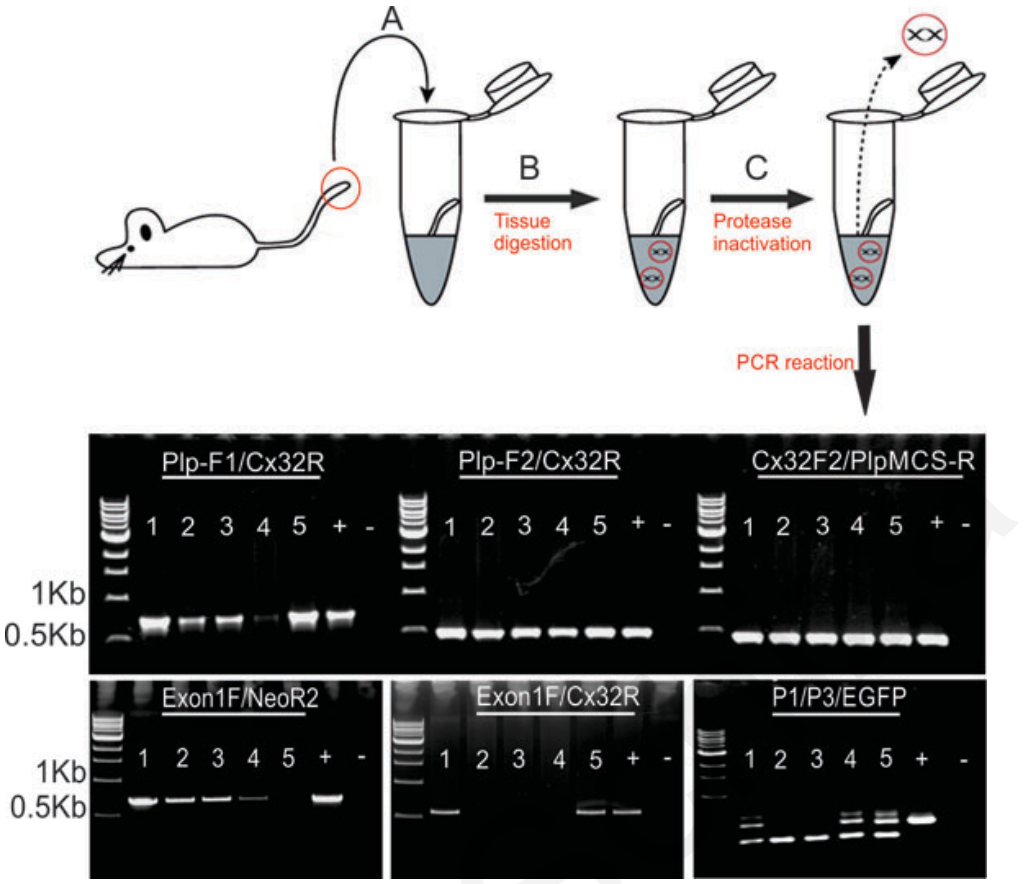

Figure 3.3: Genotyping of mice.
A small section of the mouse tail is cut (A) and incubated in lysis buffer and proteinase K at 55°C overnight (B). The proteinase K is then heat inactivated at 85°C for 45min (C). The DNA was PCR screened for the transgene using three pairs of primers (PlpF1/Cx32R, PlpF2/Cx32R and Cx32F2/PlpMCS). Positive bands in lanes 1-5 indicate the presence of the transgene in the mouse genome. PCR screening for Cx32 allele: Exon1F/NeoR2 primer set was used to detect the Cx32KO allele (Gjb1 ORF replaced by neomycin gene in Cx32KO mice) and Exon1F/Cx32R was used to detect the WT Gjb1 allele. For Cx47 allele a multiplex PCR was used P1 (Cx47 intron specific), P3 (Cx47 exon specific) and P4/EGFP (Gjc2 ORF replaced by EGFP gene in Cx47 KO mice). Mouse 1 is transgenic heterozygous for Cx32 and heterozygous for Cx47 (TG^+ X^+X^- Cx47Het); mouse 2 is transgenic Cx32/Cx47 double KO (dKO) same as mouse 3; mouse 4 is TG^+Cx32KO Cx47Het and mouse 5 is TG^+Cx32WTCx47Het.

3.3 Confirm the presence and correct localisation of hCx32 in oligodendrocytes in TG^{+}Cx32KO mice

3.3.1 Expression of transgenic and endogenous Cx32 mRNA

Here we validated if the cloned hCx32 was expressed at the correct localization in oligodendrocytes in the CNS and Schwann cells in the PNS and if the levels of expression are high enough to rescue the peripheral neuropathy of Cx32 deficient mice. In order to confirm this we used three different methods. We first checked if any hCx32 RNA is expressed in the tissues, we then examined the protein levels by Western Blotting, and finally we analyzed by immunohistochemistry the expression and localisation of hCx32 protein.

Levels of exogenous hCx32 from brain and spinal cord tissues of TG^{+}Cx32KO were compared to the endogenous expression levels in WT mice at 1 month of age. RNA was successfully isolated from the tissues and by Reverse Transcription (RT) PCR was converted to cDNA which was then amplified using specific primers (see M&M) that are identical in both human and mouse Cx32. The PCR product resulted in a 553bp product. The product was then digested using restriction enzymes specific for the human, MscI (M) or the mouse, HhaI (H) Cx32. Digest was run on 1.5% agarose gel. After digesting with MscI the TG^{+}Cx32KO tissues resulted in two separate fragments at 280 and 273bp, whereas in digestion with HhaI enzyme the original PCR product (553bp) remained uncut. In the WT tissues, HhaI uniquely cuts the mouse Cx32 cDNA into two fragments at 230 and 323bp whereas when digesting with MscI remained uncut. This indicated that hCx32 was present in brain and spinal cord tissues from the transgenic mice and also showed two to three-fold higher levels of hCx32 mRNA than of mouse Cx32 in the WT tissues (***Fig.3.4***). TG^{+}Cx32KO transgenic lines, Plp-1 and Plp-3 showed similar expression at the RNA level (data not shown).

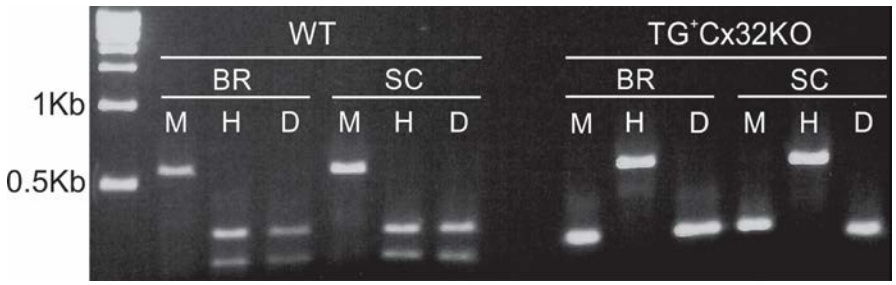

Figure 3.4: Analysis of mouse and human Cx32 transcripts.
RT-PCR and digestion by MscI (M; cuts the human Cx32 cDNA) or HhaI (H; cuts the mouse Cx32 cDNA), or with both (D; "double-cut" with MscI and HhaI) shows that M-digested human Cx32 and cDNA is detected only in transgenic but not in WT tissues (BR: brain; SC: spinal cord), whereas the H-digested mouse Cx32 cDNA is present only in the WT mouse.

3.3.2 Expression levels of the transgenic hCx32 protein by immunoblotting analysis

Since hCx32 mRNA was present in the transgenic brain and spinal cord tissues at higher levels than the WT we further wanted to check the protein levels. To determine this we obtained sacrificed brain (BR), brain stem cerebellum (BSC), spinal cord (SC) and liver (LV) tissues from 1-month old WT, TG^+Cx32KO and Cx32KO mice for comparison. Immunoblot analysis was performed using Cx32 antibody. Accordingly, immunoblot results showed a positive Cx32 band in all TG^+ and WT tissue lysates. Cx32 was absent from Cx32KO lysates, as expected. The levels of Cx32 protein in TG^+Cx32KO spinal cord were much higher compared to WT spinal cord (***Fig.3.5 A***). Liver tissue is rich in Cx32 protein; it was used to confirm that our transgenic line is on a Cx32KO background. Thus, the WT liver revealed very high levels of Cx32, whereas the liver from the TG^+ and the Cx32KO SC did not contain any Cx32 specific band. To show that these results are not due to unequal loading of the samples; we further blotted the membrane with GAPDH and used it as a loading control (***Fig.3.5 B***). Similar levels of Cx32 expression were detected by immunoblot also in tissue lysates from CNS areas of Plp-1 line (data not shown).

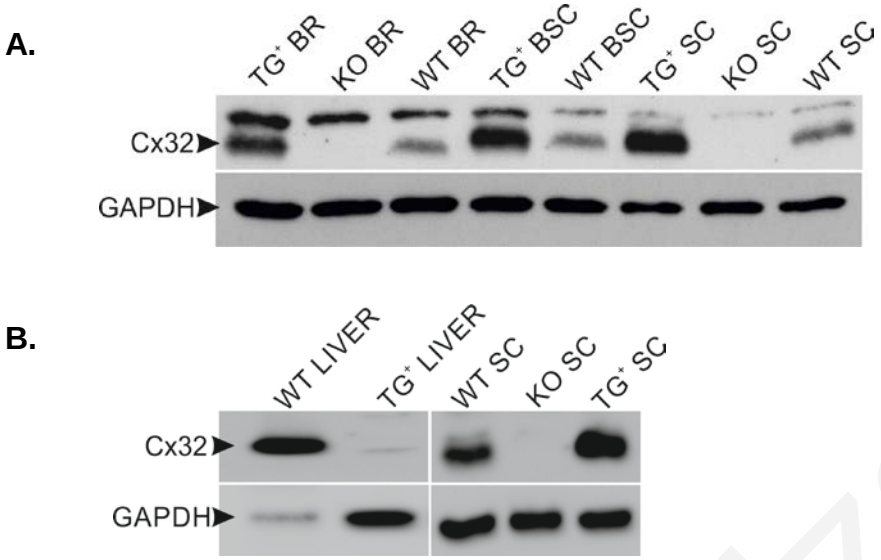

Figure 3.5: Immunoblot analysis of Cx32 expression.
A-B Immunoblot of brain (BR), brain stem cerebellum (BSC) and spinal cord (SC) lysates from transgenic line Plp-3 as well as WT and Cx32KO mice as indicated. The blot was incubated with RbCx32/918 antibody and then with GAPDH to demonstrate the loading. Cx32 protein was present in all transgenic and WT tissues. The levels of Cx32 in the transgenic tissues were much higher than the WT. In Cx32KO mice tissues the band is absent. Cx32 was also detected in the WT liver and absent from TG^+ (B).

3.3.3 Localisation of hCx32 in the CNS

To assess the correct localisation and expression levels of the transgene in TG^+Cx32KO oligodendrocytes, we immunostained different CNS areas including the spinal cord, cerebellum and cerebrum with Cx32 antibody combined with oligodendrocyte marker, CC-1, always in comparison with tissues from Cx32KO mice (negative control) and with WT mice (positive control). In the WT spinal cord Cx32 was localized mainly along large myelinated fibers while in the gray matter Cx32 formed GJ-like plaques only around oligodendrocyte cell bodies. In contrast, in TG^+Cx32KO mice Cx32 was expressed around oligodendrocyte cell bodies not only in the gray but also in the white matter, in addition to myelinated fibers (***Fig.3.6 A-C***). In the cerebrum at the level of the hippocampus Cx32 was localized in deep neocortex of WT mice along the myelinated fibers, adjacent but not within the corpus callosum (CC), whereas in the TG^+Cx32KO mice Cx32 was localized additionally in CC along small diameter fibers and around oligodendrocyte cell bodies (***Fig.3.6 D-F***). In the cerebellum of WT mice Cx32 was mainly expressed in white matter fibers, while TG^+Cx32KO mice also showed Cx32 immunoreactivity in the granule cell layer (***Fig.3.6 G-I***). No specific Cx32 staining was detected in any

Cx32KO tissues (***Fig.3.6 A, D, G***). We also stained same CNS areas for Plp-1 line and showed similar results (data not shown). Thus, overall it appears that transgenically expressed Cx32 was present in all subsets of oligodendrocytes, consistent with the expression pattern of the Plp promoter, in contrast to restricted expression in certain subpopulations of oligodendrocytes under normal conditions in WT mice.

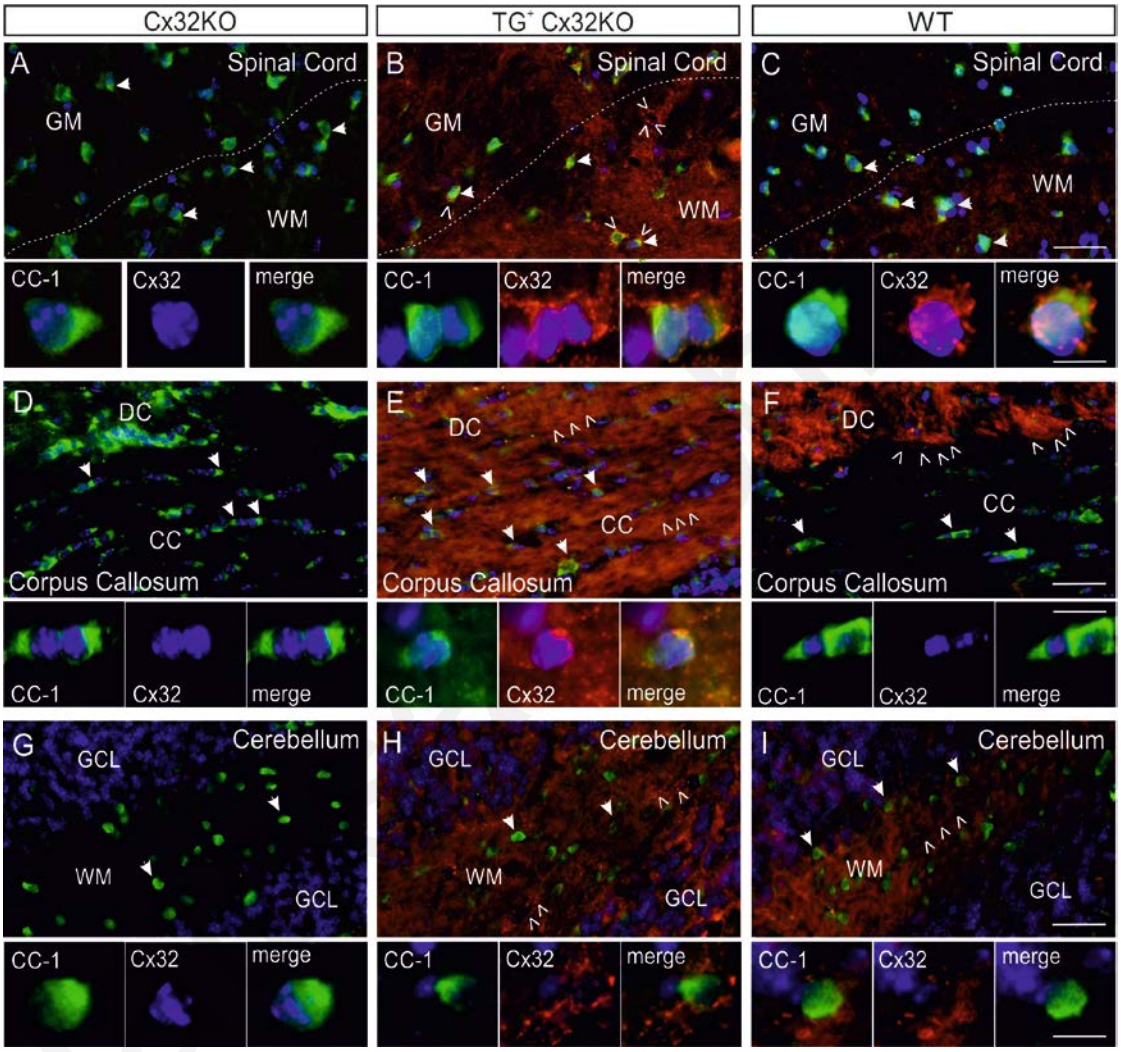

Figure 3.6: Transgenic expression of hCx32 in Cx32KO oligodendrocytes.
These are images of spinal cord (A–C), cerebrum (D–F) and cerebellar cortex (G–I) sections from 1-month-old WT, Cx32KO and TG$^+$Cx32KO mice as indicated double labelled with Cx32 (red) and oligodendrocyte marker CC-1 (A–I). Cell nuclei are stained with DAPI (blue). Cx32 is absent from all Cx32KO tissues (A, D, G) while it is expressed in the spinal cord of WT (C) and TG$^+$Cx32KO (B) mice. Cx32 forms GJ-like plaques (open arrowheads) along white matter fibers and around gray matter oligodendrocyte cell bodies (arrowheads) in the WT (C), while stronger expression also around white matter oligodendrocytes is seen in the TG$^+$Cx32KO. In the cerebrum WT mice show Cx32 expression in deep neocortex (DC) fibers but not in the corpus callosum (CC) (F), whereas TG$^+$Cx32KO mice (E) show Cx32 additionally within CC along fibers and around oligodendrocyte cell bodies. In the cerebellum of WT mice Cx32 is restricted to WM fibers (I) while in TG$^+$Cx32KO (H) it is also strongly expressed in granule cell layer (GCL) oligodendrocytes. Overview merged images and insets of separate channels are shown. Scale bars: 20 µm; in insets: 10 µm.

3.4 Presence of hCx32 in Schwann cells on Cx32KO mice

Although the Plp promoter was shown to drive restricted expression in oligodendrocytes in the CNS, we also examined the possibility of expression in the peripheral myelinating Schwann cells. We therefore immunostained sciatic nerve teased fibers of Cx32KO, TG$^+$Cx32KO and WT mice for comparison. Teased fibers were double labelled with Cx32 antibody and juxtaparanodal marker, Kv1.2. Surprisingly; Cx32 was expressed and normally localized at non-compact myelin areas in TG$^+$Cx32KO nerves similar to the positive control, WT nerve. Cx32 was absent from Cx32KO sciatic nerve fibers (***Fig.3.7 A-C***).

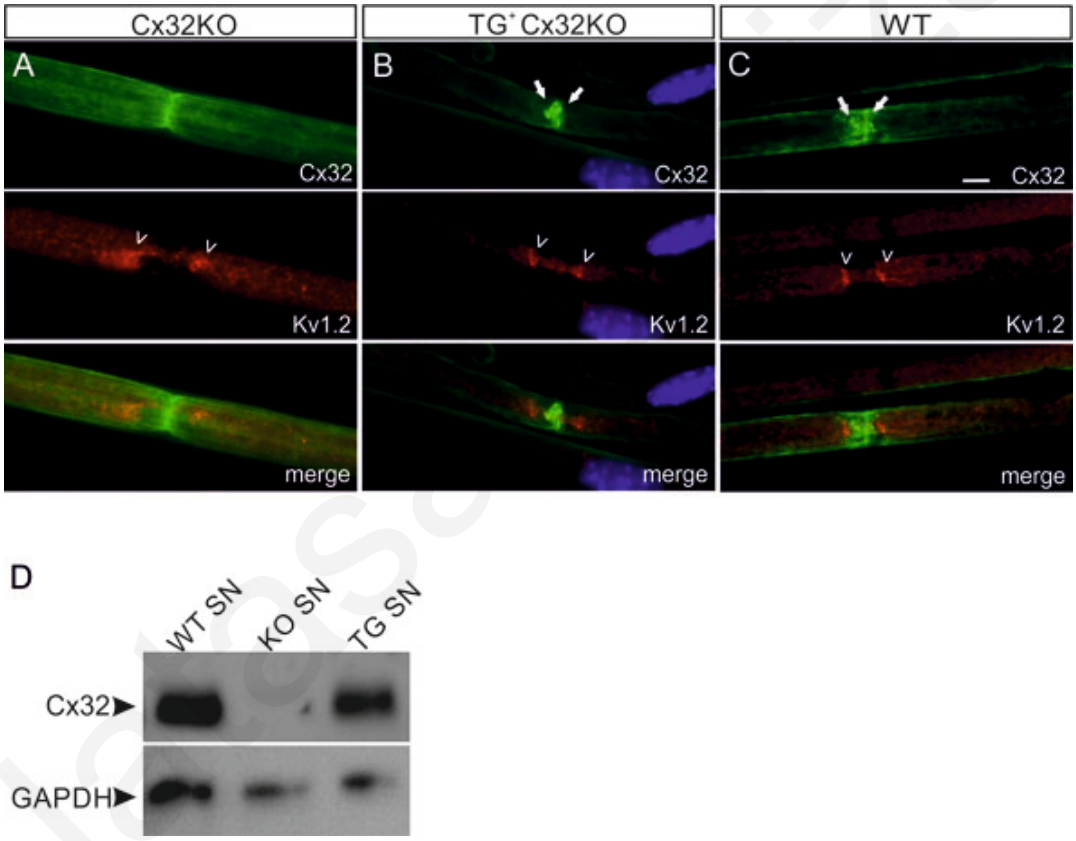

Figure 3.7: Transgenic Cx32 expression in Schwann cells in TG$^+$Cx32KO mice.
A-C: Sciatic nerve teased fibers double labeled with Cx32 and a juxtaparanodal marker, Kv1.2 (open arrowheads). Cx32 is present in non-compact myelin areas including paranodal loops (arrows) in TG$^+$Cx32KO (B) as in WT fibers (C) but is absent from Cx32KO fibers (A). Scale bars in A-C: 10 µm. D: Immunoblot analysis of Cx32 expression in sciatic nerve (SN) lysates from the transgenic line (TG$^+$Cx32KO) as well as WT and Cx32KO mice, as indicated. Cx32 band (arrowhead ~27kDa) is detected in the SN of the transgenic mouse, as well as in the WT tissue but not in Cx32KO. GAPDH blot is shown for loading control.

To further determine the expression levels of hCx32 in peripheral nerves of TG$^+$Cx32KO mice we examined by immunoblot sciatic nerve lysates from transgenic mice compared to WT nerves (***Fig.3.7 D***). The intensity of the bands was measured and quantified using Tina Scan software version 2.07d. This comparison showed that the amount of transgenically expressed Cx32 in TG$^+$Cx32KO sciatic nerves was increased by approximately 70% compared to the endogenous WT Cx32 levels.

3.5 hCx32 expression in Schwann cells rescues the peripheral neuropathy

To further verify that hCx32 expression in Cx32KO Schwann cells can rescue the development of peripheral neuropathy starting after 3 month of age (Anzini et al., 1997, Scherer et al., 1998), we examined semithin sciatic nerve sections from groups of 8-month-old TG$^+$Cx32KO and Cx32KO mice (n=4 per genotype). Morphometric analysis was performed on abnormally myelinated fibers as previously described (Sargiannidou et al., 2009a). TG$^+$Cx32KO mice showed significantly lower rates of abnormally myelinated fibers compared to Cx32KO littermates (p=0.0023), confirming that Plp promoter-driven Cx32 expression can rescue the peripheral neuropathy in Cx32KO mice (***Fig.3.8 A-C***) as was shown previously with P0 promoter-driven expression (Scherer et al., 2005). These results show that the 11Kb Plp promoter efficiently drives expression of hCx32 in all oligodendrocytes, even in subpopulations normally not expressing Cx32 (Kleopa et al., 2004), and interestingly, also in myelinated Schwann cells of TG$^+$Cx32KO mice.

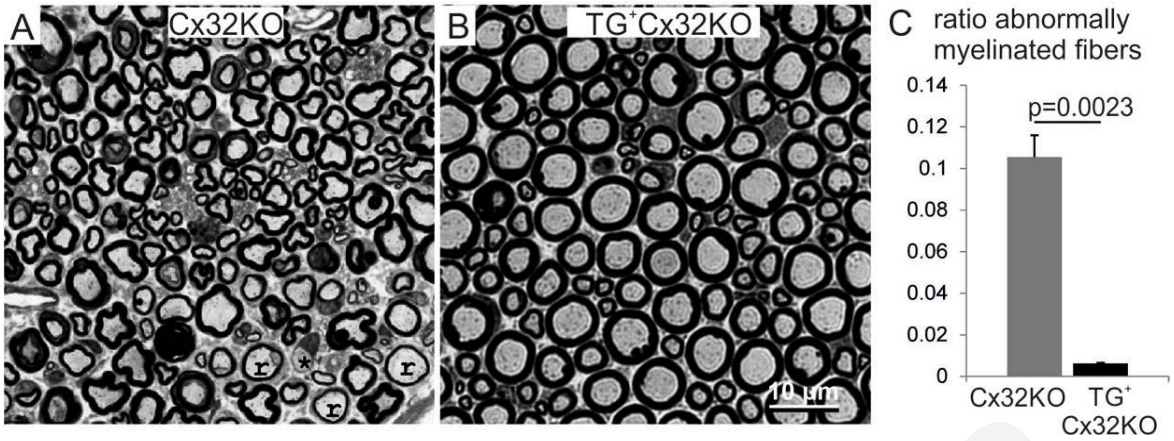

Figure 3.8: Rescue of the peripheral neuropathy in TG$^+$Cx32KO mice at the age of 8 months.
A-B: Representative semithin sections from mid- sciatic nerves of 8-month-old mice. In Cx32KO nerve (A) many axons appear to be thinly myelinated indicating previous demyelination and remyelination (r) and some are completely demyelinated (asterisk), whereas in TG$^+$Cx32KO sciatic nerve (B) all axons appear normally myelinated. C: Counts of abnormally myelinated fibers from both genotypes (n=4 per genotype) shows a significant reduction in the ratio of abnormally myelinated sciatic nerve fibers TG$^+$Cx32KO compared to Cx32KO mice.

3.6 Transgenic Cx32 expression was restricted to oligodendrocytes

Transgenic hCx32 expression was previously shown with the above results to be correctly localised around oligodendrocytes cell bodies and large fibers as well as in non-compact myelin areas of myelinated fibers in the periphery. Given the immunostaining, immunoblot and RNA results we examined if this hCx32 expression was exclusively present in oligodendrocytes. We double labelled CNS sections by immunohistochemistry with different cell markers such as GFAP-positive astrocytes, NeuN-positive neurons and Iba1-positive microglial cells in combination with Cx32 antibodies. This analysis showed that transgenic Cx32 expression was restricted to oligodendrocytes and was not detected in other CNS cell types (***Fig.3.9***).

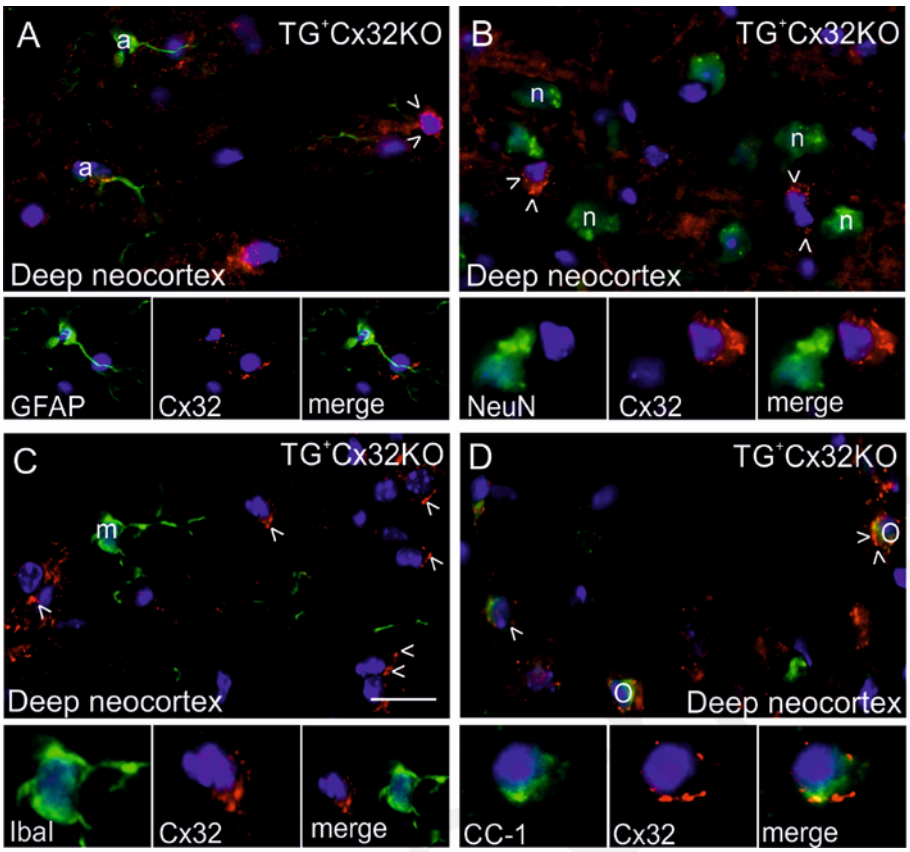

Figure 3.9: Transgenic Cx32 expression is restricted in oligodendrocytes.
Expression of Cx32 in TG$^+$Cx32KO CNS is not seen in GFAP positive astrocytes (a) (A), in NeuN positive neurons (n) (B) or in Iba-1 positive microglia (m) (C). Transgenic hCx32 forms gap junctions in CC-1 positive oligodendrocytes (D). Overview merged images and insets of separate channels are shown. Scale bars: 20 µm; in insets: 10 µm.

3.7 Generation of Cx32/Cx47dKO and TG$^+$Cx32/Cx47dKO

Given the above results we confirmed the presence and correct localisation of transgenically expressed Cx32 in the CNS and PNS. Both lines, Plp-1 and Plp-3, showed similar expression levels, therefore only one line, Plp-3, was expanded for further crossing into Cx47KO background. In order to obtain groups of double knock-out mice (Cx32/Cx47dKO) and transgenic double knock-out mice (TG$^+$Cx32/Cx47dKO) TG$^+$Cx32KO mice were crossed with Cx47KO mice obtaining initially TG$^+$Cx32KOCx47het mice and then by further breeding between offspring to obtain TG$^+$Cx32/Cx47dKO and Cx32/Cx47dKO mice. These two groups were used in the following experiments for comparison to test whether exogenous hCx32 can rescue the CNS (Menichella et al., 2003, Odermatt et al., 2003) and PNS phenotype in GJ deficient oligodendrocytes. The clinical phenotype, pathology and survival rates of Cx32/Cx47dKO littermates were

compared to those of the TG$^+$Cx32/Cx47dKO, as well as to Cx47KO from the same line and in some cases to WT mice during the 4th week of life.

To make sure that the TG$^+$Cx32/Cx47dKO mice we used do not form any Cx47 gap junctions and the rescue of the phenotype is due to the hCx32 we double labelled for oligodendrocyte marker (CC-1) and Cx47 antibody. The four genotypes, Cx47KO, Cx32/Cx47dKO, TG$^+$Cx32/Cx47dKO and WT were compared. Cx47 gap junctions were absent from all genotypes except the WT one, as expected (***Fig.3.10 A-C***). In the WT phenotype Cx47 formed gap junction plaques which showed co localisation with oligodendrocyte specific marker, CC-1 (***Fig.3.10 D***).

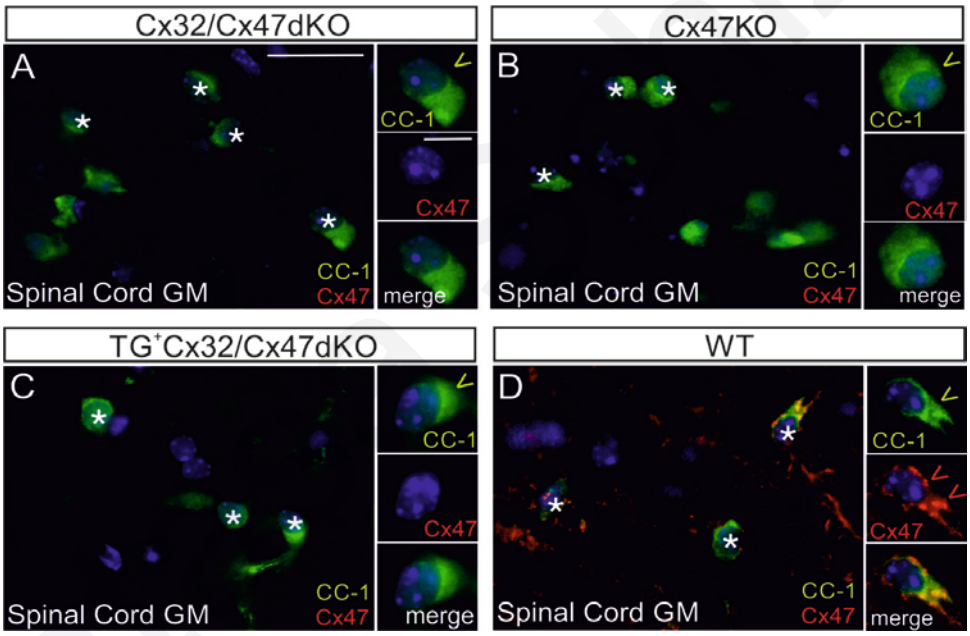

Figure 3.10: Confirm the absence of Cx47 expression in Cx47KO and double KO mice.
These are images of transverse sections from spinal cord from Cx47KO, Cx32/Cx47dKO, TG$^+$Cx32/Cx47dKO and WT mice. Sections were double labelled with Cx47 (red open arrowheads) and an oligodendrocyte marker, CC-1 (green open arrowheads). CC-1 is present in all mature oligodendrocytes (A-C). Cx47 forms gap junction plaques around oligodendrocytes (red) in the WT mouse (D). Scale bars: 20 µm; in insets: 10 µm.

We further confirmed the expression of hCx32 in TG$^+$Cx32/Cx47dKO as opposed to Cx32/Cx47dKO. Spinal cord lysates from all four genotypes, brain lysates from Cx32/Cx47dKO, TG$^+$Cx32/Cx47dKO and optic nerve lysates from Cx32/Cx47dKO, TG$^+$Cx32/Cx47dKO were used. Cx32 protein was present at

almost 3-fold levels (280%) compared to WT mice in the TG$^+$Cx32/Cx47dKO tissues and was absent from Cx32KO and Cx32/Cx47dKO tissues (***Fig.3.11***).

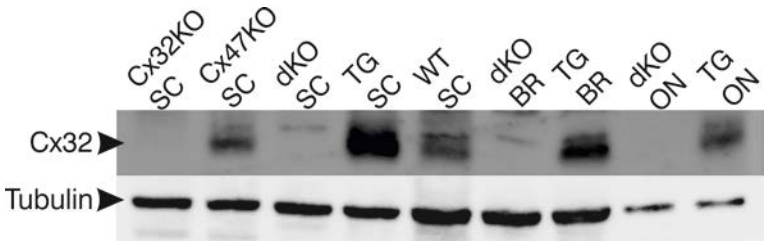

Figure 3.11: Transgenic Cx32 expression in Cx32/Cx47dKO mice.
Immunoblot analysis of CNS Cx32 expression in Cx32/Cx47dKO mice shows the absence in all Cx32KO and Cx32/Cx47dKO tissues and expression in TG$^+$Cx32/Cx47dKO at higher levels compared with the corresponding WT or Cx47KO tissues (ON: optic nerve).Tubulin blot is used for loading control.

3.8 Behavioural analysis of TG$^+$Cx32/Cx47dKO mice reveals rescue of the defects detected in Cx32/Cx47dKO mice

In this section our aim was to analyze the behavior of TG$^+$Cx32/Cx47dKO compared to the Cx32/Cx47dKO, WT and in some cases with Cx47KO. For the study of motor coordination and balance, mice were subjected to the foot print analysis, foot slip test and rotarod test.

3.8.1 Foot Print analysis

For this motor behaviour test mice paws were coloured with non-toxic ink. Forelimbs and hindlimbs were colored with different color ink: blue for the front and red for the hindlimbs and allowed to walk in the runway (***Fig.3.12 A***). Six mice (n=6) from each genotype were used for comparison. Two parameters were taken in consideration: a) the overlap width between the fore and hindlimbs in cm, and b) the stride length of right and left fore and hindlimbs. All parameters of foot print analysis, including stride length for all limbs and overlap width, were significantly improved in TG$^+$Cx32/Cx47dKO compared to Cx32/Cx47dKO mice, and reached similar levels as those of the WT animals (***Fig.3.12 B,C***).

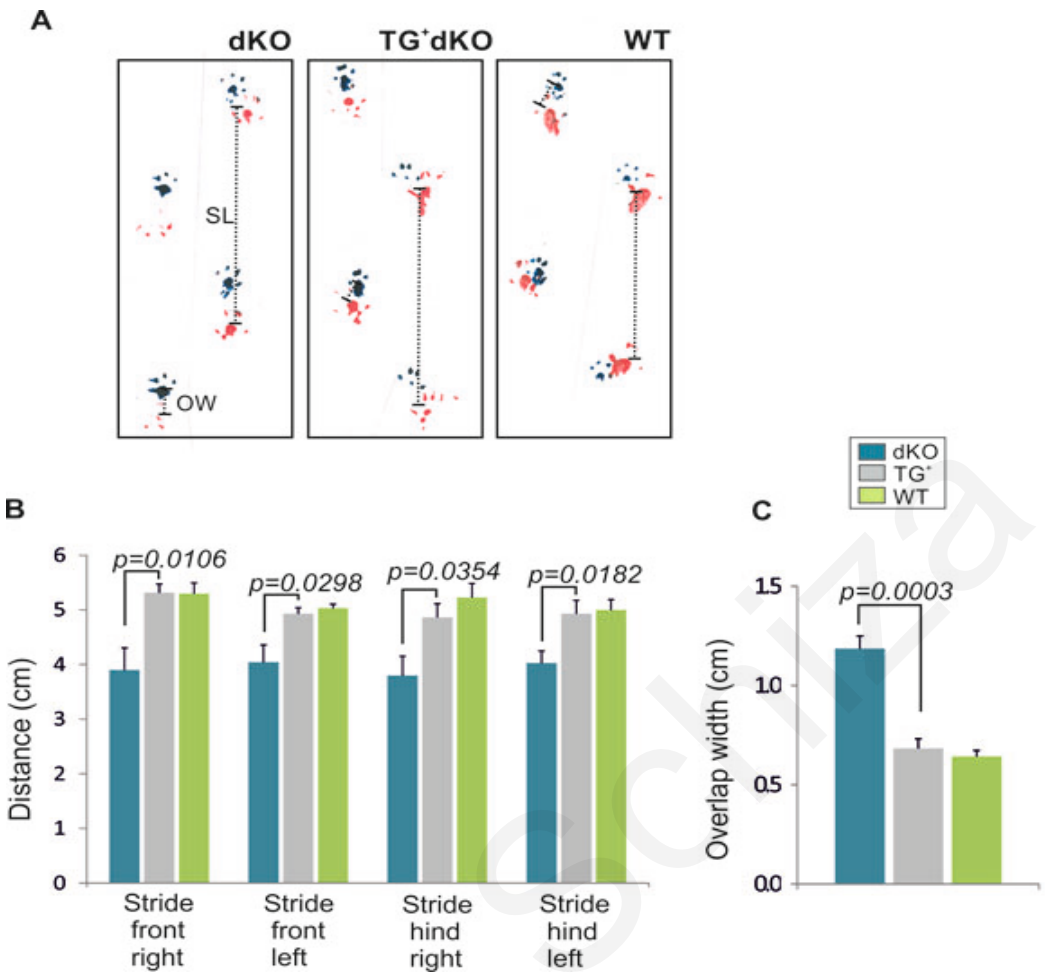

Figure 3.12: Foot Print Test analysis.
Results of behavioral analysis of Cx32/Cx47dKO phenotype compared with TG⁺Cx32/Cx47dKO, WT and Cx47KO mice. (A) Representative photographs of footprint analysis from Cx32/Cx47dKO (n = 6 mice in each genotype tested), TG⁺Cx32/Cx47dKO (n = 6) and WT (n = 4) animals, indicating the parameters measured: overlap width (OW) and stride length (SL) of left, right hind and forelimbs. (B-C) Bar graphs of the parameters considered above (in cm) indicating significant improvement to WT levels in transgenic compared to non-transgenic double KO mice.

3.8.2 Foot Slip analysis

Another way to test the motor behaviour of Cx32/Cx47dKO mice compared to TG⁺Cx32/Cx47dKO is the foot slip test modified by Britt (Britt et al., 2010). Mice were allowed to walk on a metal wire grid. If a hindlimb or forelimb falls from the grid prior to touching the floor is scored 1, if it touches the floor is scored 2. The first 50 steps were recorded. For this test we used eight mice (n=8) from each genotype Cx32/Cx47dKO, TG⁺Cx32/Cx47dKO, Cx47KO and WT were used for comparison. TG⁺Cx32/Cx47dKO mice had an average of 1±0.5 missteps whereas Cx32/Cx47dKO mice had an average of 9±1.8 missteps (p=0.0048), WT and Cx47KO mice had an average of 1±0.3 missteps (***Fig.3.13***). The improvement in

missteps of the TG+Cx32/Cx47dKO mice was significantly reduced compared to Cx32/Cx47dKO and similar to WT recordings.

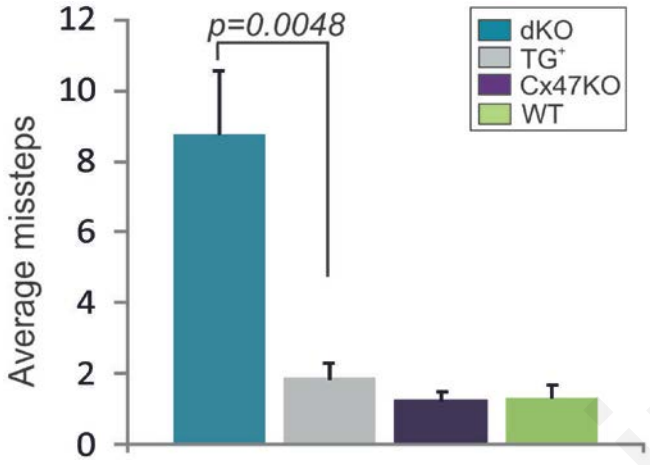

Figure 3.13: Foot Slip Analysis.
Performance in foot slip test shows significant improvement in TG+Cx32/Cx47dKO mice with reduced number of missteps compared to the Cx32/Cx47dKO reaching the level of the WT and Cx47KO mice.

3.8.3 Rotarod analysis

For rotarod analysis mice were trained to walk on motor-driven rotating spindle and the mean latency to fall off the spindle was recorded. For comparison we used nine mice (n=9) from each genotype Cx32/Cx47dKO, TG+Cx32/Cx47dKO, Cx47KO and WT. TG+Cx32/Cx47dKO showed significant improvement in time spent on the rotarod at different speeds compared to Cx32/Cx47dKO mice, although they did not reach the performance of WT and Cx47KO mice (***Fig.3.14***).

Taking into consideration all behavioural results, TG+Cx32/Cx47dKO mice outperformed Cx32/Cx47dKO animals in their ability for motor coordination and balance.

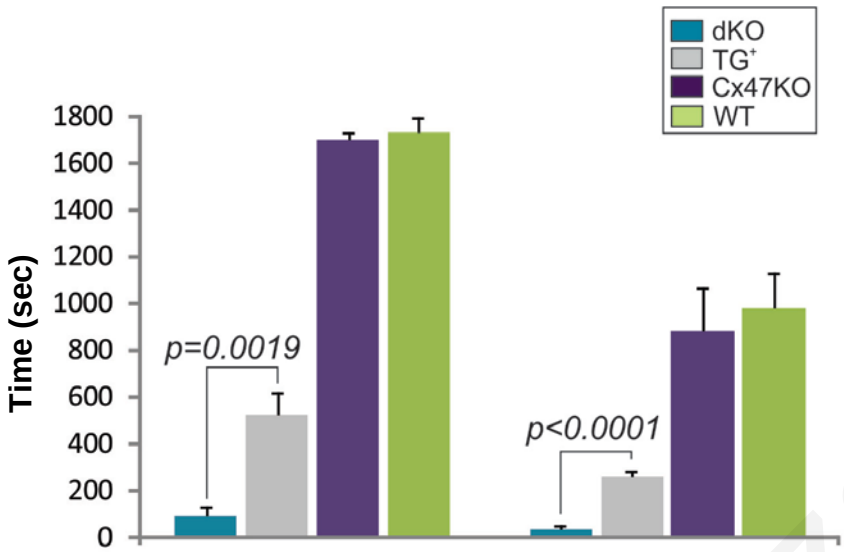

Figure 3.14: Rotarod analysis.
Results show that TG+Cx32/Cx47dKO mice performed significantly better than Cx32/Cx47dKO, although they did not reach the performance of WT and Cx47KO mice.

3.8.4 Survival Rate- Kaplan Meier

Kaplan Mayer analysis of the survival rates showed that Cx32/Cx47dKO mice (n=11) began to die from the 4th week of age and less than 20% survived beyond the 6th week, while all mice died by 12 weeks. In contrast, TG+Cx32KO/Cx47dKO mice (n=14) showed normal life span for up to 47 weeks of observation with only one mouse that died without previous signs of encephalopathy (p<0.0001) (***Fig.3.15***). Moreover, up until this age of 47 weeks TG+Cx32/Cx47dKO mice showed no evidence of tremor, seizures or other clinical symptoms that have been described to uniformly occur starting from 4-6 weeks of life in Cx32/Cx47dKO mice.

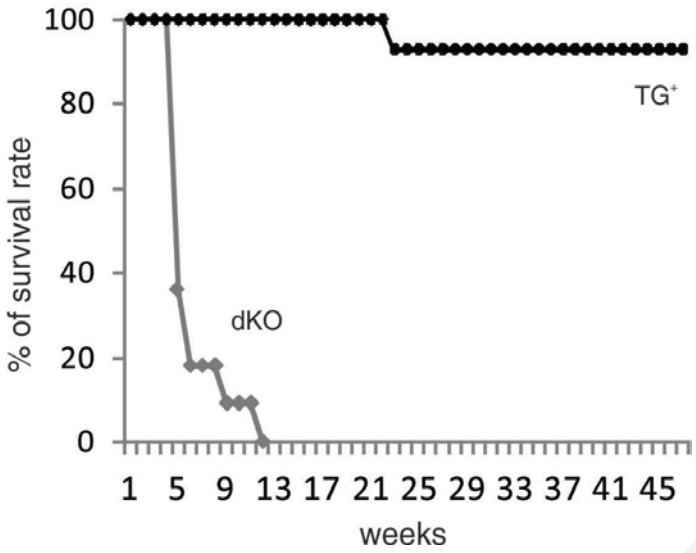

Figure 3.15: Kaplan–Meier curve.
Shows the survival rates of Cx32/Cx47dKO versus TG+Cx32/Cx47dKO mice, clearly documenting a rescue of the early mortality seen in the Cx32/Cx47dKO group. TG+Cx32/Cx47dKO show a normal life span.

In conclusion, all three behavioural tests and the survival analysis showed a clear phenotypic rescue of the motor deficits and long life span in TG+Cx32/Cx47dKO mice.

3.9 Inflammation and demyelination are prevented in the CNS of the TG+Cx32/Cx47dKO mice

We investigated whether the profound and early pathological changes developing in Cx32/Cx47dKO CNS (Menichella et al., 2003, Odermatt et al., 2003) could be prevented in TG+Cx32/Cx47dKO mice. In order to examine the degree of myelination and inflammation at one month of age we immunostained sections of the cerebrum, spinal cord and optic nerves from TG+Cx32/Cx47dKO and Cx32/Cx47dKO mice. Tissues were stained for myelin oligodendrocyte glycoprotein (MOG) and CD68, a macrophage marker and further with Cx32 protein and myelin basic protein (MBP). A great number of CD68 positive macrophages were detected in deep neocortex of the cerebrum as well as in the gray matter of the spinal cord and optic nerves of Cx32/Cx47dKO mice; in the transgenic mice no macrophages were present (***Fig.3.16 B,G,M***). Furthermore two myelin markers were used, MOG and MBP. Both showed reduced immunoreactivity in Cx32/Cx47dKO mice due to demyelination affecting thin and

large fibers whereas in TG+Cx32/Cx47dKO tissues myelination appeared normal (***Fig. 3.16 B,F,L,P***).

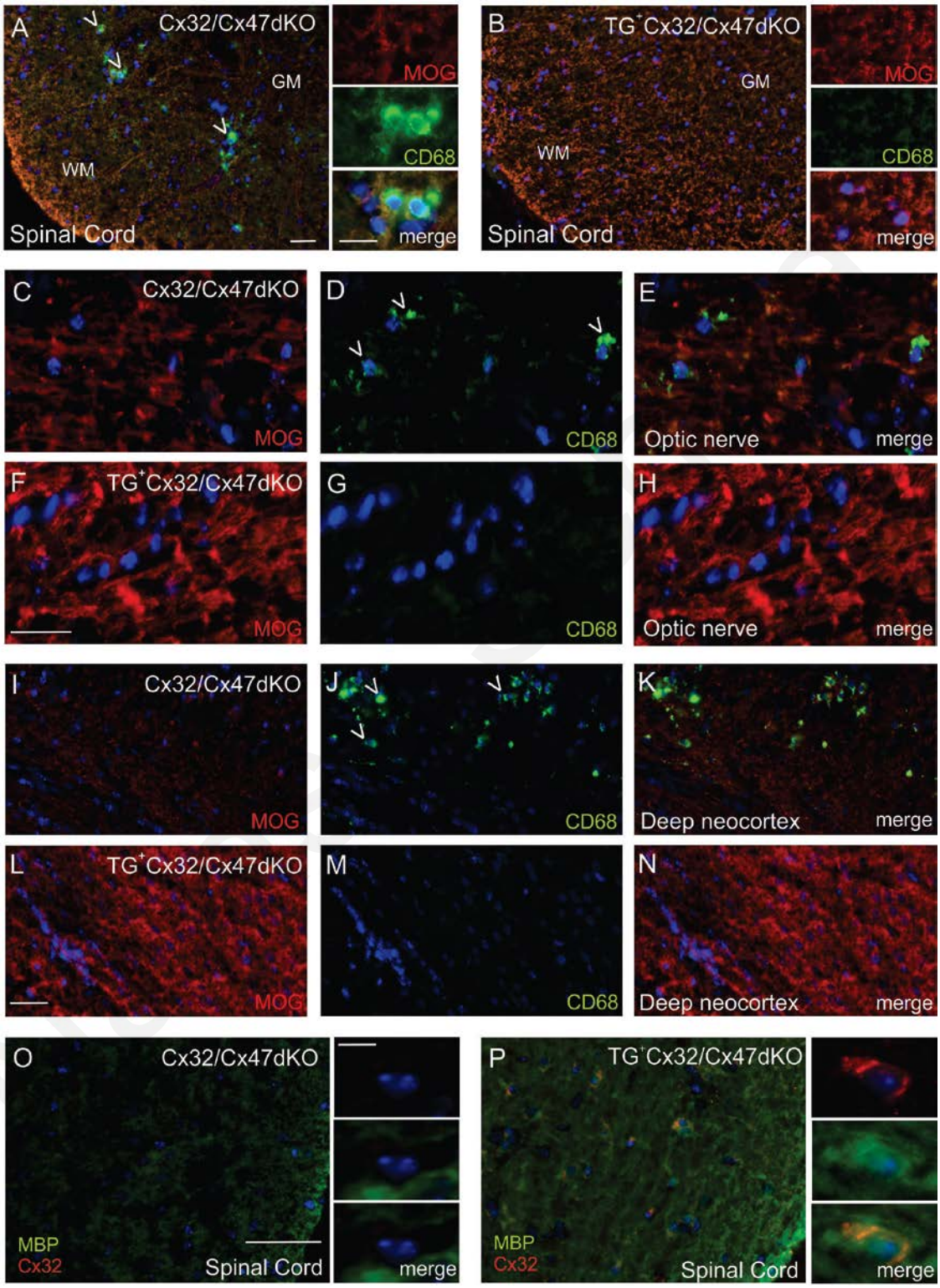

Figure 3.16: Rescue of demyelination in transgenic Cx32/Cx47dKO mice.
Spinal cord including white matter and gray matter (A-B), as well as optic nerve (C-H) and cerebrum (I-N) sections from Cx32/Cx47dKO and TG+Cx32/Cx47dKO mice as indicated double labeled for myelin oligodendrocyte protein (MOG, red) and macrophage marker (CD68, green) show improved myelin immunoreactivity and absence of macrophages

(arrowheads) in TG⁺Cx32/Cx47dKO as opposed to Cx32/Cx47dKO mice. (O-P) Longitudinal sections of the spinal cord double labelled with MBP (green) and Cx32 proteins (red). Scale bars: (A–B) 200 μm; (C–P) 20 μm; in insets: 10 μm.

In addition to the immunostaining results, we assessed the levels of myelin proteins by quantitative immunoblot analysis in spinal cord lysates from each group (n=3 per genotype) including myelin oligodendrocyte glycoprotein (MOG) and myelin basic protein (MBP). This analysis confirmed that both the MOG as well as the MBP levels were significantly higher in 1-month old TG⁺Cx32/Cx47dKO compared to Cx32/Cx47dKO littermates (*p=0.0140* and *p=0.0334*, respectively), in line with the immunostaining results (***Fig.3.17***).

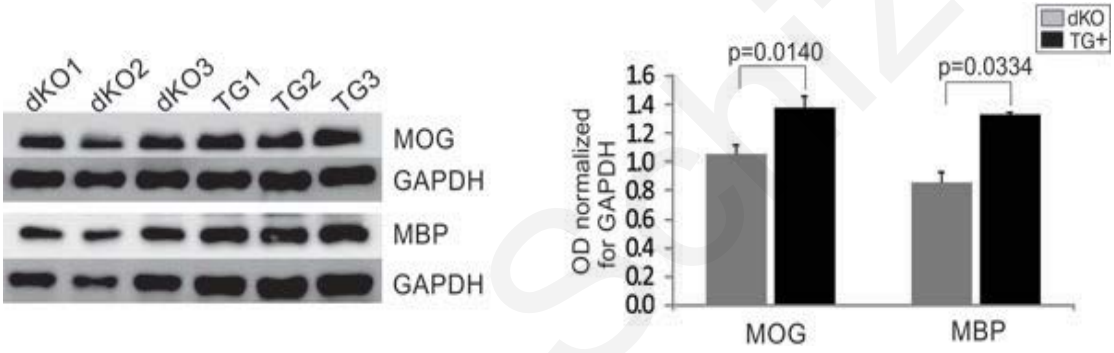

Figure 3.17: Improved myelin protein levels in TG⁺Cx32/Cx47dKO mice.
Quantitative immunoblot analysis of MBP and MOG in spinal cord lysates of Cx32/Cx47dKO (dKO) and TG⁺Cx32/Cx47dKO (TG⁺) mice (n = 3 per genotype) at 1 month of age shows that the levels of both myelin proteins normalized for loading are significantly increased in transgenic tissues. GAPDH blots are shown as loading control.

3.10 Transgenic expression of hCx32 CNS prevents astrogliosis and activated microglial cells

In order to investigate the degree of astrogliosis and inflammation in Cx32/Cx47dKO mice and whether it can be prevented in the transgenic mice we stained for astrocytes with glial fibrillary acidic protein (GFAP) and microglia with IbaI different CNS areas such as cerebrum, spinal cord and optic nerve. Immunohistochemistry results revealed increased activation of microglia in Cx32/Cx47dKO along with increased GFAP immunoreactivity indicating astrogliosis. These abnormalities were not seen in TG^{+}Cx32/Cx47dKO mice indicating a rescue of secondary inflammatory and astrogliotic changes in this leukodystrophy model. Similar rescue of inflammation and astrogliosis was seen in the other tissues including spinal cord and brain (***Fig.3.18 A-F***).

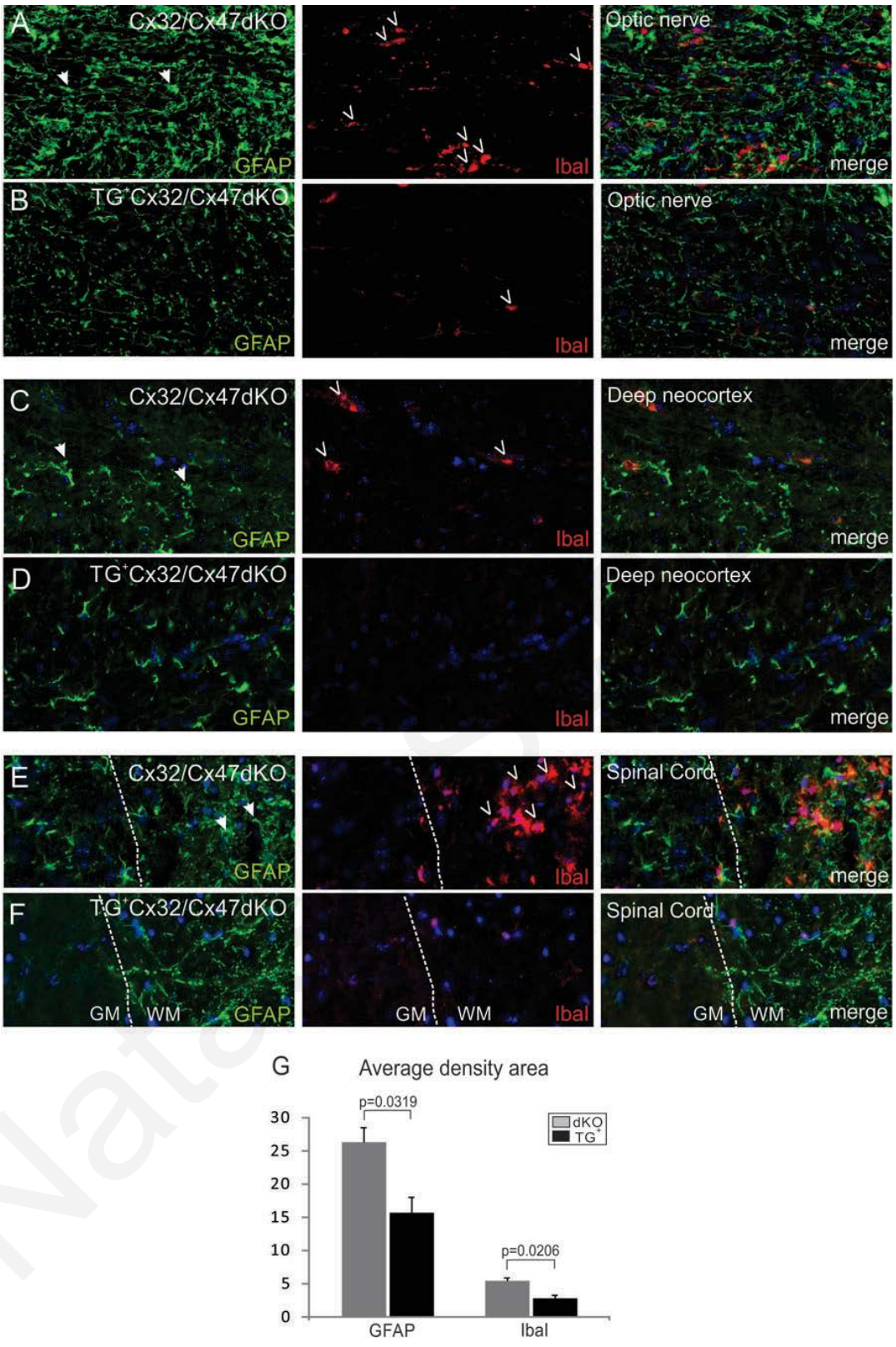

Figure 3.18: Rescue of inflammation and astrogliosis in TG⁺Cx32/Cx47dKO mice. Double labeling of optic nerve sections (A-B), cerebrum (C-D) and spinal cord (E-F) with astrocytic marker GFAP (green) and microglial marker Ibal (red), shows astrogliosis and microglial activation in the Cx32/Cx47dKO which are absent in the TG⁺Cx32/Cx47dKO. (G) The average area of immunoreactivity for GFAP and Ibal reflecting astrogliosis and microglial activation is significantly decreased in TG⁺Cx32/Cx47dKO.

To corroborate these findings we quantified the optic nerve area covered with IbaI as well as with GFAP immunoreactivity in each group (n=3 per genotype) using Image J software. This analysis confirmed that there was a significant decrease of microglia activation (*p=0.0206*) and astrogliosis (*p=0.0319*) in TG^{+}Cx32/Cx47dKO compared to Cx32/Cx47dKO mice (***Fig.3.18 G***).

3.11 Prevention of oligodendrocyte apoptosis in TG^{+}Cx32/Cx47dKO mice

The severe early pathological changes in the Cx32/Cx47dKO mice are known to be associated with oligodendrocyte apoptosis and eventual loss over time. To further investigate this issue, we stained cross sections of the spinal cord at 1-month of age from both groups for CC-1, and counted mature oligodendrocytes. This analysis showed that the total oligodendrocyte numbers were not significantly different among the two groups at the age of 1 month (***Fig.3.19 A,B,*****E**).

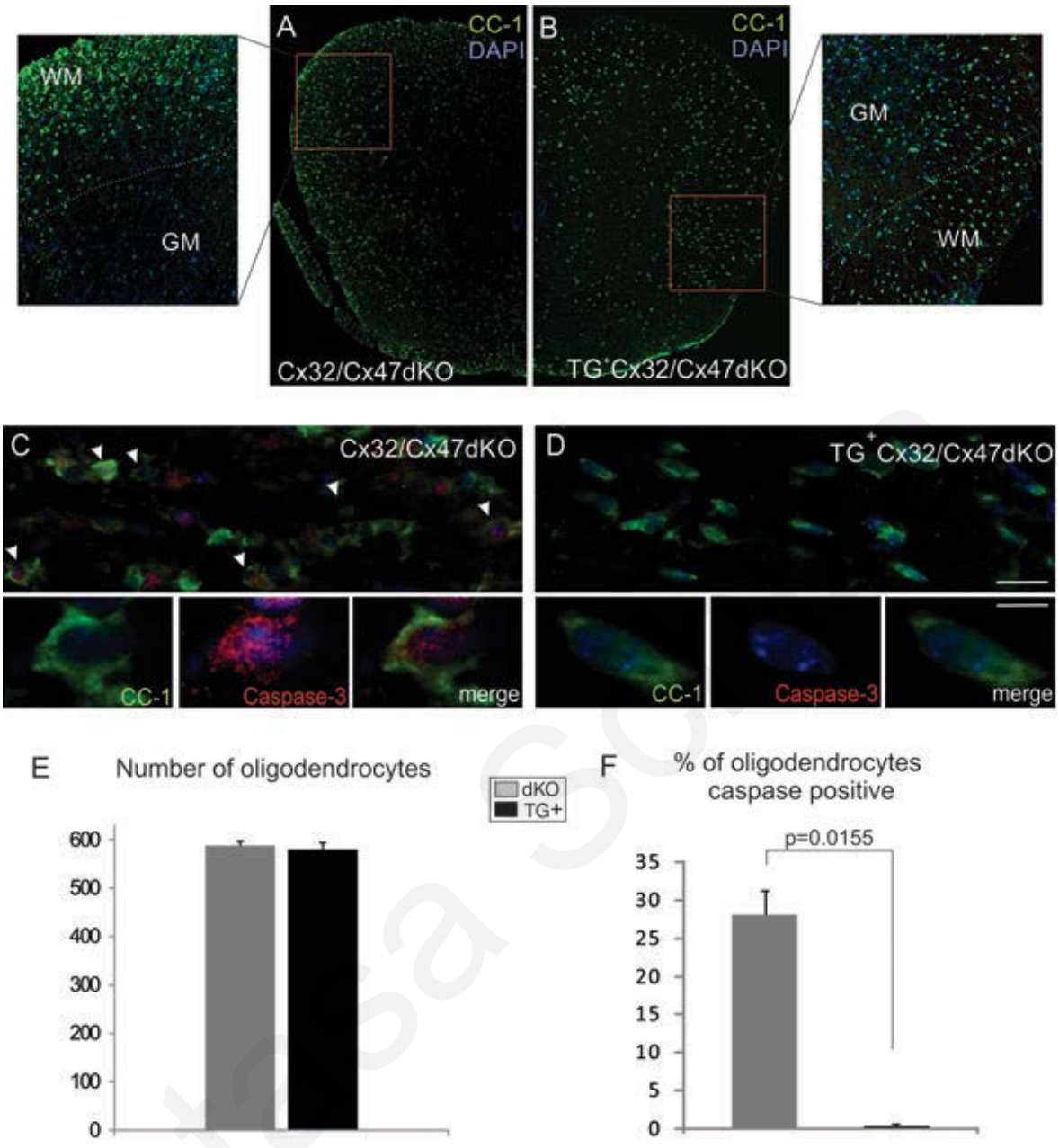

Figure 3.19: Rescue of oligodendrocyte apoptosis in TG$^+$Cx32/Cx47dKO mice.
(A-B) Overview of spinal cord transverse sections at low magnification labeled with oligodendrocyte marker CC-1 (green). Nuclei are stained with DAPI (blue). Oligodendrocytes were counted in white matter (WM) and gray matter (GM) areas, no significant difference between the two groups (E).
(C-D) Optic nerve sections double labeled with apoptosis marker caspase-3 and oligodendrocyte marker CC-1 confirms that many oligodendrocytes undergo apoptosis in Cx32/Cx47dKO (arrowheads) but none in TG$^+$Cx32/Cx47dKO. Nuclei are labeled with DAPI (blue). (F) Counts of caspase-3 positive apoptotic oligodendrocytes are significantly reduced in TG$^+$Cx32/Cx47dKO compared with Cx32/Cx47dKO.

To test the possibility that oligodendrocytes in the Cx32/Cx47dKO mice might undergo apoptosis, immunohistochemistry was performed. We double labelled spinal cord and optic nerve sections for oligodendrocytes with CC1 and caspase-3, an apoptotic marker (***Fig.3.19 C,D***). Many CC1-positive oligodendrocytes in Cx32/Cx47dKO optic nerve and spinal cord were also positive for the apoptotic marker suggesting beginning apoptosis, whereas TG$^+$Cx32/Cx47dKO oligodendrocytes showed no caspase-3 immunoreactivity. Counts of caspase-3 immunoreactive optic nerve oligodendrocytes were on average 27% in the Cx32/Cx47dKO group, and less than 1% in TG$^+$Cx32/Cx47dKO, confirming that hCx32 expression also prevented oligodendrocyte apoptosis (***Fig.3.19 F***).

3.12 Improvement of CNS myelination in TG$^+$Cx32/Cx47dKO mice

To further confirm the immunostaining results suggesting improved CNS myelination in TG$^+$Cx32/Cx47dKO mice, we examined spinal cord and optic nerve semithin and ultrathin sections from groups of one-month old Cx32/Cx47dKO and TG$^+$Cx32/Cx47dKO mice. Overviews of toluidine blue stained spinal cord and optic nerve transverse sections revealed reduced myelin staining with loss of white-gray matter contrast in the spinal cord and numerous large vacuoles in Cx32/Cx47dKO tissues, while TG$^+$Cx32/Cx47dKO showed normal appearance (***Fig.3.20 A-G***).

In higher magnification semithin and electron microscopy images of anterior and posterior funiculi of the spinal cord from Cx32/Cx47dKO mice the majority of large axons showed enlarged extracellular spaces separating the myelin sheath from the axon. Some were thinly myelinated and most of them completely demyelinated. Similar findings were present in the optic nerve with vacuolization and demyelination of most axons. These pathological changes were absent in TG$^+$Cx32/Cx47dKO spinal cord or optic nerve (***Fig.3.21 A-F***). Quantification of myelin volume density in the anterior and posterior spinal cord funiculi as well as in the optic nerve in groups of one-month-old mice confirmed that myelin density was significantly increased (*p=0.0078, 0.0101, and 0.0032* respectively) in TG$^+$Cx32/Cx47dKO mice compared to the Cx32/Cx47dKO mice in all areas examined (***Fig.3.21 G***).

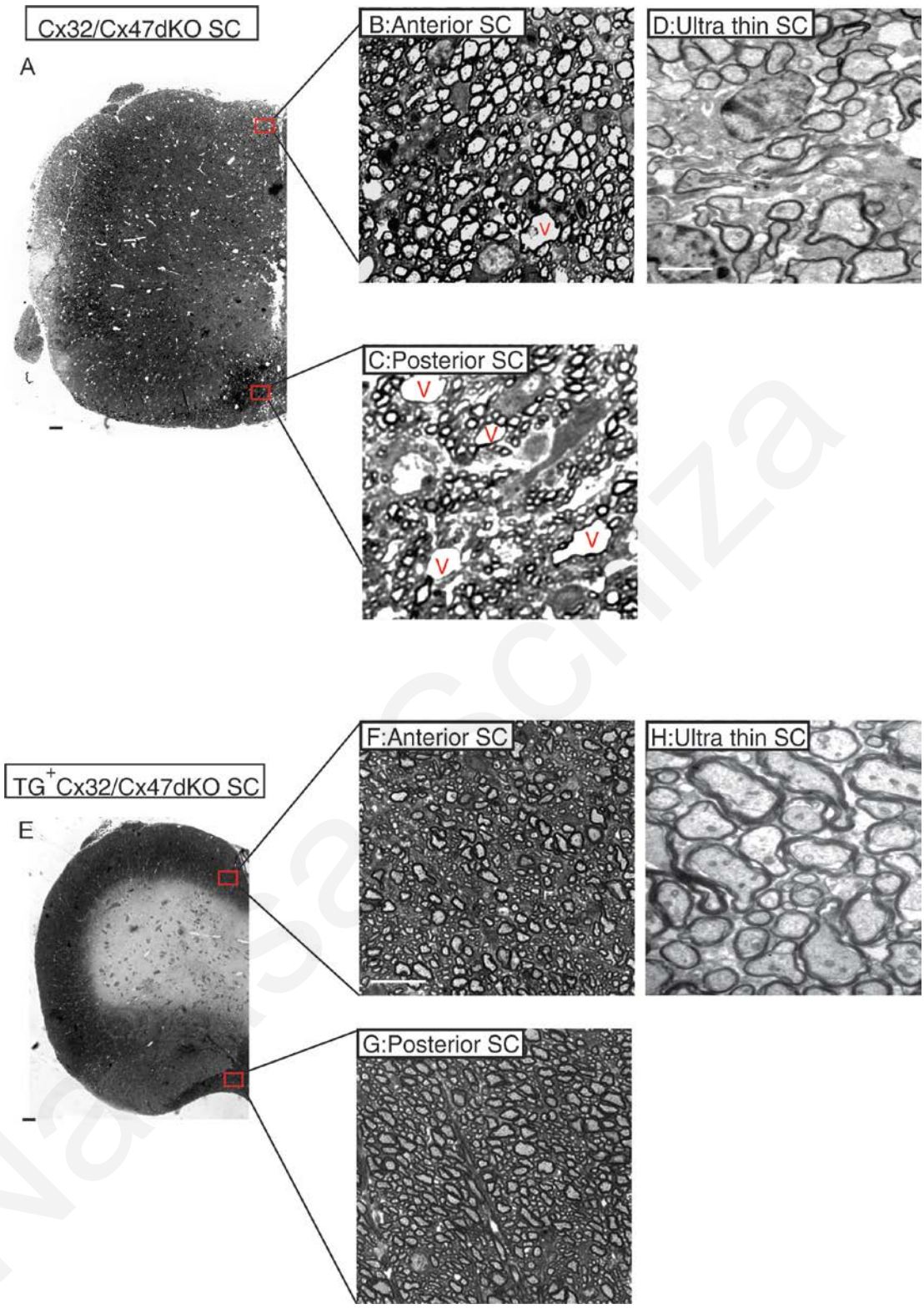

Figure 3.20: Prevention of severe spinal cord demyelination in TG$^+$Cx32/Cx47dKO mice.
Photomicrographs of semithin (A–G) and ultrathin (D-H) sections from spinal cord from 1-month-old mice. Overview of transverse sections from Cx32/Cx47dKO and TG$^+$Cx32/Cx47dKO spinal cords (A and E), as indicated as well as higher magnification images of Cx32/Cx47dKO anterior and posterior spinal cord (A, B and C) reveal that many axons appear thinly myelinated and some demyelinated with extensive vacuolation (V) whereas in TG$^+$Cx32/Cx47dKO mice (E, F and G) axons appear normally myelinated. Scale bars: (A and E) 200 µm; (B-C, F-G) 10 µm; (M and N) 2.5 µm.

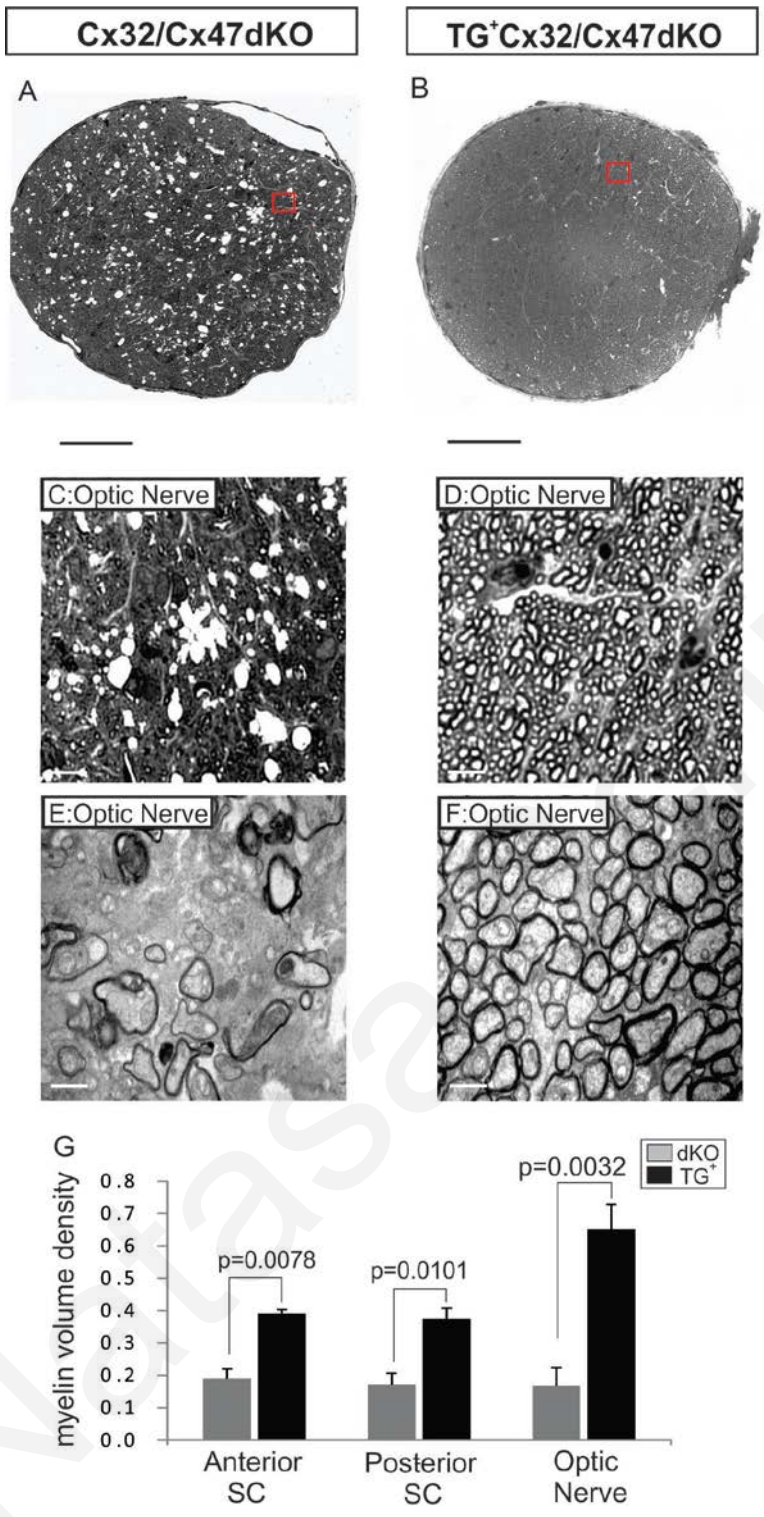

Figure 3.21: Prevention of severe optic nerve demyelination in TG⁺Cx32/Cx47dKO mice.

A marked loss of myelinated axons and vacuole formation in the myelin sheaths are noticed in Cx32/Cx47dKO optic nerves whereas in TG⁺Cx32/Cx47dKO most optic nerve axons are normally myelinated (A-F) Scale bars: (A-B) 10 µm; (C-F) 2 µm (G) Myelin volume density measured in semithin sections from anterior and posterior spinal cord funiculus as well as optic nerves (n = 4 mice in each group) reveals that myelin density is significantly increased in TG⁺Cx32/Cx47dKO compared with Cx32/Cx47dKO in both spinal cord and optic nerve.

3.13 Gap junction formation in oligodendrocytes of TG$^+$Cx32/Cx47dKO mice

To determine whether the transgenic expression of hCx32 was sufficient to allow the re-establishment of oligodendrocyte GJ connectivity in TG$^+$Cx32/Cx47dKO mice, including O/O, O/A and intra-myelin GJs, we double labelled for Cx32 and all other major astrocyte and oligodendrocyte connexins including Cx30, Cx43 and Cx29, comparing TG$^+$Cx32/Cx47dKO to Cx32/Cx47dKO and Cx47KO mice. The latter should have comparable GJ connectivity to the TG$^+$ since they endogenously express Cx32 but not Cx47 in oligodendrocytes. In all TG$^+$Cx32/Cx47dKO CNS regions examined including the spinal cord, cerebrum and cerebellum, Cx32 showed the same localization in cell bodies and along myelinated fibers in all subpopulations of oligodendrocytes as in TG$^+$Cx32KO CNS (***Fig.3.6***).

Double staining of Cx32 with astrocytic Cx30, known to partner with Cx32 (Orthmann-Murphy et al., 2007b) showed that Cx30 was diffusely expressed mostly in the gray matter forming GJ-like plaques, which colocalized with Cx32 GJ plaques around oligodendrocytes in TG$^+$Cx32/Cx47dKO similar to Cx47KO mice. In contrast, Cx30 showed no colocalization with oligodendrocytes in Cx32/Cx47dKO mice in which Cx32 was absent (***Fig.3.22 A-C***). Double staining with Cx43 showed the typical expression of Cx43 forming diffuse GJ plaques in gray matter with weak colocalization with Cx32 GJ plaques around oligodendrocytes in TG$^+$Cx32/Cx47dKO and even less in Cx47KO mice. Cx32/Cx47dKO mice showed stronger Cx43 immunoreactivity in gray matter areas, likely reflecting astrogliosis, with absence of Cx32 (***Fig.3.22 D-F***). Cx29 was normally localized along thinly myelinated fibers in the spinal cord gray matter, in the cerebellum and in the cerebrum in all three genotypes without apparent differences. Cx32 was expressed along medium and large myelinated fibers mostly without colocalization with Cx29 in TG$^+$Cx32/Cx47dKO and Cx47KO mice, while it was absent in Cx32/Cx47dKO (***Fig.3.22 G-I***).

Counts of GJ plaques surrounding oligodendrocytes in confocal images of spinal cord gray matter revealed similar numbers of Cx30 GJ plaques in all genotypes, while Cx32 GJ plaques were increased in TG$^+$Cx32/Cx47dKO compared to Cx47KO mice and showed higher overlap ratios with Cx30 GJ

plaques (***Fig.3.22 J***). Counts of Cx43 plaques were significantly increased in Cx32/Cx47dKO compared to TG^{+}Cx32/Cx47dKO or Cx47KO mice, likely reflecting astrogliosis. Also with this double labelling Cx32 GJ plaques showed higher counts in transgenic compared to Cx47KO mice, as well as increasing overlap with Cx43 (***Fig.3.22 K***). However, Cx32 GJ plaques around TG^{+}Cx32/Cx47dKO oligodendrocytes showed significantly lower overlap levels with Cx43 than with Cx30 ($p<0.0001$), indicating that transgenically expressed Cx32 forms O/A GJs mainly through coupling with Cx30.

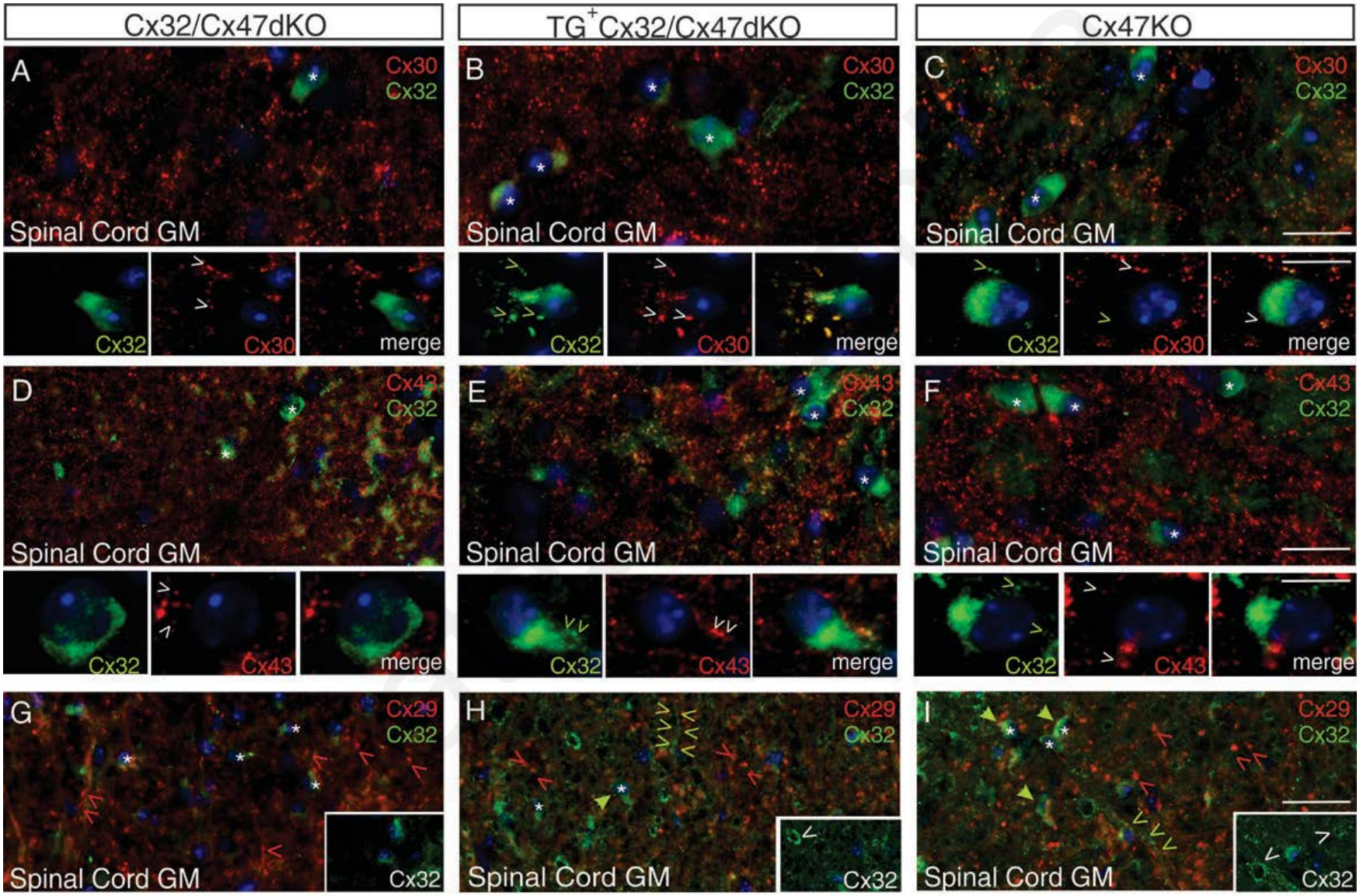
Cx32/Cx47dKO
TG+Cx32/Cx47dKO
Cx47KO
A
B
C
Cx30
Cx32
Spinal Cord GM
Cx32
Cx30
merge
D
E
F
Cx43
Cx32
Spinal Cord GM
Cx32
Cx43
merge
G
H
I
Cx29
Cx32
Spinal Cord GM
Cx32

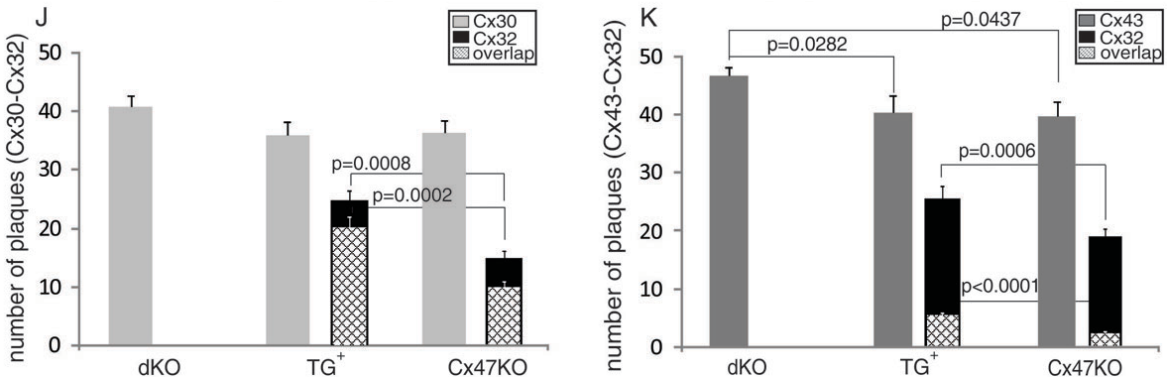

Figure 3.22: Gap junction formation by hCx32 in TG$^+$Cx32/Cx47dKO gray matter oligodendrocytes.
These are images of transverse sections from the indicated CNS gray matter (GM) regions of Cx32/Cx47dKO, TG$^+$Cx32/Cx47dKO and Cx47KO mice. Sections were double labeled with anti-Cx32 (green) and either anti-Cx30 (A–C), anti-Cx43 (D–F) or anti-Cx29 (G–I) antibodies (red). Cell nuclei are visualized with DAPI (blue). Note that due to the replacement of Cx47 ORF with EGFP in Cx47KO mice oligodendrocyte cell bodies are green fluorescent in all three genotypes (asterisks). (A–C) Cx30 forms GJ plaques (open arrowheads) diffusely in the gray matter in all genotypes, but shows colocalization with Cx32 GJ plaques around oligodendrocytes only in TG$^+$Cx32/Cx47dKO and Cx47KO mice indicating the formation of O/A channels, but not in Cx32/Cx47dKO mice in which Cx32 is absent. In TG$^+$Cx32/Cx47dKO and Cx47KO mice, Cx32 forms GJ plaques also along medium size myelinated fibers (green open arrowheads). (D–F) Cx43 forms diffusely GJ plaques that appear increased in Cx32/Cx47dKO in which Cx32 is absent, compared with TG$^+$Cx32/Cx47dKO and Cx47KO. Some Cx43 GJ plaques colocalize with Cx32 around oligodendrocytes in TG$^+$Cx32/Cx47dKO and Cx47KO mice but less than Cx30. (G–I) Cx29 shows expression along thin myelinated fibers in all three genotypes (red open arrowheads), while Cx32 is expressed along larger fibers (green open arrowheads) only in Cx47KO and TG$^+$Cx32/Cx47dKO mice without colocalization with Cx29. Scale bars, 20 μm; in insets, 10 μm. Counts of GJ plaques formed by Cx30 and Cx32 (J) or by Cx43 and Cx32 (K) around individual spinal cord GM oligodendrocytes show that Cx32 GJs are significantly increased in TG$^+$Cx32/Cx47dKO compared with Cx47KO mice and are absent from Cx32/Cx47dKO. Moreover, the percentage of Cx32 GJ plaques overlapping with Cx30 as well as with Cx43 is increased in TG$^+$Cx32/Cx47dKO compared with Cx47KO. Cx30 GJ plaque counts do not differ between genotypes, while Cx43 GJ plaque counts are significantly increased in Cx32/Cx47dKO mice.

Transgenic expression of Cx32 was also examined in different white matter (WM) areas of TG$^+$Cx32/Cx47dKO compared to Cx32/Cx47dKO and Cx47KO mice, including the spinal cord WM, cerebellum, optic nerve and cerebrum at the level of CC. In the spinal cord and cerebellar WM of TG$^+$Cx32/Cx47dKO and Cx47KO mice, Cx32 was expressed along large diameter myelinated fibers, but TG$^+$Cx32/Cx47dKO mice additionally showed Cx32 GJ plaques at oligodendrocyte cell bodies. Cx32 did not co-localize with Cx43 GJ plaques that were diffusely present in all WM areas (***Fig.3.23 A-C***). While Cx47KO mice showed the expected mutually exclusive expression of Cx29 along thin fibers and Cx32 along large fibers (Altevogt et al., 2002), in TG$^+$Cx32/Cx47dKO there was some expression of

Cx32 also along thin fibers colocalizing with Cx29 (***Fig.3.23 D-F***). Similar expression pattern was found in cerebellum, in which Cx32 formed GJ plaques in WM fibers in both Cx47KO and TG^+Cx32/Cx47dKO mice, but in addition there was expression along thin fibers of the molecular layer only in the TG^+ (***Fig.3.23 G-L***). In WM areas were Cx32 is not physiologically expressed, including the optic nerve and CC (Kleopa et al., 2004), Cx47KO showed no Cx32 expression, while TG^+Cx32/Cx47dKO showed Cx32 forming GJ plaques at oligodendrocyte cell bodies with partial colocalization with Cx43, as well as along thinly myelinated fibers colocalizing with Cx29. In Cx47KO and Cx32/Cx47dKO optic nerve and CC Cx32 was absent (***Fig.3.23 M-R,*** *and data not shown*).

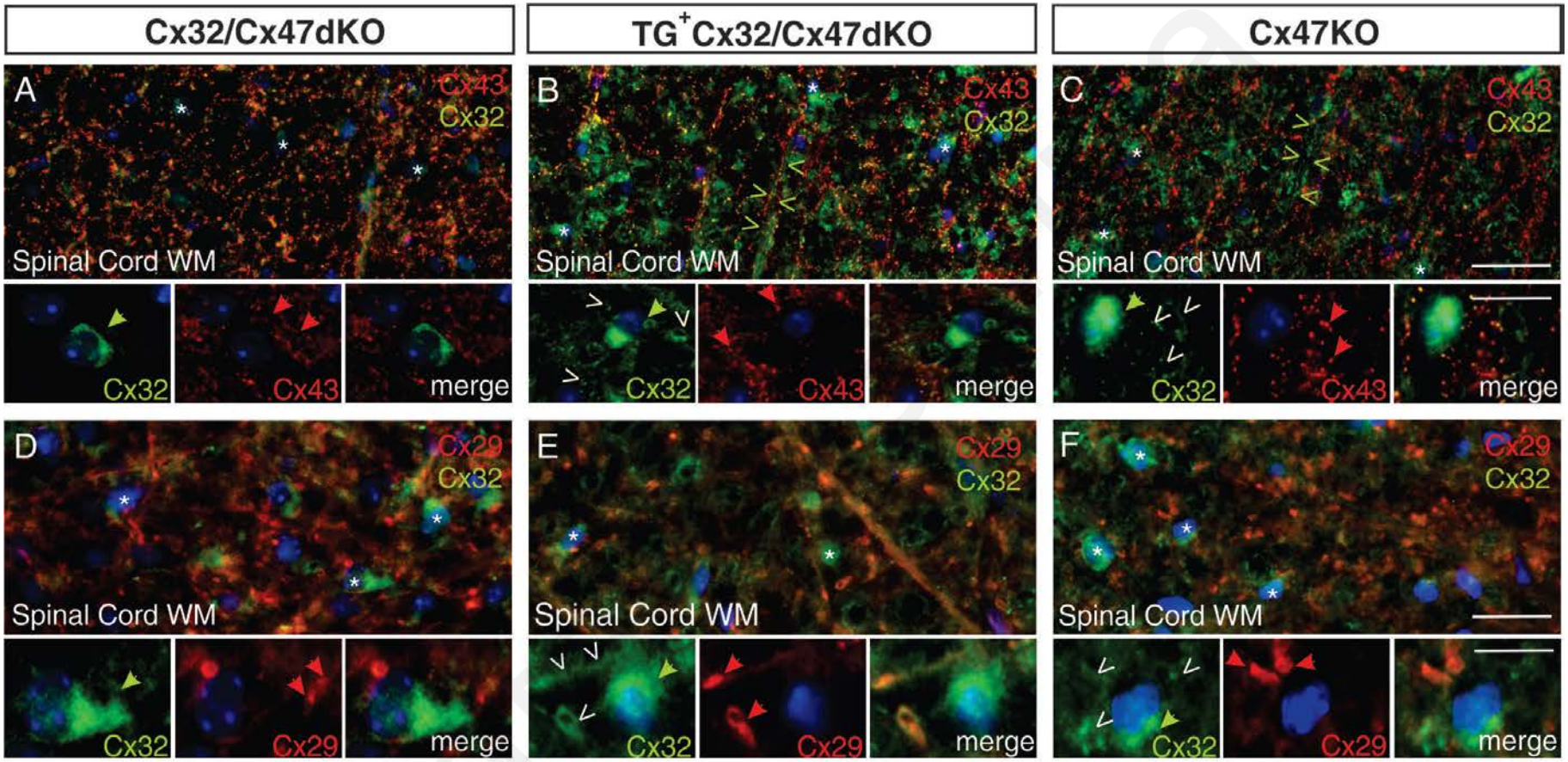
Cx32/Cx47dKO
TG+Cx32/Cx47dKO
Cx47KO
A
B
C
D
E
F
Cx43
Cx32
Cx29
Spinal Cord WM
Cx32
Cx43
Cx29
merge

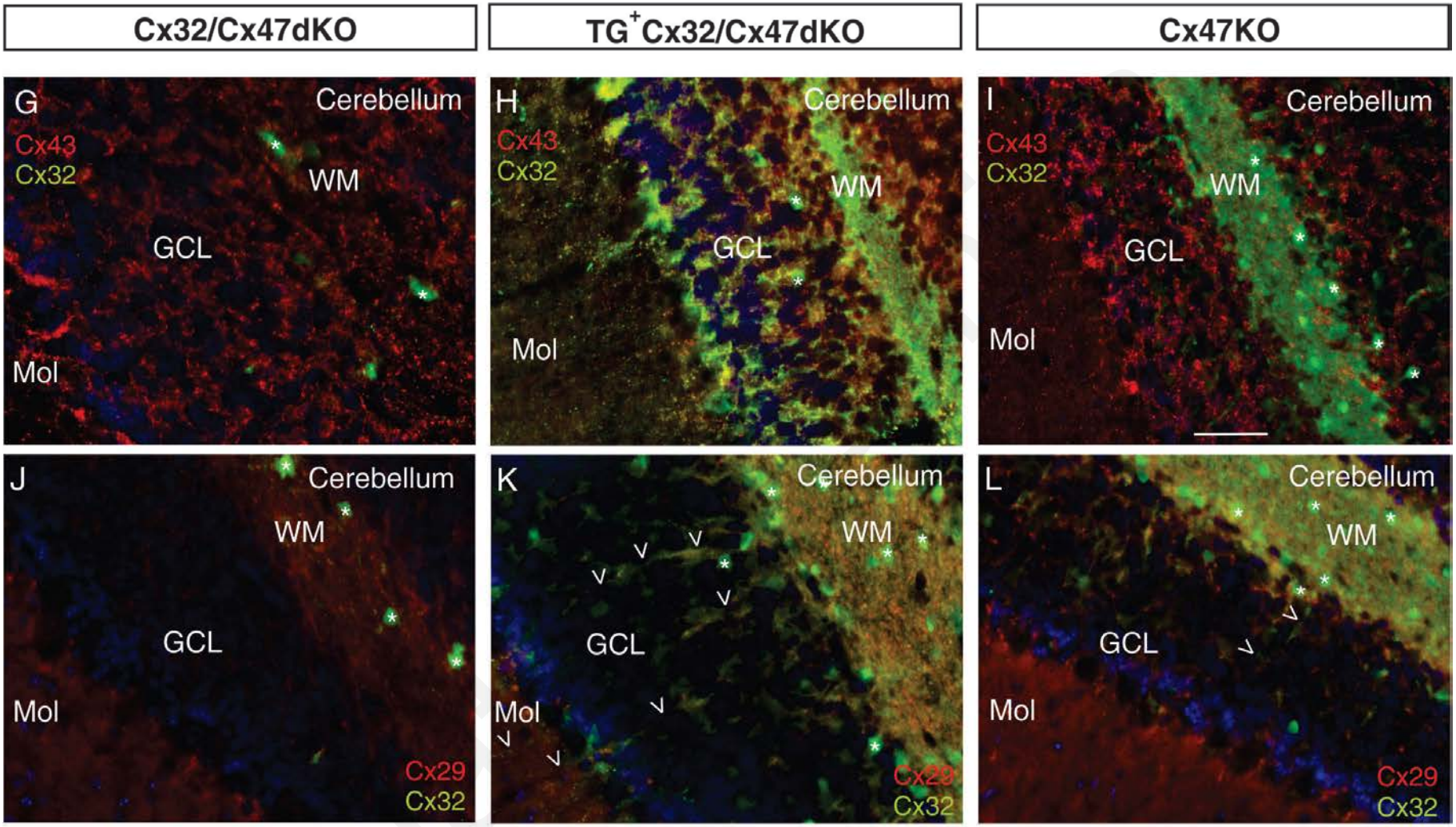
Cx32/Cx47dKO
TG+Cx32/Cx47dKO
Cx47KO
G
H
I
J
K
L
Cerebellum
Cx43
Cx32
WM
GCL
Mol
Cx29
Cx32

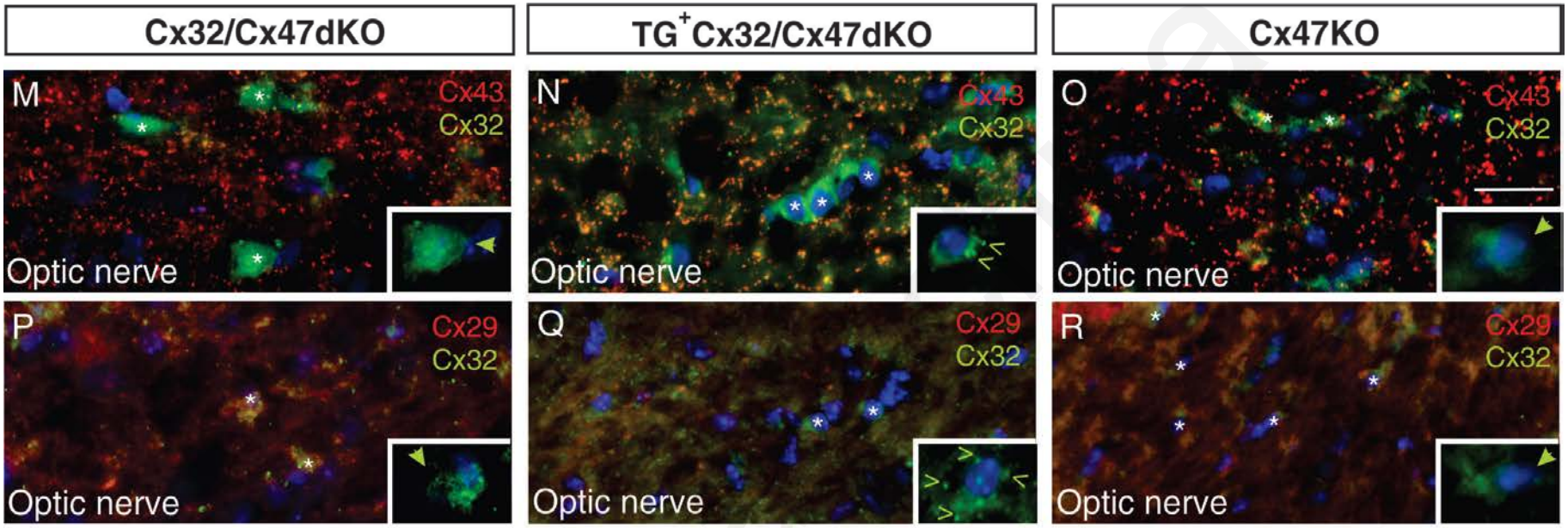

Figure 3.23: Gap junction formation by hCx32 in TG$^+$Cx32/Cx47dKO white matter oligodendrocytes.
Images of transverse sections from different CNS white matter (WM) areas as indicated from Cx32/Cx47dKO, TG$^+$Cx32/Cx47dKO and Cx47KO mice. Sections were double labeled with anti-Cx32 (green) and either anti-Cx43 (A-C, G-I, M-O) or anti-Cx29 (D-F, J-L, P-R) antibodies (red). Cell nuclei are visualized with DAPI (blue). Oligodendrocyte cell bodies are green fluorescent in all three genotypes (green arrows). In the spinal cord, cerebellum and optic nerve Cx32 is localized along the large myelinated fibers (white arrowheads) in TG$^+$Cx32/Cx47dKO and Cx47KO mice while Cx43 forms GJ plaques (red arrows) diffusely in the WM in all genotypes and shows colocalization with some Cx32 GJ plaques around oligodendrocytes only in TG$^+$Cx32/Cx47dKO and Cx47KO mice. Cx43 GJ plaques appear increased in Cx32/Cx47dKO in which Cx32 is absent (A-C, G-I, M-O). Double staining with Cx29 and Cx32 shows Cx29 expression along thin myelinated fibers in all three genotypes (red arrows). Cx32 is expressed along larger fibers only in Cx47KO mice without co localization with Cx29, whereas in TG$^+$Cx32/Cx47dKO Cx32 is also expressed in the thinly myelinated fibers colocalizing with Cx29 (D-F, J-L, P-R). Scale bars, 20 µm; in insets, 10 µm.

In conclusion, these findings suggest that transgenic expression of hCx32 in GJ deficient oligodendrocytes of Cx32/Cx47dKO leads to strong GJ formation along the myelinated fibers, with some ectopic expression along thin fibers as well. Furthermore, Cx32 expression leads to reestablishment of O/A heterotypic connections mainly between Cx32 and Cx30 in the GM, and in the WM also by homotypic O/O GJs, similar to the connectivity in Cx47KO CNS. However, Cx32 does not appear to be able to replace Cx47 in O/A connections with Cx43.

Chapter 4

CONCLUSION

CONCLUSION

4.1 Phenotypic and pathological rescue of the Cx32/Cx47dKO mice

We have successfully generated transgenic lines strongly expressing hCx32 specifically in oligodendrocytes throughout the CNS, as confirmed by our expression analysis on Cx32KO background. Reestablishment of GJ connectivity in oligodendrocytes rescued the severe phenotype of early CNS demyelination and death in Cx32/Cx47dKO mice. Furthermore, expression of Cx32 in Schwann cells prevented the peripheral neuropathy in Cx32KO mice, confirming that connexin loss in both central and peripheral myelinating cells causes disease through cell autonomous effects.

The Plp promoter has been shown to drive expression specifically in oligodendrocytes (Anderson et al., 1997, Jiang et al., 2000, Savvaki et al., 2010). Interestingly, our results confirm that the Plp promoter is also active in Schwann cells, although at lower levels compared with oligodendrocytes, as also reported in previous studies. Plp transgenic expression levels in the CNS were overall higher, up to 3-fold, compared with WT Cx32 expression. This is both due to higher expression in each oligodendrocyte, as shown by the increased number of Cx32 GJ plaques per cell compared with the Cx47KO (**Fig.3.21**), as well as due to the extra-physiological expression in all oligodendrocytes, such as those in the CC and optic nerves, in contrast to restricted Cx32 expression in specific subpopulations in WT CNS (Kleopa et al., 2004). Plp driven expression levels were higher compared with CNP-driven expression in previously generated mutants, reflecting the higher expression per cell, since CNP promoter also provided expression in all subsets of oligodendrocytes (Sargiannidou et al., 2009a).

There was no obvious adverse effect of Cx32 expression beyond the physiologically expressing subsets of oligodendrocytes, and these expression levels were sufficient to rescue the CNS phenotype of Cx32/Cx47dKO mice, similar to what has been achieved in the PNS using the P0 promoter transgene (Scherer et al., 2005). Interestingly, peripheral neuropathy was also rescued in this model, even with expression levels slightly below the WT levels, while P0

promoter-driven transgenic Cx32 expression levels in Schwann cells were much higher than WT levels (Scherer et al., 2005).

The main goal of this project was to rescue the Cx32/Cx47dKO leukodystrophy model by replacing one of the two missing oligodendrocyte connexins, in this case hCx32. Cx32/Cx47dKO mice have been characterized in detail (Menichella et al., 2003, Odermatt et al., 2003) and provide a relevant model of hypomyelinating leukodystrophy offering an opportunity to study possible therapeutic interventions. In our hands, Cx32/Cx47dKO mice presented the previously reported phenotype of action tremor followed by tonic seizures during the fourth to fifth postnatal week, which increased in frequency and severity leading to death by the sixth postnatal week. Pathological analysis at 1 month of age showed the expected severe demyelination, axonal degeneration and apoptosis of oligodendrocytes in the spinal cord funiculi and in the optic nerve. Both the behavioral as well as the pathological comparison of Cx32/Cx47dKO with TG^{+}Cx32/Cx47dKO mice clearly demonstrated that Plp-driven Cx32 replacement rescued the Cx32/Cx47dKO phenotype. TG^{+}Cx32/Cx47dKO mice outperformed Cx32/Cx47dKO mice in all tests of motor performance reaching the performance level of Cx47KO and WT mice.

Only in the rotarod test, although clearly improved compared with Cx32/Cx47dKO littermates, TG^{+}Cx32/Cx47dKO mice remained below the performance of Cx47KO and WT mice. The reason for this discrepancy is unclear. In contrast to Cx47KO or WT mice with normal Cx32 expression in Schwann cells, lower than physiological Cx32 expression in TG^{+}Cx32/Cx47dKO Schwann cells could have caused a degree of peripheral neuropathy at 1 month of age, contributing to the lower rotarod performance.

Finally, examining the survival rates between the two groups confirmed that transgenic Cx32 expression rescued the early mortality in Cx32/Cx47dKO mice and allowed a normal life span.

The behavioral correction of TG^{+}Cx32/Cx47dKO mice was accompanied by a complete rescue of the pathological changes that are typical for Cx32/Cx47dKO

mice (Menichella et al., 2003, Odermatt et al., 2003). Immunostaining and immunoblot analysis of myelin proteins, as well as electron microscopy with morphometric analysis demonstrated that the severe demyelination and vacuole formation in spinal cord gray and WM, cerebrum, cerebellum and optic nerve were prevented, while oligodendrocyte apoptosis was significantly reduced. Furthermore, secondary inflammatory changes that have been described in PMLD models with GJ-deficient oligodendrocytes (Tress et al., 2011), including activation of microglial cells and recruitment of macrophages, as well as astrogliosis, reflected in increased GFAP and Cx43 immunoreactivity, were prevented in our TG$^+$Cx32/Cx47KO mice. These inflammatory changes are likely to play a role in disease progression similar to what has been shown for Cx32KO mice in the PNS (Kobsar et al., 2003, Groh et al., 2010), as well as in experimental models of CNS myelin gene defects (Ip et al., 2006, Ip et al., 2007, Ip et al., 2012). mRNA levels of several microglial genes which are involved in neuroprotection have been analyzed and increased levels were noticed (Hickman et al., 2013).

4.2 Oligodendrocyte GJs in TG$^+$Cx32/Cx47dKO mice

Our analysis of GJ formation in oligodendrocytes in TG$^+$Cx32/Cx47dKO mice revealed that Cx32 was extensively expressed along myelinated fibers, forming the homotypic intracellular channels, and also along fibers that normally express only Cx29, such as the CC and optic nerves (Kleopa et al., 2004, Kamasawa et al., 2005). Furthermore, numerous Cx32 GJ plaques were formed around the cell bodies and were overall increased compared with Cx47KO mice, colocalizing mostly with Cx30 and to a much lesser degree with Cx43. Thus, transgenic replacement of Cx32 in the Cx32/Cx47dKO mouse appears to re-establish in part oligodendrocyte GJ connectivity, but does not replace Cx47 in O/A GJs, the majority of which are formed by Cx47 paired with Cx43 (Nagy et al., 2003b, Altevogt and Paul, 2004, Kamasawa et al., 2005, Wallraff et al., 2006). Therefore, the TG$^+$Cx32/Cx47dKO phenotype resembles that of Cx47KO mice.

Even with the high levels of Cx32 expression achieved in all oligodendrocytes, Cx32 is likely to form only heterotypic O/A GJs with astrocytic Cx30, and homotypic O/O GJs with itself. This is in keeping with previous studies showing lack of coupling between transfected cells where one expresses Cx32

and the other Cx47 (Orthmann-Murphy et al., 2007b, Magnotti et al., 2011). Furthermore, Cx32 is unlikely to replace Cx47 in pairing with Cx43, since the available literature indicates that no functional Cx32/Cx43 channels can be formed (Orthmann-Murphy et al., 2007b, Bruzzone et al., 1994, Magnotti et al., 2011).

Mice that lack Cx32 (Anzini et al., 1997, Sutor et al., 2000) or express Cx32 mutants on Cx32KO background, such as T55I and R75W (Sargiannidou et al., 2009a) develop a progressive demyelinating peripheral neuropathy after 3 month of age with subtle changes in the CNS myelin. Cx47KO mice show sporadic vacuolation of CNS myelinated fibers starting from the optic nerve. Myelination of the peripheral nerves is not affected by the deletion of Cx47 (Menichella et al., 2003, Odermatt et al., 2003).

In humans, unlike mice, loss of Cx47 function leads to PMLD or spastic paraparesis (Uhlenberg et al., 2004, Orthmann-Murphy et al., 2009), while loss of Cx32 only rarely (Al-Mateen et al., 2013), suggesting that Cx47 is more crucial for oligodendrocyte function and survival. Cx47 may play more important roles during development and oligodendrocyte differentiation and myelination (Odermatt et al., 2003) its expression in developing oligodendrocytes precedes those of Cx32 and Cx29 (Parenti et al., 2010). Moreover, oligodendrocytes throughout the CNS express Cx47 but only certain subpopulations express Cx32 (Kleopa et al., 2004, Kamasawa et al., 2005). Supporting these findings from rodent models, oligodendrocyte precursor cells in postmortem human brain studies were shown to express Cx47 but not Cx32, while mature oligodendrocytes express Cx47 throughout the human brain, similar to the expression pattern in rodents (Markoullis et al., 2012, Markoullis et al., 2014). Taken together, while our study provides the proof of principle for amelioration of phenotype by replacing at least in part GJ connectivity in oligodendrocytes in this PMLD model, it may be necessary to replace Cx47 in future clinical studies, since the presence of Cx32 in PMLD patients does not prevent the disease.

Interestingly, a GJC2 mutation affecting O/O but not O/A GJ connectivity was found in a subclinical leukodystrophy patient (Abrams et al., 2014), indicating that even partial restoration of oligodendrocyte connectivity as described in our model

may be sufficient to ameliorate the clinical phenotype, also in the human disease. Why the loss of Cx47 is more detrimental for humans with PMLD as opposed to Cx47KO mice is not clear, but may be related to several factors operating in humans that are not present in mice. Greater life span and brain size is a consideration, as well as stressful conditions that increase metabolic demand and requirements on GJ connectivity in oligodendrocytes, as also recognized for the CNS phenotypes resulting from Cx32 mutations (Paulson et al., 2002, Al-Mateen et al., 2013). This metabolic stress occurs only under experimental conditions in laboratory mice and has indeed caused increased myelin vacuolation flowing increased axonal activity in Cx47KO mice (Menichella et al., 2006). Another consideration is that Cx32/Cx30 channels can compensate for the loss of Cx47/Cx43 channels in mice more effectively than in humans, although the overall distribution of glial connexin expression appears to be similar between human and rodent brain (Kleopa et al., 2004, Sargiannidou et al., 2008, Markoullis et al., 2012, Markoullis et al., 2014).

4.3 Oligodendrocyte connectivity to panglial network

Oligodendrocytes are closely connected to astrocytes via GJs. Both human disorders such as occulodental digital dysplasia syndrome resulting from GJA1/Cx43 mutations (Paznekas et al., 2003), as well as mouse models with astrocyte connexin deletions may cause demyelination, highlighting the importance of the panglial network connectivity for oligodendrocytes. Besides the Cx32/Cx47dKO model, various other double connexin mutants including astrocytic connexins have shown similar phenotypes. The deletion of two astrocytic connexins in Cx30/Cx43AstrodKO resulted in early onset vacuolation, edema, astrogliosis and oligodendrocyte apoptosis in the brain, aswell as multiple behavioral deficits, although life span was normal (Wallraff et al., 2006, Lutz et al., 2009). Overall, the WM abnormalities in these mutants resembled the ones in Cx32/Cx47dKO mice, but their milder phenotype highlighted the importance of O/O GJs (Maglione et al., 2010, Wasseff and Scherer, 2011) that were preserved as opposed to the Cx32/Cx47dKO.

Deletion of one astrocytic and one oligodendrocytic connexin proved to be more pathogenic than the loss of two astrocytic connexins, and resembled more

the loss of two oligodendrocyte connexins. Cx32/Cx43AstroKO mice (with mGFAP-cre driven deletion of Cx43) developed WM vacuolation by the fifth week and seizures by the eighth week with early mortality by 20 weeks (Magnotti et al., 2011). However, mGFAP-cre driven Cx43AstroKOmight have been incomplete and subsequent generation of another Cx32/Cx43AstrodKO (with nestin-cre driven deletion of Cx43) resulting in complete deletion of Cx43 in astrocytes demonstrated loss of oligodendrocytes with demyelination and more phenotypic similarities to Cx32/Cx47dKO (May et al., 2013). Furthermore, Cx47 expression in oligodendrocytes and stability on the cell membrane was shown to depend in the presence of Cx43 in astrocytes, indicating that in the Cx32/Cx43dKO Cx47:Cx30 O/A is also lost and only homotypic O/O Cx47 GJs may be preserved, explaining the severity of the phenotype resembling Cx32/Cx47dKO. Likewise, Cx30/Cx47dKO mice showed early onset myelin pathology, severe vacuolation in the WM and activation of microglia and astrocytes, leading to early mortality (Tress et al., 2012). As described in our study, this double mutant demonstrates that Cx32 cannot replace Cx47 in O/A GJs, but can only form channels with Cx30 in astrocytes. Overall, the results of glial connexin mutants highlight the importance of both O/O and O/A GJs for CNS myelination and homeostasis.

In conclusion, we show that the severe phenotype of the hypomyelinating leukodystrophy model with GJ-deficient oligodendrocytes can be rescued by replacement of one, in this case Cx32, oligodendrocyte connexins, by reestablishing, at least in part, the O/O and O/A connectivity. This study has implications for future therapeutic trials targeting CNS and PNS disorders resulting from connexin mutations, including PMLD and CMT1X.

Development of gene replacement strategies targeting specifically the myelinating cells either in the CNS, or in the PNS, or in both, has the potential to provide a therapy for inherited human disorders resulting from loss of connexin function, and such strategies should be further studied.

REFERENCES

REFERENCES

Abel A, Bone LJ, Messing A, Scherer SS, Fischbeck KF (1999) Studies in transgenic mice indicate a loss of connexin32 function in X-linked Charcot-Marie-Tooth disease. J Neuropathol Exp Neurol 58:702-710.

Abrams CK, Scherer SS, Flores-Obando R, Freidin MM, Wong S, Lamantea E, Farina L, Scaioli V, Pareyson D, Salsano E (2014) A new mutation in GJC2 associated with subclinical leukodystrophy. Journal of neurology 261:1929-1938.

Abrams CK, Oh S, Ri Y, Bargiello TA (2000) Mutations in connexin 32: the molecular and biophysical bases for the X-linked form of Charcot-Marie-Tooth disease. Brain Res Rev 32:203-214.

Abrams CK, Freidin MM, Verselis VK, Bennett MV, Bargiello TA (2001) Functional alterations in gap junction channels formed by mutant forms of connexin 32: evidence for loss of function as a pathogenic mechanism in the X-linked form of Charcot-Marie-Tooth disease. Brain Res 900:9-25.

Abrams CK, Bennett MVL, Verselis VK, Bargiello TA (2002) Voltage opens unopposed gap junction hemichannels formed by a connexin 32 mutant associated with X-linked Charcot-Marie-Tooth disease. Proc Natl Acad Sci U S A 99:3980-3984.

Ahn M, Lee J, Gustafsson A, Enriquez A, Lancaster E, Sul J, Haydon P, Paul D, Huang Y, Abrams C, Scherer S (2008) Cx29 and Cx32, two connexins expressed by myelinating glia, do not interact and are functionally distinct. J Neurosci Res 86:992-1006.

Al-Mateen M, Craig AK, Chance PF (2013) The Central Nervous System Phenotype of X-Linked Charcot-Marie-Tooth Disease: A Transient Disorder of Children and Young Adults. J Child Neurol Feb 11. [Epub ahead of print]:doi: 10.1177/0883073812474343

Altevogt BM, Kleopa KA, Postma FR, Scherer SS, Paul DL (2002) Connexin29 is uniquely distributed within myelinating glial cells of the central and peripheral nervous systems. J Neurosci 22:6458-6470.

Altevogt BM, Paul DL (2004) Four classes of intercellular channels between glial cells in the CNS. J Neurosci 24:4313-4323.

Anderson TJ, Montague P, Nadon N, Nave KA, Griffiths IR (1997) Modification of Schwann cell phenotype with Plp transgenes: Evidence that the PLP and DM20 isoproteins are targeted to different cellular domains. J Neurosci Res 50:13-22.

Anzini P, Neuberg DH-H, Schachner M, Nelles E, Willecke K, Zielasek J, Toyka K, Suter U, Martini R (1997) Structural abnormalities and deficient maintenance of peripheral nerve myelin in mice lacking the gap junction protein connexin32. J Neurosci 17:4545-4561.

Balice-Gordon RJ, Bone LJ, Scherer SS (1998) Functional gap junctions in the Schwann cell myelin sheath. J Cell Biol 142:1095-1104.

Bell C, Willison H, Clark C, Haites N (1996) CNS abnormalities in a family with a connexin32 mutation and peripheral neuropathy. Eur J Hum Genet 4:S136.

Bergoffen J, Scherer SS, Wang S, Oronzi-Scott M, Bone L, Paul DL, Chen K, Lensch MW, Chance P, Fischbeck K (1993) Connexin mutations in X-linked Charcot-Marie-Tooth disease. Science 262:2039-2042.

Birouk N, Le Guern E, Maisonobe T, Rouger H, Gouider R, Gugenheim M, Tardieu S, Gugenheim M, Routon MC, Leger JM, Agid Y, Brice A, Bouche P (1998) X-linked Charcot-Marie-Tooth disease with connexin 32 mutations - clinical and electrophysiological study. Neurology 50:1074-1082.

Bjartmar c, Kidd G, Mork S, Rudick R, Trapp BD (2000) Neurological disability correlates with spinal cord axonal loss and reduced N-acetyl asparate in chronic multiple sclerosis patients. Ann Neurol 48:893-901.

Bort S, Nelis E, Timmerman V, Sevilla T, Cruz-Martinez A, Martinez F, Millan JM, Arpa J, Vilchez JJ, Prieto F, Van Broeckhoven C, Palau F (1997) Mutational analysis of the MPZ, PMP22 and Cx32 genes in patients of Spanish ancestry with Charcot-Marie-Tooth disease and hereditary neuropathy with liability to pressure palsies. Hum Genet 99:746-754.

Britt JM, Kane JR, Spaeth CS, Zuzek A, Robinson GL, Gbanaglo MY, Estler CJ, Boydston EA, Schallert T, Bittner GD (2010) Polyethylene glycol rapidly restores axonal integrity and improves the rate of motor behavior recovery after sciatic nerve crush injury. J Neurophysiol 104:695-703.

Bruzzone R, White TW, Scherer S, S, Fischbeck KH, Paul DL (1994) Null mutations of connexin32 in patients with X-linked Charcot-Marie-Tooth disease. Neuron 13:1253-1260.

Bruzzone R, White TW, Paul DL (1996) Connections with connexins: the molecular basis of direct intercellular signaling. Eur J Biochem 238:1-27.

Bugiani M, Al Shahwan S, Lamantea E, Bizzi A, Bakhsh E, Moroni I, Balestrini M, Uziel G, Zeviani M (2006) GJA12 mutations in children with recessive hypomyelinating leukoencephalopathy. Neurology 67:273-279.

Cailloux F, Gauthier-Barichard F, Mimault C, Isabelle V, Courtois V, Girard G, Dastugue B, Boespflug-Tanguy O (2000) Genotype-phenotype correlation in inherited brain myelination defects due to proteolipid protein gene mutations. European journal of human genetics : EJHG 8:837-845.

Castro C, Gomez-Hernandez JM, Silander K, Barrio LC (1999) Altered formation of hemichannels and gap junction channels caused by C-terminal connexin-32 mutations. J Neurosci 19:3752-3760.

Chandross KJ, Kessler JA, Cohen RI, Simburger E, Spray DC, Bieri P, Dermietzel R (1996) Altered connexin expression after peripheral nerve injury. Mol Cell Neurosci 7:501-518.

Deschênes SM, Bone LJ, Fischbeck KH, Scherer SS (1996) Connexin32 and X-linked Charcot-Marie-Tooth disease. In: The Biology of Gap Junctions(Spray, D. and Dermietzel, R., eds), pp 213-227 Georgetown, TX: R.G. Landes.

Deschênes SM, Walcott JL, Wexler TL, Scherer SS, Fischbeck KH (1997) Altered trafficking of mutant connexin32. J Neurosci 17:9077-9084.

Duffy HS, Delmar M, Spray DC (2002) Formation of the gap junction nexus: binding partners for connexins. Journal of physiology, Paris 96:243-249.

Ferrell RE, Baty CJ, Kimak MA, Karlsson JM, Lawrence EC, Franke-Snyder M, Meriney SD, Feingold E, Finegold DN (2010) GJC2 missense mutations cause human lymphedema. Am J Hum Genet 943-948.

Fiori MC, Reuss L, Cuello LG, Altenberg GA (2014) Functional analysis and regulation of purified connexin hemichannels. Frontiers in physiology 5:71.

Foran DR, Peterson AC (1992) Myelin acquisition in the central nervous system of the mouse revealed by an MBP-Lac-Z transgene. J Neurosci 12:4890-4897.

Forghani R, Garofalo L, Foran D, Farhadi H, Lepage P, Hudson T, Tretjakoff I, Valera P, Peterson A (2001) A distal upstream enhancer from the myelin basic protein gene regulates expression in myelin-forming schwann cells. J Neurosci 21:3780-3787.

Fuss B, Mallon B, Phan T, Ohlemyer c, Kirchoff F, Nishiyama A, Macklin WB (2000) Purification and analysis of in vivo-differentiated oligodendrocytes expressing the green fluorescent protein. Dev Biol 218:259-274.

Gage GJ, Kipke DR, Shain W (2012) Whole animal perfusion fixation for rodents. Journal of visualized experiments : JoVE.

Garbern J, Cambi F, Shy M, Kamholz J (1999) The molecular pathogenesis of Pelizaeus—Merzbacher disease. Archives of neurology 56:1210–1214.

Garbern JY (2007) Pelizaeus-Merzbacher disease: genetic and cellular pathogenesis. Cell Mol Life Sci 64:50–65.

Gow A, Friedrich VL, Lazzarini RA (1992) Myelin basic protein gene contains separate enhancers for oligodendrocyte and Schwann cell expression. J Cell Biol 119:605-616.

Groh J, Heinl K, Kohl B, Wessig C, Greeske J, Fischer S, Martini R (2010) Attenuation of MCP-1/CCL2 expression ameliorates neuropathy in a mouse model for Charcot-Marie-Tooth 1X. Human molecular genetics 19:3530-3543.

Gutierrez A, England JD, Sumner AJ, Ferer S, Warner LE, Lupski JR, Garcia CA (2000) Unusual electrophysiological findings in X-linked dominant Charcot-Marie-Tooth disease. Muscle & nerve 23:182-188.

Hahn AF, Brown WF, Koopman WJ, Feasby TE (1990) X-linked dominant hereditary motor and sensory neuropathy. Brain : a journal of neurology 113:1511-1525.

Hahn AF, Bolton CF, White CM, Brown WF, Tuuha SE, Tan CC, Ainsworth PJ (1999) Genotype/phenotype correlations in X-linked Charcot-Marie-Tooth disease. Ann N Y Acad Sci 883:366-382.

Hahn AF, Ainsworth PJ, Naus CCG, Mao J, Bolton CF (2000) Clinical and pathological observations in men lacking the gap junction protein connexin 32. Muscle & nerve S39-S48.

Hahn AF, Ainsworth PJ, Bolton CF, Bilbao JM, Vallat J-M (2001) Pathological findings in the X-linked form of Charcot-Marie-Tooth disease: a morphometric and ultrastructural analysis. Acta Neuropathol 101:129-139.

Halbrich M, Barnes J, Bunge M, Joshi C (2008) A V139M mutation also causes the reversible CNS phenotype in CMTX. Can J Neurol Sci 35:372-374.

Hanemann CO, Bergmann C, Senderek J, Zerres K, Sperfeld A (2003) Transient, recurrent, white matter lesions in X-linked Charcot-Marie-Tooth disease with novel connexin 32 mutation. Arch Neurol 60:605-609.

Hattori N, Yamamoto M, Yoshihara T, Koike H, Nakagawa M, Yoshikawa H, Ohnishi A, Hayasaka K, Onodera O, Baba M, Yasuda H, Saito T, Nakashima K, Kira J, Kaji R, Oka N, Sobue G (2003) Demyelinating and axonal features of Charcot-Marie-Tooth disease with mutations of myelin-related proteins (PMP22, MPZ and Cx32): a clinicopathological study of 205 Japanese patients. Brain : a journal of neurology 126:134-151.

Henneke M, Combes P, Diekmann S, Bertini E, Brockmann K, Burlina AP, Kaiser J, Ohlenbusch A, Plecko B, Rodriguez D, Boespflug-Tanguy O, Gartner J (2008) GJA12 mutations are a rare cause of Pelizaeus-Merzbacher-like disease. Neurology 70:748-754.

Hickman SE, Kingery ND, Ohsumi TK, Borowsky ML, Wang LC, Means TK, El Khoury J (2013) The microglial sensome revealed by direct RNA sequencing. Nature neuroscience 16:1896-1905.

Huang Y, Sirkowski EE, Stickney JT, Scherer SS (2005) Prenylation-defective human connexin32 mutants are normally localized and function equivalently to wild-type connexin32 in myelinating Schwann cells. The Journal of neuroscience : the official journal of the Society for Neuroscience 25:7111-7120.

Hudson LD, Garbern JY, Kamholz JA (2004) Pelizaeus-Merzbacher disease. In: Myelin biology and disorders, vol. 2 (RA, L., ed), pp 867–885 San Diego: Elsevier.

Inoue K (2005) PLP1-related inherited dysmyelinating disorders: Pelizaeus-Merzbacher disease and spastic paraplegia type 2. Neurogenetics 6:1–16.

Ip CW, Kroner A, Crocker PR, Nave KA, Martini R (2007) Sialoadhesin deficiency ameliorates myelin degeneration and axonopathic changes in the CNS of PLP overexpressing mice. . Neurobiol Dis 25:105-111

Ip CW, Kroner A, Fischer S, Berghoff M, Kobsar I, Mäurer M, Martini R (2006) Role of immune cells in animal models for inherited peripheral neuropathies. Neuromolecular medicine 8:175-190.

Ip CW, Kroner A, Groh J, Huber M, Klein D, Spahn I, Diem R, Williams SK, Nave KA, Edgar JM, Martini R (2012) Neuroinflammation by cytotoxic T-lymphocytes impairs retrograde axonal transport in an oligodendrocyte mutant mouse. PloS one 7:e42554.

Jeng LJ, Balice-Gordon RJ, Messing A, Fischbeck KH, Scherer SS (2006) The effects of a dominant connexin32 mutant in myelinating Schwann cells. Mol Cell Neurosci 32:283-298.

Jiang HY, Duchala CS, Awatramani R, Shumas S, Carlock L, Kamholz J, Garbern J, Scherer SS, Shy ME, Macklin WB (2000) Proteolipid protein mRNA stability is regulated by axonal contact in the rodent peripheral nervous system. J Neurobiol 44:7-19.

Kamasawa N, Sik A, Morita M, Yasumura T, Davidson K, Nagy J, Rash J (2005) Connexin-47 and connexin-32 in gap junctions of oligodendrocyte somata, myelin sheaths, paranodal loops and Schmidt-Lanterman incisures: Implications for ionic homeostasis and potassium siphoning. Neuroscience 136:65-86.

Kawakami H, Inoue K, Sakakihara I, Nakamura S (2002) Novel mutation in X-linked Charcot-Marie-Tooth disease associated with CNS impairment. Neurology 59:923-926.

Kleopa KA, Yum SW, Scherer SS (2002) Cellular mechanisms of connexin32 mutations associated with CNS manifestations. J Neurosci Res 68:522-534.

Kleopa KA, Orthmann JL, Enriquez A, Paul DL, Scherer SS (2004) Unique distribution of gap junction proteins connexin29, connexin32, and connexin47 in oligodendrocytes. Glia 47:346-357.

Kleopa KA, Scherer SS (2006a) Molecular genetics of X-linked Charcot-Marie-Tooth disease. Neuromolecular medicine 8:107-122.

Kleopa KA, Zamba-Papanicolaou E, Alevra X, Nicolaou P, Georgiou DM, Hadjisavvas A, Kyriakides T, Christodoulou K (2006b) Phenotypic and cellular expression of two novel connexin32 mutations causing CMT1X. Neurology 66:396-402.

Kleopa KA (2011) The role of gap junctions in Charcot-Marie-Tooth disease. The Journal of neuroscience : the official journal of the Society for Neuroscience 31:17753-17760.

Kobsar I, Berghoff M, Samsam M, Wessig C, Maurer M, Toyka KV, R. M (2003) Preserved myelin integrity and reduced axonopathy in connexin32-deficient mice lacking the recombination activating gene-1. Brain : a journal of neurology 126:804-813

Kuntzer T, Dunand M, Schorderet DF, Vallat JM, Hahn AF, Bogousslavsky J (2003) Phenotypic expression of a Pro 87 to Leu mutation in the connexin 32 gene in a large Swiss family with Charcot-Marie-Tooth neuropathy. J Neurol Sci 207:77-86.

Laird DW (2006) Life cycle of connexins in health and disease. The Biochemical journal 394:527-543.

Lauf U, Giepmans BN, Lopez P, Braconnot S, Chen SC, Falk MM (2002) Dynamic trafficking and delivery of connexons to the plasma membrane and accretion to gap junctions in living cells. Proceedings of the National Academy of Sciences of the United States of America 99:10446-10451.

Lee M-J, Nelson I, Houlden H, Sweeney M, Hilton-Jones D, Blake J, Wood N, Reilly M (2002) Six novel connexin32 (GJB1) mutations in X-linked Charcot-Marie-Tooth disease. Journal of neurology, neurosurgery, and psychiatry 73:304-306.

Liang GSL, de Miguel M, Gomez-Hernandez JM, Glass JD, Scherer SS, Mintz M, Barrio LC, Fischbeck KH (2005) Severe neuropathy with leaky connexin32 hemichannels. Ann Neurol 57:749-754.

Lutz SE, Zhao Y, Gulinello M, Lee SC, Raine CS, Brosnan CF (2009) Deletion of astrocyte connexins 43 and 30 leads to a dysmyelinating phenotype and hippocampal CA1 vacuolation. J Neurosci 29:7743-7752.

Maglione M, Tress O, Haas B, Karram K, Trotter J, Willecke K, Kettenmann H (2010) Oligodendrocytes in mouse corpus callosum are coupled via gap junction channels formed by connexin47 and connexin32. Glia 58:1104-1117.

Magnotti LM, Goodenough DA, Paul DL (2011) Deletion of oligodendrocyte Cx32 and astrocyte Cx43 causes white matter vacuolation, astrocyte loss and early mortality. Glia 59:1064-1074.

Markoullis K, Sargiannidou I, Schiza N, Hadjisavvas A, Roncaroli F, Reynolds R, Kleopa KA (2012) Gap junction pathology in multiple sclerosis lesions and in normal appearing white matter. Acta Neuropathol 123:873-886.

Markoullis K, Sargiannidou I, Schiza N, Roncaroli F, Reynolds R, Kleopa KA (2014) Oligodendrocyte gap junction loss and disconnection from reactive astrocytes in multiple sclerosis gray matter. Journal of neuropathology and experimental neurology 73:865-879.

Marques W, Sweeney MG, Wood NW, Wroe SJ (1999) Central nervous system involvement in a novel connexin 32 mutation affecting identical twins. J Neurol Neurosurg Psychiat 66:803-804.

Martin PEM, Mambetisaeva ET, Archer DA, George CH, Evans WH (2000) Analysis of gap junctions assembly using mutated connexins detected in Charcot-Marie-Tooth X-linked disease. J Neurochem 74:711-720.

Matsuyama W, Nakagawa M, Moritoyo T, Takashima H, Umehara F, Hirata K, Suehara M, Osame M (2001) Phenotypes of X-linked Charcot-Marie-Tooth disease and altered trafficking of mutant *Connexin 32* (*GJB1*). J Hum Genet 46:307-313.

May D, Tress O, Seifert G, Willecke K (2013) Connexin47 protein phosphorylation and stability in oligodendrocytes depend on expression of Connexin43 protein in astrocytes. The Journal of neuroscience : the official journal of the Society for Neuroscience 33:7985-7996.

Meier C, Dermietzel R, Davidson KG, Yasumura T, Rash JE (2004) Connexin32-containing gap junctions in Schwann cells at the internodal zone of partial myelin compaction and in Schmidt-Lanterman incisures. The Journal of neuroscience : the official journal of the Society for Neuroscience 24:3186-3198.

Menichella DM, Goodenough DA, Sirkowski E, Scherer SS, Paul DL (2003) Connexins are critical for normal myelination in the CNS. J Neurosci 23:5963-5973.

Menichella DM, Majdan M, Awatramani R, Goodenough DA, Sirkowski E, Scherer SS, Paul DL (2006) Genetic and physiological evidence that oligodendrocyte gap junctions contribute to spatial buffering of potassium released during neuronal activity. The Journal of neuroscience : the official journal of the Society for Neuroscience 26:10984-10991.

Michalski JP, Anderson C, Beauvais A, De Repentigny Y, Kothary R (2011) The proteolipid protein promoter drives expression outside of the oligodendrocyte lineage during embryonic and early postnatal development. PloS one 6:e19772.

Mullins LJ, Bailey MA, Mullins JJ (2006) Hypertension, kidney, and transgenics: a fresh perspective. Physiological reviews 86:709-746.

Nagy JI, Rash JE (2000) Connexins and gap junctions of astrocytes and oligodendrocytes in the CNS. Brain Res Rev 32:29-44.

Nagy JI, Ionescu AV, Lynn BD, Rash JE (2003a) Connexin29 and connexin32 at oligodendrocyte and astrocyte gap junctions and in myelin of the mouse central nervous system. J Comp Neurol 22:356-370.

Nagy JI, Ionescu AV, Lynn BD, Rash JE (2003b) Coupling of astrocyte connexins Cx26, Cx30, Cx43 to oligodendrocyte Cx29, Cx32, Cx47: Implications from normal and connexin32 knockout mice. Glia 44:205-218.

Nave K-A, Boespflug-Tanguy O (1996) Developmental defects of myelin formation: from X-linked mutations to human dysmyelinating diseases. Neuroscientist 2:33-43.

Nicholson G, Nash J (1993) Intermediate nerve conduction velocities define X-linked Charcot-Marie-Tooth neuropathy families. Neurology 43:2558-2564.

Nicholson G, Corbett A (1996) Slowing of central conduction in X-linked Charcot-Marie-Tooth neuropathy shown by brain auditory evoked responses. J Neurol Neurosurg Psychiatry 61:43-46.

Nicholson GA, Yeung L, Corbett A (1998) Efficient neurophysiological selection of X-linked Charcot-Marie-Tooth families. Neurology 51:1412-1416.

Odermatt B, Wellershaus K, Wallraff A, Seifert G, Degen J, Euwens C, Fuss B, Bussow H, Schilling K, Steinhauser C, Willecke K (2003) Connexin 47 (Cx47)-deficient mice with enhanced green fluorescent protein reporter gene reveal predominant oligodendrocytic expression of Cx47 and display vacuolized myelin in the CNS. J Neurosci 23:4549-4559.

Oh S, Ri Y, Bennett MVL, Trexler EB, Verselis VK, Bargiello TA (1997) Changes in permeability caused by connexin 32 mutations underlie X-linked Charcot-Marie-Tooth disease. Neuron 19:927-938.

Omori Y, Mesnil M, Yamasaki H (1996) Connexin 32 mutations from X-linked Charcot-Marie-Tooth disease patients: functional defects and dominant negative effects. Mol Biol Cell 7:907-916.

Orthmann-Murphy JL, Enriquez AD, Abrams CK, Scherer SS (2007a) Loss-of-function connexin47 mutations cause Pelizaeus-Merzbacher-like disease. Mol Cell Neurosci 34:629-641.

Orthmann-Murphy JL, Freidin M, Fischer E, Scherer SS, Abrams CK (2007b) Two distinct heterotypic channels mediate gap junction coupling between astrocyte and oligodendrocyte connexins. The Journal of neuroscience : the official journal of the Society for Neuroscience 27:13949-13957.

Orthmann-Murphy JL, Salsano E, Abrams CK, Bizzi A, Uziel G, Freidin MM, Lamantea E, Zeviani M, Scherer SS, Pareyson D (2009) Hereditary spastic paraplegia is a novel phenotype for GJA12/GJC2 mutations. Brain 132:426-438.

Panas M, Karadimas C, Avramopoulos D, Vassilopoulos D (1998) Central nervous system involvement in four patients with Charcot-Marie-Tooth disease with connexin 32 extracellular mutations. J Neurol Neurosurg Psychiat 65:947-948.

Panas M, Kalfakis N, Karadimas C, Vassilopoulos D (2001) Episodes of generalized weakness in two sibs with the C164T mutation of the connexin 32 gene. Neurology 57:1906-1908.

Parenti R, Cicirata F, Zappalà A, Catania A, La Delia F, Cicirata V, Tress O, Willecke K (2010) Dynamic expression of Cx47 in mouse brain development and in the cuprizone model of myelin plasticity. Glia 58:1594-1609.

Paulson HL, Garbern JY, Hoban TF, Krajewski KM, Lewis RA, Fischbeck KH, Grossman RI, Lenkinski R, Kamholz JA, Shy ME (2002) Transient central nervous system white matter abnormality in X-linked Charcot-Marie-Tooth disease. Ann Neurol 52:429-434.

Paznekas WA, Boyadjiev SA, Shapiro R, Daniels O, Wollnik B, Keegan CE, Innis JW, Dinulos MB, Christian C, Hannibal MC, Jabs EW (2003) Connexin 43 (GJA1) mutations cause the pleiotropic phenotype of oculodentodigital dysplasia. Am J Hum Genet 72:408-418

Rabadan-Diehl C, Dahl G, Werner R (1994) A connexin-32 mutation associated with Charcot-Marie-Tooth disease does not affect channel formation in oocytes. FEBS Lett 351:90-94.

Rash JE, Yasumura T, Dudek FE, Nagy JI (2001) Cell-specific expression of connexins and evidence of restricted gap junctional coupling between glial cells and between neurons. The Journal of neuroscience : the official journal of the Society for Neuroscience 21:1983-2000.

Ressot C, Bruzzone R (2000) Connexin channels in Schwann cells and the development of the X-linked form of Charcot-Marie-Tooth disease. Brain Res Rev 32:192-202.

Rouger H, Le Guern E, Birouk N, Gouider R, Tardieu S, Plassart E, Gugenheim M, Vallat J-M, Louboutin JP, Bouche P, Agid E, Brice A (1997) Charcot-Marie-Tooth disease with intermediate motor nerve conduction velocities: Characterization of 14 Cx32 mutations in 35 families. Hum Mutat 10:443-450.

Rozear MP, Pericak-Vance MA, Fischbeck K, Stajich JM, Gaskell PC, Jr., Krendel DA, Graham DG, Dawson DV, Roses AD (1987) Hereditary motor and sensory neuropathy, X-linked: a half century follow-up. Neurology 37:1460-1465.

Salviati L, Trevisson E, Baldoin MC, Toldo I, Sartori S, Calderone M, Tenconi R, Laverda AM (2007) A novel deletion in the GJA12 gene causes Pelizaeus-Merzbacher-like disease. Neurogenetics 8:57-60.

Sander S, Nicholson GA, Ouvrier RA, McLeod JG, Pollard JD (1998) Charcot-Marie-Tooth disease: histopathological features of the peripheral myelin protein (PMP22) duplication (CMT1A) and connexin32 mutations (CMTX1). Muscle & nerve 21:217-225.

Sandri C, Van Buren JM, Akert K (1982) Membrane morphology of the vertebrate nervous system. Prog Brain Res 46:201-265.

Sargiannidou I, Ahn M, Enriquez AD, Peinado A, Reynolds R, Abrams CK, Scherer SS, Kleopa KA (2008) Human oligodendrocytes express Cx31.3: function and interactions with Cx32 mutants. Neurobiol Dis 30:221-233.

Sargiannidou I, Vavlitou N, Aristodemou S, Hadjisavvas A, Kyriacou K, Scherer SS, Kleopa KA (2009a) Connexin32 mutations cause loss of function in Schwann cells and oligodendrocytes leading to PNS and CNS myelination defects. The Journal of neuroscience : the official journal of the Society for Neuroscience 29:4748-4761.

Savvaki M, Theodorakis K, Zoupi L, Stamatakis A, Tivodar S, Kyriacou K, Stylianopoulou F, Karagogeos D (2010) The expression of TAG-1 in glial cells is sufficient for the formation of the juxtaparanodal complex and the phenotypic rescue of tag-1 homozygous mutants in the CNS. The Journal of neuroscience : the official journal of the Society for Neuroscience 30:13943-13954.

Segretain D, Falk MM (2004) Regulation of connexin biosynthesis, assembly, gap junction formation, and removal. Biochimica et biophysica acta 1662:3-21.

Senderek J, Bergmann C, Quasthoff S, Ramaekers VT, Schroder JM (1998) X-linked dominant Charcot-Marie-Tooth disease: nerve biopsies allow morphological evaluation and detection of connexin32 mutations (Arg15Trp, Arg22Gln). Acta Neuropathol 95:443-449.

Senderek J, Hermanns B, Bergmann C, Boroojerdi B, Bajbouj M, Hungs M, Ramaekers VT, Quasthoff S, Karch D, Schroder JM (1999) X-linked dominant Charcot-Marie-Tooth neuropathy: clinical, electrophysiological, and morphological phenotype in four families with different connexin32 mutations. J Neurol Sci 167:90-101.

Schelhaas HJ, Van Engelen BG, Gabreels-Festen AA, Hageman G, Vliegen JH, Van Der Knaap MS, Zwarts MJ (2002) Transient cerebral white matter lesions in a patient with connexin 32 missense mutation. Neurology 59:2007-2008.

Scherer SS, Deschênes SM, Xu Y-T, Grinspan JB, Fischbeck KH, Paul DL (1995) Connexin32 is a myelin-related protein in the PNS and CNS. J Neurosci 15:8281-8294.

Scherer SS, Xu Y-T, Nelles E, Fischbeck K, Willecke K, Bone LJ (1998) Connexin32-null mice develop a demyelinating peripheral neuropathy. Glia 24:8-20.

Scherer SS, Bone LJ, Deschênes SM, Abel A, Balice-Gordon R, Fischbeck K (1999) The role of the gap junction protein connexin32 in the pathogenesis of X-linked Charcot-Marie-Tooth disease. In: Gap Junction-Mediated Intercellular Signalling in Health and Disease, vol. Novartis Foundation

Symposium 219 (Cardew, G., ed), pp 175-185 New York: John Wiley & Sons.

Scherer SS, Xu YT, Messing A, Willecke K, Fischbeck KH, Jeng LJ (2005) Transgenic expression of human connexin32 in myelinating Schwann cells prevents demyelination in connexin32-null mice. J Neurosci 25:1550-1559.

Schnapp BJ, Mugnaini E (1978) Membrane architecture of myelinated fibers as seen by freeze-fracture. In: Physiology and Pathobiology of Axons(Waxman, S. G., ed), pp 83-123 New York: Raven Press.

Söhl G, Gillen C, Bosse F, Gleichmann M, Muller HW, Willecke K (1996) A second alternative transcript of the gap junction gene connexin32 is expressed in murine Schwann cells and modulated in injured sciatic nerve. Eur J Cell Biol 69:267-275.

Söhl G, Theis M, Hallas G, Brambach S, Dahl E, Kidder G, Willecke K (2001) A new alternatively spliced transcript of the mouse connexin32 gene is expressed in embryonic stem cells, oocytes, and liver. Exp Cell Res 266:177-186.

Srinivasan J, Leventer RJ, Kornberg AJ, Dahl HH, Ryan MM (2008) Central nervous system signs in X-linked Charcot-Marie-Tooth disease after hyperventilation. Pediatr Neurol 38:293-295.

Sutor B, Schmolke C, Teubner B, Schirmer C, Willecke K (2000) Myelination defects and neuronal hyperexcitability in the neocortex of connexin 32-deficient mice. Cereb Cortex 10:684-697.

Tabaraud F, Lagrange E, Sindou P, Vandenberghe A, Levy N, Vallat JM (1999) Demyelinating X-linked Charcot-Marie-Tooth disease: Unusual electrophysiological findings. Muscle & nerve 22:1442-1447.

Tang Y, Nyengaard JR (1997) A stereological method for estimating the total length and size of myelin fibers in human brain white matter. J Neurosci Methods 73:193-200.

Taylor RA, Simon EM, Marks HG, Scherer SS (2003) The CNS phenotype of X-linked Charcot-Marie-Tooth disease: more than a peripheral problem. Neurology 61:1475-1478.

Tetzlaff W (1982) Tight junction contact events and temporary gap junctions in the sciatic nerve fibres of the chicken during Wallerian degeneration and subsequent regeneration. J Neurocytol 11:839-858.

Tress O, Maglione M, May D, Pivneva T, Richter N, Seyfarth J, Binder S, Zlomuzica A, Seifert G, Theis M, Dere E, Kettenmann H, Willecke K (2012) Panglial gap junctional communication is essential for maintenance of myelin in the CNS. The Journal of neuroscience : the official journal of the Society for Neuroscience 32:7499-7518.

Tress O, Maglione M, Zlomuzica A, May D, Dicke N, Degen J, Dere E, Kettenmann H, Hartmann D, Willecke K (2011) Pathologic and phenotypic

alterations in a mouse expressing a connexin47 missense mutation that causes pelizaeus-merzbacher-like disease in humans. PLoS Genet 7:e1002146. Epub 1002011 Jul 1002147

Uhlenberg B, Schuelke M, Ruschendorf F, Ruf N, Kaindl AM, Henneke M, Thiele H, Stoltenburg-Didinger G, Aksu F, Topaloglu H, Nurnberg P, Hubner C, Weschke B, Gartner J (2004) Mutations in the gene encoding gap junction protein alpha 12 (Connexin 46.6) cause Pelizaeus-Merzbacher-like disease. Am J Hum Genet 75:251-260.

Unger VM, Kumar NM, Gilula NB, Yeager M (1999) Three-dimensional structure of a recombinant gap junction membrane channel. Science 283:1176-1180.

VanSlyke JK, Deschênes SM, Musil LS (2000) Intracellular transport, assembly, and degradation of wild-type and disease-linked mutant gap junction proteins. Molecular biology of the cell 11:1933-1946.

Vital A, Ferrer X, Lagueny A, Vandenberghe A, Latour P, Goizet C, Canron MH, Louiset P, Petry KG, Vital C (2001) Histopathological features of X-linked Charcot-Marie-Tooth disease in 8 patients from 6 families with different connexin32 mutations. J Peripher Nerv Syst 6:79-84.

Vondracek P, Seeman P, Hermanova M, Fajkusova L (2005) X-linked Charcot-Marie-Tooth disease: phenotypic expression of a novel mutation Ile127Ser in the GJB1 (connexin 32) gene. Muscle & nerve 31:252-255.

Wallraff A, Kohling R, Heinemann U, Theis M, Willecke K, Steinhauser C (2006) The impact of astrocytic gap junctional coupling on potassium buffering in the hippocampus. The Journal of neuroscience : the official journal of the Society for Neuroscience 26:5438-5447.

Wasseff SK, Scherer SS (2011) Cx32 and Cx47 mediate oligodendrocyte:astrocyte and oligodendrocyte:oligodendrocyte gap junction coupling. Neurobiol Dis 42:506-513.

White TW, Paul DL (1999) Genetic diseases and gene knockouts reveal diverse connexin functions. Annu Rev Physiol 61:283-310.

Wight PA, Duchala CS, Readhead C, Macklin WB (1993) A myelin proteolipid protein-lacZ fusion protein is developmentally regulated and targeted to the myelin membrane in transgenic mice. J Cell Biol 123:443-454.

Willecke K, Eiberger J, Degen J, Eckardt D, Romualdi A, Guldenagel M, Deutsch U, Sohl G (2002) Structural and functional diversity of connexin genes in the mouse and human genome. Biol Chem 383:725-737.

Wolf NI, Cundall M, Rutland P, Rosser E, Surtees R, Benton S, Chong WK, Malcolm S, Ebinger F, Bitner-Glindzicz M, Woodward KJ (2007) Frameshift mutation in GJA12 leading to nystagmus, spastic ataxia and CNS dys-/demyelination. Neurogenetics 8:39-44.

Yeager M, Unger VM, Falk MM (1998) Synthesis, assembly and structure of gap junction intercellular channels. Current opinion in structural biology 8:517-524.

Yoshimura T, Satake M, Ohnishi A, Tsutsumi Y, Fujikura Y (1998) Mutations of connexin32 in Charcot-Marie-Tooth disease type X interfere with cell-to-cell communication but not cell proliferation and myelin-specific gene expression. J Neurosci Res 51:154-161.

Yum SW, Kleopa KA, Shumas S, Scherer SS (2002) Diverse trafficking abnormalities of Connexin32 mutants causing CMTX. Neurobiol Dis 11:43-52.

APPENDIX

APPENDIX

Table A1: Solutions

REAGENT	RECIPE
10x Running Buffer for Western Blot	30.3gr Tris-hydroxide 144.42gr Glycine 10gr SDS *Bring dH_2O up to a liter*
1x Transfer Buffer for Western Blot	3gr Tris-hydroxide 14gr Glycine 200ml Methanol *Bring dH_2O up to a liter* *Adjust pH to 7.6*
12% Running gel (for 1 gel)	3.35ml ddH_2O 4ml 30% bis-acrylamide 2.5ml 1.5M Tris-HCl (pH8.8) 100µl 10% SDS 100µl 10%Ammonium Persulfate (APS) 8µl TEMED
4% Stacking gel (for 1gel)	3.05ml ddH_2O 0.65ml 30% bis-acrylamide 1.25ml 0.5M Tris-HCl (pH6.8) 50µl 10% SDS 50µl 10%Ammonium Persulfate (APS) 8µl TEMED
10x Phosphate buffered Saline (PBS) Buffer	80gr NaCl 2gr KCl 11.5gr $Na_2HPO_4 \cdot 2H_2O$ 2gr KH_2PO_4 *Bring dH_2O up to a liter*
RIPA Buffer	1x PBS 1% NP-40 0.5% Sodium deoxycholate 0.1% SDS 2mM EDTA *Add protease inhibitors (Roche)*
Blocking solution for Western Blot	2.5gr regilait non-fat powder milk 500µl Tween-20 50ml PBS
Blocking solution for Immnofluorescence	5gr Bovine serum albumin powder 500ml TRITON X-100 98.5ml 1xPBS

0.2M Solution A	13.8gr of Sodium dihydrogen phosphate monohydrate (NaH_2PO4H_2O) *Bring dH_2O up to 500ml*
0.2M Solution B	14.2gr of Sodium hydrogen phosphate anhydrous (Na_2HPO_4) *Bring dH_2O up to 500ml*
0.1M PB	23.5ml Solution A 76.5ml Solution B *Add 100ml dH_2O* *Adjust pH 7.2 using solutions A or B*
10%SDS	25gr Sodium Dodecyl Sulfate 250ml dH_2O
4% PFA	4gr PFA powder 100ml 0.1M PB Stir and warm at 60^oC After dissolving add 2 drops of 1M NaOH
Coomasie Stain (200ml)	100ml methanol 20ml acetic acid 80ml H_2O 200mg Coomassie Brilliant blue
Coomasie Destain (500ml)	150ml methanol 35ml acetic acid 315ml H2O
LB-Broth	10gr Peptone 5gr yeast 5gr NaCl Bring dH2O up to a liter
LB Agar	15gr agar 10gr Peptone 5gr yeast 5gr NaCl Bring dH2O up to a liter
SOC medium (100ml)	2gr Bacto Trypton 0.5gt yeast extract 200µl 5M NaCl 250µl 1M KCl 1ml 1M MgCl2 1ml 1M MgSO4 2ml 1M Glucose
Ampicillin (100mg/ml)	0.5g of powder ampicillin Dissolve in 5ml dH2O

Table A2: PCR Primers

NAME	SEQUENCE 5' TO 3'
AscI-F1	TAC GCG TAC GGC GCG CCC GCG GAC A
PacI-R	CCT TAA TTA AGG GGC GGA TCC TCA GCA GGC CGA GCA
Plp-F1	TGG GTG TTG GTT TTT GGA GA
Plp-F2	CTG AGT ATT GTA GGC AAG GG
PlpMCS-F	AGG TTT AAA CAG TCG ACT CTA G
Cx32-F2	GGC TCA CCA GCA ACA CAT AG
Cx32-R	CGC TGT TGC AGC CAG GCT GG
P1	CAG GAT CAA TGG AAG ATT CTC GGT CCC
P3	GCC AAG CGG TGG ACT GCA TAG CCC AGG
P4	GAC ACG CTG AAC TTG TGG CCG TTT ACG
Cx32-F	TGA GGC AGG ATG AAC TGG ACA GGT
Cx32-R	CAC GAA GCA GTC CAC TGT

Table A3: Sequencing Primers

NAME	SEQUENCE 5' TO 3'
Cx32-F1	CAG GTT TGT ACA CCT TGC TCA G
Cx32-R	CCA GCC TGG CTG CAA CAG CG
Cx32-F2	GGC TCA CCA GCA ACA CAT AG
Cx32-R2	GTT TGA GGC CGT CTT CAT GT
Cx32-F	AGC TGC TGA GTG AGC AGG ATG G
Cx32-R1	CTG AAA AGA GCG ACC GCT GCT CGG CCT

Table A4: Reverse Transcription Primers

NAME	SEQUENCE 5' TO 3'
Cx32-F	TGAGGCAGGATGAACTGGACAGGT
Cx32-R	CACGAAGCAGTCCACTGT

Table A5: Primary Antibodies

PRIMARY ANTIBODY	SPECIES	DILUTION	SOURCE
Cx32	RABBIT POLYCLONAL	1:50	ZYMED (*71-0600)*
Cx32	MOUSE MONOCLONAL	1:50	ZYMED (*35-8900)*
Cx32	RABBIT POLYCLONAL	1:5000	USA
Cx47	RABBIT POLYCLONAL	1:50	INVITROGEN (*36-4700)*
Cx47	MOUSE MONOCLONAL	1:200	INVITROGEN (*37-4500)*
Cx43	RABBIT POLYCLONAL	1:50	CELL SIGNALING (*#3512)*
Cx43	MOUSE MONOCLONAL	1:200	MILLIPORE (*MAB3067)*
Cx30	RABBIT POLYCLONAL	1:500	INVITROGEN *(71-2200)*
Cx29	RABBIT POLYCLONAL	1:300	ZYMED *(34-4200)*
CASPASE-3	RABBIT POLYCLONAL	1:10	MILLIPORE (*AB3623*)
CC-1	MOUSE MONOCLONAL	1:50	CALBIOCHEM
APP	RABBIT POLYCLONAL	1:300	CHEMICON (*AB5352*)
PLP	RAT MONOCLONAL	1:10	UK
CD68-ALEXA488	RAT MONOCLONAL	1:50	SEROTEC (*MCA1957A488)*
MOG	MOUSE MONOCLONAL	1:50	UK

Iba1	RABBIT POLYCLONAL	1:300	BIOCARE MEDICAL (*CP290A)*
GFAP	MOUSE MONOCLONAL	1:400	SIGMA (*G3893)*
MBP	MOUSE MONOCLONAL	1:400	ABCAM (*AB24567)*
MBP	RABBIT POLYCLONAL	1:1000	UK
NeuN	MOUSE MONOCLONAL	1:400	CHEMICON (*MAB377)*
Kv1.2	RABBIT POLYCLONAL	1:200	ALOMONE LABS (*APC009)*
PMP22	RABBIT POLYCLONAL	1:50	ABCAM (*AB61220)*

Table A6: Secondary Antibodies

SECONDARY ANTIBODY	SPECIES	DILUTION	SOURCE
DyLight488 (FITC)	Rabbit polyclonal	1:500	Jackson Immunoresearch Laboratories (*111-486-003*)
Fluorescein (FITC)	Mouse monoclonal	1:500	Jackson Immunoresearch Laboratories (*115-096-003*)
Rhodamine (TRITC)	Mouse monoclonal	1:500	Jackson Immunoresearch Laboratories (*115-026-068*)
Rhodamine (TRITC)	Rabbit polyclonal	1:500	Jackson Immunoresearch Laboratories (111-026-003)
Horseradish peroxidase	Rabbit polyclonal	1:3000	Jackson Immunoresearch Laboratories (*111-036-003*)
Horseradish Peroxidase	Mouse monoclonal	1:3000	Jackson Immunoresearch Laboratories (*115-036-068*)

Preparation of frozen competent XL1-Blue bacterial cells

1. Set up an overnight culture XL1-Blue in 2ml of LB broth
2. Add 500µl of the overnight culture to 100ml LB in a 1L flask
3. Shake at 37^{o}C until the OD600nm =0.48
4. Split into 2x 50ml falcon tubes and incubate on ice for 30 minutes
5. Spin in a chilled centrifuge (4^{o}C) at 400rpm for 10 minutes
6. Resuspend in 25ml cold $CaCl_2$ in each tube
7. Leave on ice for 30 minutes
8. Spin in a chilled centrifuge (4^{o}C) at 4000rpm for 20 minutes
9. Resuspend in 4ml cold $CaCl_2$ in each tube
10. Leave on ice overnight
11. Add 2ml of cold sterile 100% glycerol
12. Dispense into 100µl aliquots (in the cold room)
13. Freeze in liquid nitrogen or on dry ice
14. Store at -80^{o}C

3-Aminopropyltriethoxysilane (APES) coating slides

1. Place slides in racks and wash in washing up liquid for 30 minutes
2. Wash away liquid using running tap water for 15 minutes
3. Wash in tap water for 10 minutes (2x)
4. Wash in distilled water for 10 minutes (2x)
5. Wash in 96% ethanol for 10 minutes (2x)
6. Wash in 100% ethanol (2x)
7. Let the slides dry
8. Dip the slides in 2% APES in acetone for 30seconds
9. Dip the acetone for 30 seconds (2x)
10. Let the slides dry at 37^{o}C

OXFORD

Human Molecular Genetics, 2015, 1–16

doi: 10.1093/hmg/ddu725
Advance Access Publication Date: 18 December 2014
Original Article

ORIGINAL ARTICLE

Transgenic replacement of Cx32 in gap junction-deficient oligodendrocytes rescues the phenotype of a hypomyelinating leukodystrophy model

Natasa Schiza[1], Irene Sargiannidou[1], Alexia Kagiava[1], Christos Karaiskos[1], Marianna Nearchou[3] and Kleopas A. Kleopa[1,2,*]

[1]Neuroscience Laboratory, [2]Neurology Clinics and [3]Department of Molecular Pathology and Electron Microscopy, The Cyprus Institute of Neurology and Genetics, Nicosia, Cyprus

*To whom correspondence should be addressed at: Neurology Clinics and Neuroscience Laboratory, The Cyprus Institute of Neurology and Genetics, 6 International Airport Avenue, PO Box 23462, 1683, Nicosia, Cyprus. Tel: +357 22358600; Fax: +357 22392786; Email: kleopa@cing.ac.cy

Abstract

Oligodendrocytes are coupled by gap junctions (GJs) formed mainly by connexin47 (Cx47) and Cx32. Recessive *GJC2*/Cx47 mutations cause Pelizaeus–Merzbacher-like disease, a hypomyelinating leukodystrophy, while *GJB1*/Cx32 mutations cause neuropathy and chronic or acute-transient encephalopathy syndromes. Cx32/Cx47 double knockout (Cx32/Cx47dKO) mice develop severe CNS demyelination beginning at 1 month of age leading to death within weeks, offering a relevant model to study disease mechanisms. In order to clarify whether the loss of oligodendrocyte connexins has cell autonomous effects, we generated transgenic mice expressing the wild-type human Cx32 under the control of the mouse proteolipid protein promoter, obtaining exogenous hCx32 expression in oligodendrocytes. By crossing these mice with Cx32KO mice, we obtained expression of hCx32 on Cx32KO background. Immunohistochemical and immunoblot analysis confirmed strong CNS expression of hCx32 specifically in oligodendrocytes and correct localization forming GJs at cell bodies and along the myelin sheath. TG$^+$Cx32/Cx47dKO mice generated by further crossing with Cx47KO mice showed that transgenic expression of hCx32 rescued the severe early phenotype of CNS demyelination in Cx32/Cx47dKO mice, resulting in marked improvement of behavioral abnormalities at 1 month of age, and preventing the early mortality. Furthermore, TG$^+$Cx32/Cx47dKO mice showed significant improvement of myelination compared with Cx32/Cx47dKO CNS at 1 month of age, while the inflammatory and astrogliotic changes were fully reversed. Our study confirms that loss of oligodendrocyte GJs has cell autonomous effects and that re-establishment of GJ connectivity by replacement of least one GJ protein provides correction of the leukodystrophy phenotype.

Introduction

Connectivity through gap junctions (GJs) mediates inter- and intracellular communication that is vital for myelinating cells. *GJC2*/Cx47 mutations cause a hypomyelinating leukodystrophy known as Pelizaeus–Merzbacher-like disease (PMLD) (1) while *GJB1*/Cx32 mutations cause X-linked Charcot–Marie-Tooth (CMT1X), a peripheral neuropathy that may be accompanied by chronic or acute-transient encephalopathy syndromes, often induced by conditions of metabolic stress (2–4). Accumulating evidence indicates that *GJC2*/Cx47 mutations (5), as well as most *GJB1*/Cx32 mutations (6,7) result in loss of function, suggesting that strategies to replace connexin function in oligodendrocytes may be a promising future therapeutic strategy.

Oligodendrocytes express at least three different GJ proteins, Cx29, Cx32 and Cx47 (8–10). Cx47 is found in perikarya and proximal processes of all oligodendrocytes (11–13) forming

Received: October 23, 2014. **Revised and Accepted:** December 10, 2014

homotypic oligodendrocyte–oligodendrocyte (O/O) or heterotypic oligodendrocyte–astrocyte (O/A) GJs with Cx43 as astrocytic partner (10,14–16). Cx32 is mainly expressed along large myelinated fibers of the white matter (WM) (8,11) forming intracellular GJs within the myelin sheath but also in cell bodies of mainly gray matter oligodendrocytes forming O/A GJs with Cx30 as astrocytic partner (9,10,14,17). Cx29 and its human ortholog Cx31.3 appear to mainly form hemichannels along thin myelinated fibers (11,18,19).

Mice lacking Cx32 or Cx47 develop minimal CNS pathology and no obvious CNS phenotype indicating that these proteins have partially overlapping functions. However, loss of both oligodendrocyte connexins in Cx32/Cx47 double knockout (Cx32/Cx47dKO) mice leads to severe and early CNS demyelination (12,13). Cx32/Cx47dKO mice develop a progressive, coarse action tremor during the third postnatal week followed by tonic seizures, which increase in frequency and severity until the animals die, typically during the sixth postnatal week. At 1 month of age, these mice show severe CNS demyelination, axonal degeneration and apoptosis of oligodendrocytes in the spinal cord funiculi and in the optic nerves, confirming that GJ connectivity is vital for oligodendrocytes (12,13).

Transgenic replacement of Cx32 expression in Schwann cells of Cx32KO mice resulted in full rescue of the peripheral neuropathy, confirming the cell autonomous mechanisms in CMT1X (20). Such cell autonomous effect needs to be shown also for CNS pathology resulting from connexin mutations, given the more complex cell–cell interactions and restricted compatibilities between glial connexins (10,15,16). For this purpose we generated transgenic mice expressing the wild-type (WT) human Cx32 under the control of the mouse proteolipid protein (Plp) promoter, obtaining exogenous hCx32 expression in oligodendrocytes. Transgenic expression of hCx32 in Cx32/Cx47dKO mice resulted in almost complete rescue of behavioral abnormalities at 1 month of age, and prevented the severe CNS demyelination and early mortality. Oligodendrocyte GJ connectivity was re-established through homotypic Cx32 and heterotypic Cx32/Cx30 channels.

Results

Generation of TG$^+$Cx32KO and TG$^+$Cx32/Cx47dKO mice

Successful pronuclear injection of the transgenic construct (Fig. 1A) and screening of offspring revealed five transgenic founders. Two of the founders showed stable transmission to the next generation and were crossed with Cx32KO mice and further genotyped (Fig. 1B). About 30% of the mice carried the transgene (TG$^+$). These mice were crucial for the assessment of the transgenic expression and exogenous Cx32 localization on a *Gjb1*-null/Cx32KO background. Therefore, these two lines were further expanded on Cx32KO background.

Expression of hCx32 in the CNS and PNS of Cx32KO mice and rescue of the peripheral neuropathy

We compared the expression levels of exogenous hCx32 from brain and spinal cord tissues of TG$^+$Cx32KO to the endogenous expression in WT mice at 1 month of age by reverse transcriptase-polymerase chain reaction (RT-PCR). cDNA was amplified using primers which are identical in both human and mouse Cx32, resulting in a 553bp product. Restriction digest with enzymes specific for the human or the mouse Cx32 showed that tissues from transgenic mice had 2 to 3-fold higher levels of Cx32 mRNA than the WT tissues (Fig. 1C). Accordingly, immunoblot analysis showed higher levels of Cx32 protein in TG$^+$Cx32KO spinal cord compared with WT spinal cord. However, sciatic nerves from transgenic mice showed slightly lower Cx32 levels compared with WT nerves. Cx32 expression was absent in TG$^+$Cx32KO liver and in all Cx32 KO control tissues (Fig. 1D). Both TG$^+$Cx32KO transgenic lines showed similar expression at the RNA and protein level (data not shown) and only one was expanded for further analysis and crossing into Cx47KO background.

To assess the transgenic expression of Cx32 in oligodendrocytes of Cx32KO mice, we immunostained different CNS areas including the spinal cord, cerebellum and cerebrum with Cx32 antibody combined with cell markers for oligodendrocytes (CC-1), astrocytes (GFAP), neurons (NeuN) and microglial cells (IbaI) (Fig. 2). In the spinal cord (Fig. 2A–C) Cx32 was localized mainly along large myelinated fibers in WT mice and formed GJ-like plaques only around oligodendrocyte cell bodies in the gray matter, while in TG$^+$Cx32KO mice Cx32 was expressed around oligodendrocyte cell bodies not only in the gray but also in the WM, in addition to myelinated fibers. In the cerebrum at the level of the hippocampus (Fig. 2D–F) Cx32 was localized in deep neocortex of WT mice along myelinated fibers, adjacent but not within the corpus callosum (CC), whereas in the TG$^+$Cx32KO Cx32 was localized additionally in CC along small diameter fibers and around oligodendrocyte cell bodies (Fig. 2E). In the cerebellum (Fig. 2G–I) of WT mice Cx32 was mainly expressed in WM fibers, while TG$^+$Cx32KO mice also showed Cx32 immunoreactivity in the granule cell layer. No specific Cx32 staining was detected in any Cx32KO tissues. Transgenic Cx32 expression was restricted to oligodendrocytes and was not detected in GFAP-positive astrocytes, NeuN-positive neurons or Iba1-positive microglial cells (Fig. 2J–L).

Given the immunoblot results we also examined Cx32 expression in Schwann cells by immunostaining sciatic nerve teased fibers (Fig. 3A–C). Cx32 was expressed and normally localized at non-compact myelin areas in TG$^+$Cx32KO nerves similar to the WT nerve, while it was absent from Cx32KO fibers. To further verify that hCx32 expression in Cx32KO Schwann cells can rescue the development of peripheral neuropathy starting after 3 month of age (21,22), we examined semithin sciatic nerve sections from groups of 8-month-old mice ($n = 4$ per genotype) with morphometric analysis of abnormally myelinated fibers as previously described (7). TG$^+$Cx32KO mice showed significantly lower rates of abnormally myelinated fibers compared with Cx32KO littermates ($P = 0.0023$), confirming that Plp promoter-driven Cx32 expression can rescue the peripheral neuropathy in Cx32KO mice (Fig. 3D–F) as was shown previously with P0 promoter-driven expression (20). These results show that the 11 kb Plp promoter efficiently drives expression of hCx32 in all oligodendrocytes, even in subpopulations normally not expressing Cx32 (11), and interestingly, also in myelinated Schwann cells of TG$^+$Cx32KO mice.

Transgenic Cx32 expression rescues the phenotype of Cx32/Cx47dKO mice

To examine whether transgenic expression of hCx32 in oligodendrocytes can also rescue the severe CNS phenotype of Cx32/Cx47dKO mice (12,13) we crossed TG$^+$Cx32KO mice with Cx47KO mice obtaining initially TG$^+$Cx32KOCx47het mice and then by further breeding TG$^+$Cx32/Cx47dKO mice (Fig. 1B). All behavioral and pathological changes in TG$^+$Cx32/Cx47dKO mice were compared during the fourth week of life to Cx32/Cx47dKO littermates,

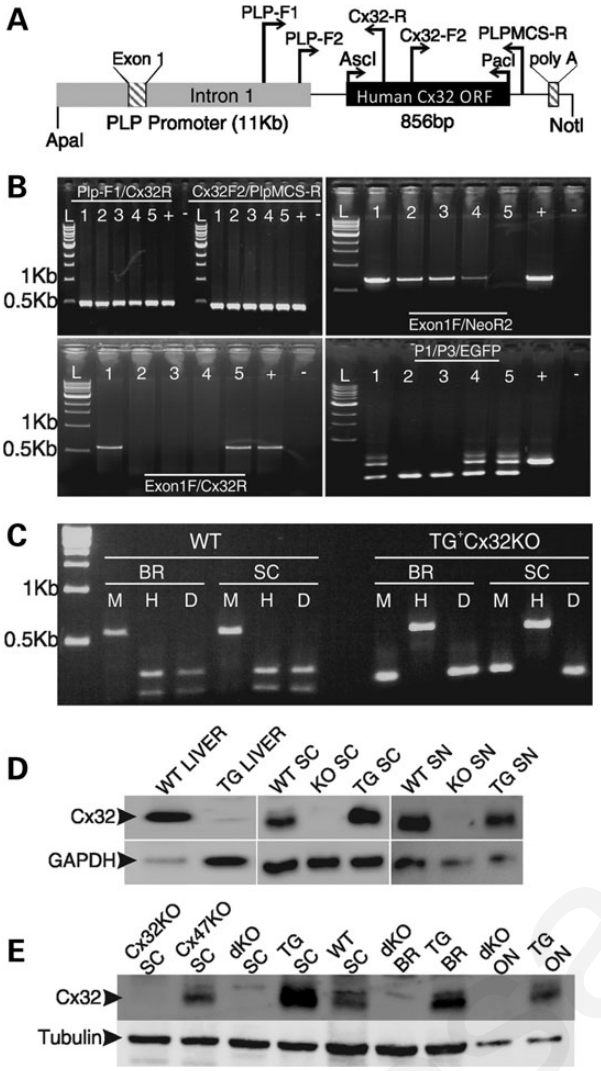

Figure 1. (**A**) Structure of the PLP-hCx32 transgenic cassette used to express hCx32 in CNS myelinating cells showing the positions of the restriction enzymes and PCR screening primers. (**B**) PCR screening for transgenic lines using two pairs of primers (Plp-F1/Cx32R, Cx32-F2/PlpMCS). Positive bands in lanes 1–5 indicate the presence of the transgene in the mouse genome. PCR screening for Cx32 allele: Exon1F/NeoR2 primer set was used to detect the Cx32KO allele (*Gjb1* ORF replaced by neomycin gene in Cx32 KO mice) and Exon1F/Cx32R was used to detect the WT *Gjb1* allele. For Cx47 allele a multiplex PCR was used P1 (Cx47 intron specific), P3 (Cx47 exon specific) and P4/EGFP (*Gjc2* ORF replaced by EGFP gene in Cx47 KO mice). Mouse 1 is transgenic heterozygous for Cx32 and heterozygous for Cx47 (TG^{+} $X^{+}X^{-}$ Cx47Het); Mouse 2 is transgenic Cx32/Cx47 double KO (dKO) same as Mouse 3; Mouse 4 is TG^{+}Cx32KO Cx47Het and Mouse 5 is TG^{+}Cx32WTCx47Het. (**C**) Analysis of mouse and human Cx32 transcripts by RT-PCR and digestion by *MscI* (M; cuts the human Cx32 cDNA) or *HhaI* (H; cuts the mouse Cx32 cDNA), or with both (D; 'double-cut' with *MscI* and *HhaI*) shows that M-digested human Cx32 cDNA is detected only in transgenic but not in WT tissues (BR: brain; SC: spinal cord), whereas the H-digested mouse Cx32 cDNA is present only in the WT mouse. (**D**) Immunoblot analysis of Cx32 expression in liver (LV), SC and sciatic nerve (SN) lysates from the transgenic line (TG^{+}Cx32KO) as well as WT and Cx32KO mice, as indicated, detects the Cx32 band (arrowhead ~27 kDa) in the SC and SN but not in the liver of the transgenic mouse, as well as in all WT tissues but not in any Cx32KO tissues. Note the Plp promoter-driven expression results in higher Cx32 levels in the SC and in lower levels in the SN compared with the WT mouse. Different exposures are shown for each tissue due to different expression levels. GAPDH blot is shown for loading control. (**E**) Immunoblot analysis of CNS Cx32 expression in Cx32/Cx47dKO mice shows the absence in all Cx32KO and Cx32/Cx47dKO tissues and expression in TG^{+}Cx32/Cx47dKO at higher levels compared with the corresponding WT or Cx47KO tissues (ON: optic nerve).Tubulin blot is used for loading control.

to Cx47KO from the same line, and in some cases to WT mice. Immunoblot analysis of spinal cord tissue from TG^{+}Cx32/Cx47dKO, Cx32/Cx47dKO, WT and Cx47KO mice confirmed the presence of Cx32 protein in the TG^{+}Cx32/Cx47dKO CNS at almost 3-fold levels (280%) compared with WT mice (Fig. 1E).

For behavioral analysis mice were subjected to foot print test ($n = 6$ per genotype), foot slip test ($n = 8$), and rotarod test ($n = 9$). All parameters of foot print analysis, including stride length for all limbs and overlap width, were significantly improved in TG^{+}Cx32/Cx47dKO compared with Cx32/Cx47dKO mice, and reached similar levels as those of the WT animals (Fig. 4A–C). Furthermore, the foot slip test revealed that TG^{+}Cx32/Cx47dKO mice had an average of 1 ± 0.5 missteps whereas Cx32/Cx47dKO mice had an average of 9 ± 1.8 missteps ($P = 0.0048$) (Fig. 4D). Finally, TG^{+}Cx32/Cx47dKO showed significant improvement in time spent on the rotarod at different speeds compared with Cx32/Cx47dKO mice, although they did not reach the performance of WT and Cx47KO mice (Fig. 4E). Taking into consideration all behavioral results, TG^{+}Cx32/Cx47dKO mice outperformed Cx32/Cx47dKO animals in their ability for motor coordination and balance.

Kaplan–Meier analysis of the survival rates showed that Cx32/Cx47dKO mice ($n = 11$) began to die from the fourth week of age and <20% survived beyond the sixth week, while all mice died by 12 weeks. In contrast, TG^{+}Cx32KO/Cx47dKO mice ($n = 14$) showed survival rates of up to 47 weeks (maximum observation) with only one mouse that died without previous signs of encephalopathy ($P < 0.0001$) (Fig. 4F). Moreover, TG^{+}Cx32/Cx47dKO mice showed no evidence of tremor, seizures or other clinical symptoms described in Cx32/Cx47dKO mice up until this age. In conclusion, behavioral and survival analysis showed a clear phenotypic rescue of the motor deficits and long life span in TG^{+}Cx32/Cx47dKO mice.

Transgenic expression of hCx32 CNS prevents inflammation, astrogliosis and demyelination in the CNS of TG^{+}Cx32/Cx47dKO mice

To investigate whether the profound and early pathological changes developing in Cx32/Cx47dKO CNS (12,13) could be prevented in TG^{+}Cx32/Cx47dKO mice, we examined by immunostaining at 1 month of age the degree of myelination, inflammation and astrogliosis in sections of the cerebrum, cerebellum, spinal cord and optic nerves from TG^{+}Cx32/Cx47dKO and Cx32/Cx47dKO mice. Tissues were stained for myelin oligodendrocyte glycoprotein (MOG), a myelin marker and CD68, a macrophage marker. Numerous CD68 positive macrophages were detected in the spinal cord and optic nerves of Cx32/Cx47dKO mice whereas in the transgenic mice no macrophages were present. Furthermore, myelin immunoreactivity was reduced in Cx32/Cx47dKO mice but appeared normal in TG^{+}Cx32/Cx47dKO tissues (Fig. 5A–D).

Further staining for astrocytes with GFAP and microglia with Iba1 revealed increased activation of microglia in Cx32/Cx47dKO optic nerve along with increased GFAP immunoreactivity indicating astrogliosis, while these abnormalities were not seen in TG^{+}Cx32/Cx47dKO (Fig. 5E–F). Similar rescue of myelin pathology, inflammation and astrogliosis was seen in other tissues such as spinal cord and brain (not shown). Further double labeling for oligodendrocytes with CC1 and caspase-3 revealed that many oligodendrocytes in Cx32/Cx47dKO optic nerve and spinal cord were positive for this apoptotic marker, in contrast to TG^{+}Cx32/Cx47dKO showing no caspase-3 immunoreactivity (Fig. 5G–H).

Quantification of the optic nerve area covered with Iba1 as well as GFAP immunoreactivity in each group ($n = 3$ per genotype) confirmed the significant decrease of microglia activation ($P = 0.0206$) and astrogliosis ($P = 0.0319$) in TG^{+}Cx32/Cx47dKO

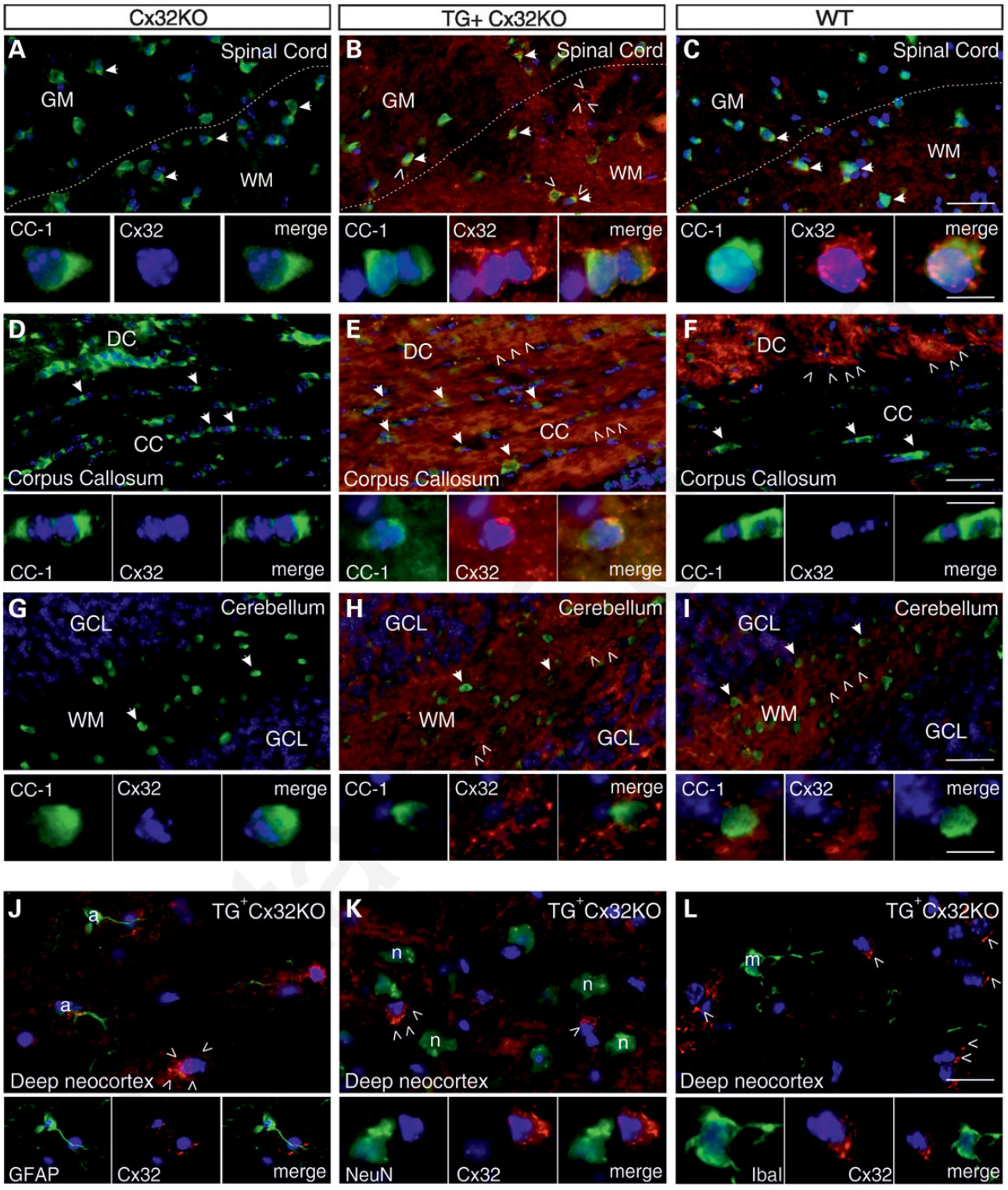

Figure 2. Transgenic expression of hCx32 in Cx32KO oligodendrocytes. These are images of spinal cord (**A–C**), cerebrum (**D–F** and **J–L**) and cerebellar cortex (**G–I**) sections from 1-month-old WT, Cx32KO and TG$^+$Cx32KO mice as indicated double labeled with Cx32 (red) and either oligodendrocyte marker CC-1 (A–I) or other cell markers as indicated (J–L) (green). Cell nuclei are stained with DAPI (blue). Cx32 is absent from all Cx32KO tissues (A, D, G) while it is expressed in the spinal cord of WT (C) and TG$^+$Cx32KO (B) mice. Cx32 forms GJ-like plaques (open arrowheads) along white matter fibers and around gray matter oligodendrocyte cell bodies (arrowheads) in the WT (C), while stronger expression also around white matter oligodendrocytes is seen in the TG$^+$Cx32KO. In the cerebrum WT mice show Cx32 expression in deep neocortex (DC) fibers but not in the corpus callosum (CC) (F), whereas TG$^+$Cx32KO mice (E) show Cx32 additionally within CC along fibers and around oligodendrocyte cell bodies. In the cerebellum of WT mice Cx32 is restricted to WM fibers (I) while in TG$^+$Cx32KO (H) it also shows strong expression in granule cell layer (GCL) oligodendrocytes. Expression of Cx32 in TG$^+$Cx32 KO CNS is not seen in GFAP+ astrocytes (a) (J), NeuN+ neurons (n) (K) or in Iba-1+ microglia (m) (L). Overview merged images and insets of separate channels are shown. Scale bars: 20 μm; in insets: 10 μm.

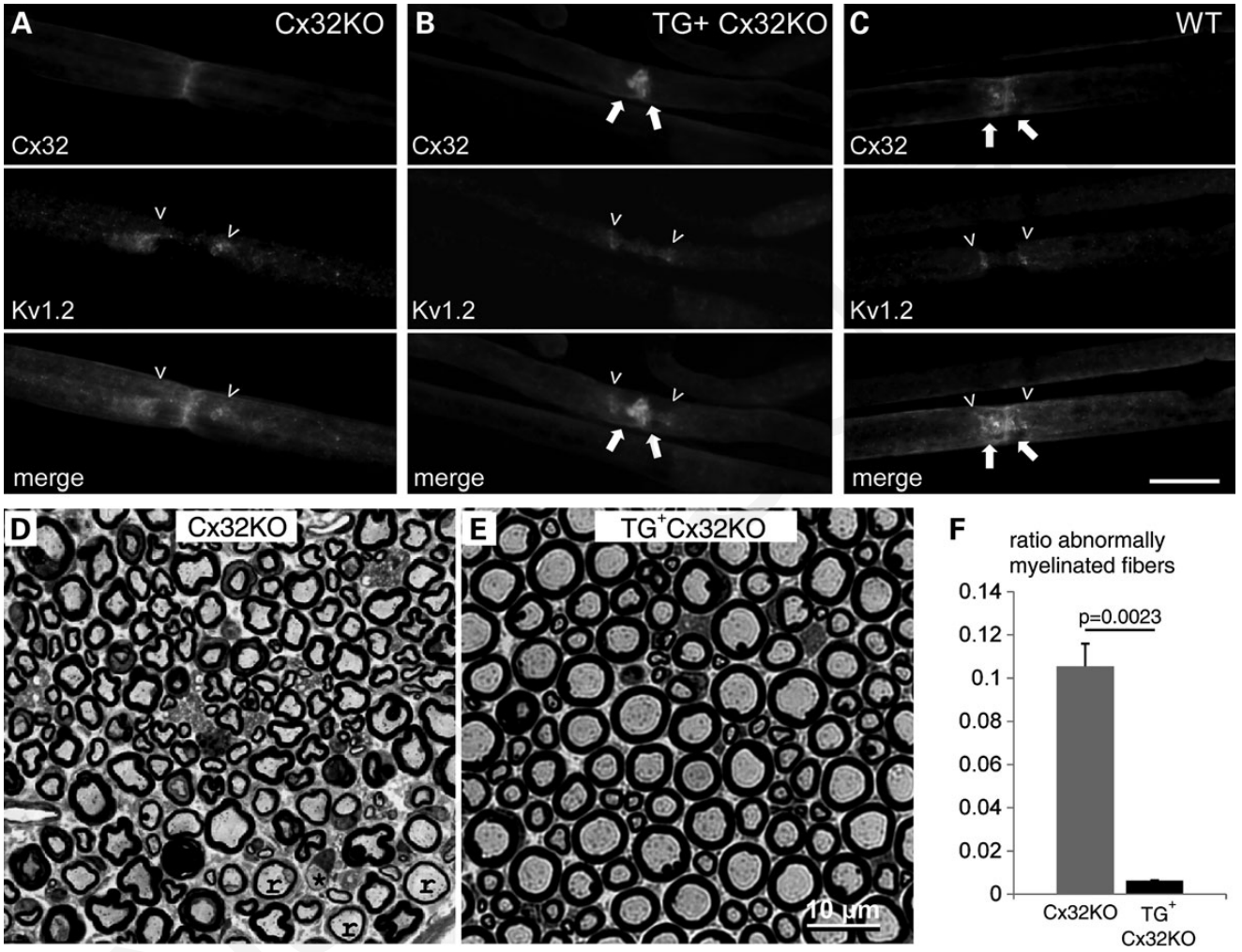

Figure 3. Transgenic Cx32 expression in Schwann cells and rescue of the peripheral neuropathy in TG+Cx32KO mice. (**A–C**) Sciatic nerve teased fibers double labeled with Cx32 and a juxtaparanodal marker, Kv1.2 (open arrowheads). Cx32 is present in non-compact myelin areas including paranodal loops (arrows) in TG+Cx32KO (B) as in WT fibers (C) but is absent from Cx32KO fibers (A). Scale bars in A–C: 10 µm. (**D–E**) Representative semithin sections from sciatic nerves of 8-month-old mice. In Cx32KO nerve (D) many axons appear to be thinly myelinated indicating previous demyelination and remyelination (**r**) and some are completely demyelinated (asterisk), whereas in TG+Cx32KO sciatic nerve (E) all axons appear normally myelinated. (**F**) Counts of abnormally myelinated fibers from both genotypes ($n = 4$ per genotype) shows a significant reduction in the ratio of abnormally myelinated fibers TG+Cx32KO compared with Cx32KO mice.

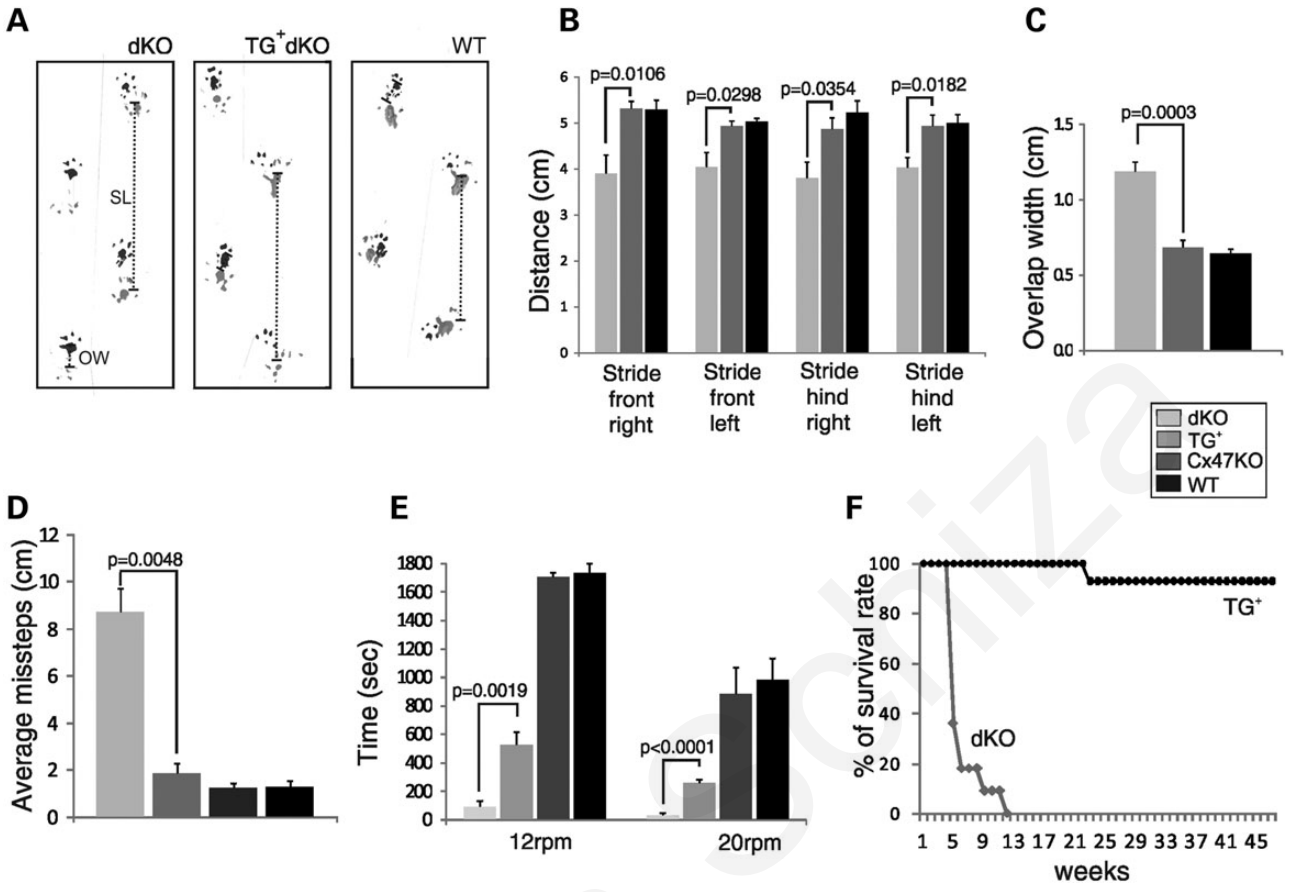

Figure 4. Phenotypic rescue of TG$^+$Cx32/Cx47dKO mice. Results of behavioral analysis of Cx32/Cx47dKO phenotype compared with TG$^+$Cx32/Cx47dKO, WT and Cx47KO mice. (**A**) Representative photographs of footprint analysis from Cx32/Cx47dKO ($n = 6$ mice in each genotype tested), TG$^+$Cx32/Cx47dKO ($n = 6$) and WT ($n = 4$) animals, indicating the parameters measured: overlap width (OW) and stride length (SL) of left and right hind- and forelimbs. (**B**) Quantification of stride length, for both right and left limbs. The front and hind stride measurements were larger in TG$^+$Cx32/Cx47dKO (and similar to WT) compared with those of the Cx32/Cx47dKO mice. (**C**) Quantification of the overlap width also shows that TG$^+$Cx32/Cx47dKO gait performance was significantly improved compared with the Cx32/Cx47dKO reaching the level of the WT mice. (**D**) Performance in foot slip test shows significant improvement in TG$^+$Cx32/Cx47dKO mice with reduced number of missteps compared with the Cx32/Cx47dKO reaching the level of the WT and Cx47KO mice. (**E**) Results of rotarod test show that TG$^+$Cx32/Cx47dKO mice performed significantly better than Cx32/Cx47dKO, although they did not reach the performance of WT and Cx47KO mice. (**F**) Kaplan–Meier curve showing the survival rates of Cx32/Cx47dKO versus. TG$^+$Cx32/Cx47dKO mice, clearly documenting a rescue of the early mortality seen in the Cx32/Cx47dKO group, TG$^+$Cx32/Cx47dKO show a normal life span.

compared with Cx32/Cx47dKO mice (Fig. 5I). Counts of caspase-3 immunoreactive optic nerve oligodendrocytes were on average 27% in the Cx32/Cx47dKO group, and <1% in TG$^+$Cx32/Cx47dKO, confirming that hCx32 expression also prevented oligodendrocyte apoptosis (Fig. 5J). Total oligodendrocyte numbers were not significantly different among the two groups at the age of 1 month (data not shown). In addition to the immunostaining results, we assessed the levels of myelin proteins by quantitative immunoblot analysis in spinal cord lysates from each group ($n = 3$ per genotype) including MOG and myelin basic protein (MBP). This analysis confirmed that both the MOG as well as the MBP levels were significantly higher in TG$^+$Cx32/Cx47dKO compared with Cx32/Cx47dKO mice ($P = 0.014$ and $P = 0.0334$, respectively) (Fig. 5K), in line with the immunostaining results.

To further confirm the immunostaining results suggesting improved CNS myelination in TG$^+$Cx32/Cx47dKO mice, we examined spinal cord and optic nerve semithin and ultrathin sections from groups of 1-month-old Cx32/Cx47dKO and TG$^+$Cx32/Cx47dKO mice. Overviews of toluidine blue stained spinal cord and optic nerve transverse sections revealed reduced myelin staining with loss of white–gray matter contrast (in the spinal cord) and numerous large vacuoles in Cx32/Cx47dKO tissues, while TG$^+$Cx32/Cx47dKO showed normal appearance (Fig. 6A–D). At higher magnification semithin and electron microscopy images of anterior and posterior funiculi of the spinal cord from Cx32/Cx47dKO mice the majority of large axons showed enlarged extracellular spaces separating the myelin sheath from the axon. Some were thinly myelinated and most of them completely demyelinated. Similar findings were present in the optic nerve with vacuolization and demyelination of most axons. These pathological changes were absent in TG$^+$Cx32/Cx47dKO spinal cord or optic nerve (Fig. 6E–N). Quantification of myelin volume density in the anterior and posterior spinal cord funiculi as well as in the optic nerve in groups of 1-month-old mice confirmed that myelin density was significantly increased in TG$^+$Cx32/Cx47dKO mice compared with the Cx32/Cx47dKO mice in all areas examined (Fig. 6O).

Gap junction formation in oligodendrocytes of TG$^+$Cx32/Cx47dKO mice

To determine whether the transgenic expression of hCx32 was sufficient to allow the re-establishment of oligodendrocyte GJ connectivity in TG$^+$Cx32/Cx47dKO mice, including O/O, O/A and

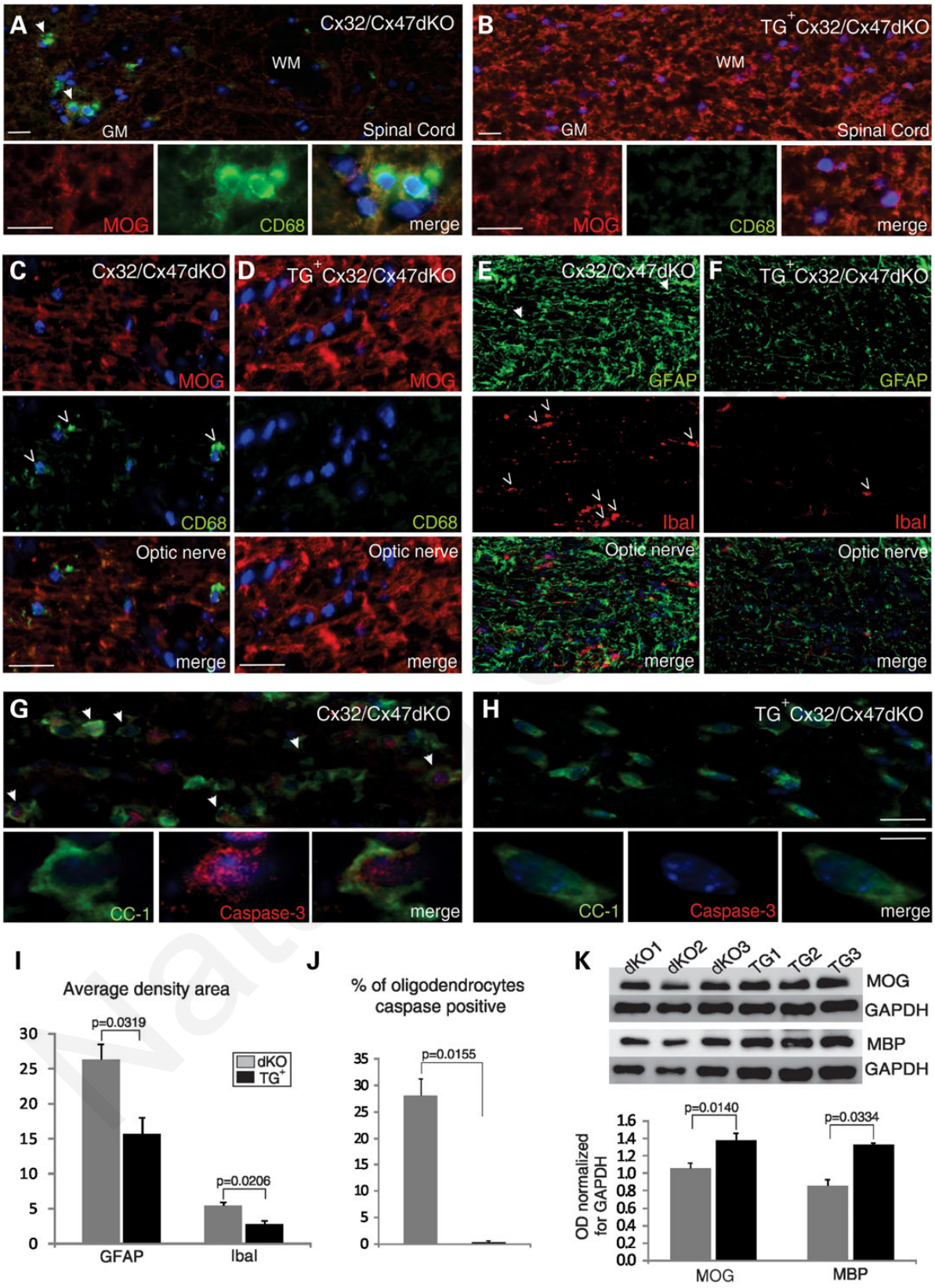

Figure 5. Rescue of demyelination, inflammation and astrogliosis in transgenic Cx32/Cx47dKO mice. Spinal cord including white matter and gray matter (**A** and **B**) and optic nerve (**C** and **D**) sections from Cx32/Cx47dKO and TG$^+$Cx32/Cx47dKO mice as indicated double labeled for myelin oligodendrocyte protein (MOG, red) and macrophage marker (CD68, green) show improved myelin immunoreactivity and absence of macrophages (arrowheads) in TG$^+$Cx32/Cx47dKO as opposed to Cx32/Cx47dKO mice. (**E** and **F**) Double labeling of optic nerve sections with astrocytic marker GFAP and microglial marker Iba1 (arrowheads), shows astrogliosis and microglial activation in the Cx32/Cx47dKO which are absent in the TG$^+$Cx32/Cx47dKO. (**G** and **H**) Optic nerve sections double labeling with apoptosis marker caspase-3

intra-myelin GJs, we double labeled for Cx32 and all other major astrocyte and oligodendrocyte connexins including Cx30, Cx43 and Cx29, comparing TG$^+$Cx32/Cx47dKO with Cx32/Cx47dKO and Cx47KO mice. The latter should have comparable GJ connectivity to the TG$^+$ since they endogenously express Cx32 but not Cx47 in oligodendrocytes. In all TG$^+$Cx32/Cx47dKO CNS regions examined including the spinal cord, cerebrum and cerebellum, Cx32 showed the same localization in cell bodies and along myelinated fibers in all subpopulations of oligodendrocytes as in TG$^+$Cx32KO CNS (Fig. 2).

Double staining of Cx32 with astrocytic Cx30, known to partner with Cx32 (15) showed that Cx30 was diffusely expressed mostly in the gray matter forming GJ-like plaques, which colocalized with Cx32 GJ plaques around oligodendrocytes in TG$^+$Cx32/Cx47dKO similar to Cx47KO mice. In contrast, Cx30 showed no colocalization with oligodendrocytes in Cx32/Cx47dKO mice in which Cx32 was absent (Fig. 7A–C). Double staining with Cx43 showed the typical expression of Cx43 forming diffuse GJ plaques in gray matter with weak colocalization with Cx32 GJ plaques around oligodendrocytes in TG$^+$Cx32/Cx47dKO and even less in Cx47KO mice. Cx32/Cx47dKO mice showed stronger Cx43 immunoreactivity in gray matter areas, likely reflecting astrogliosis, with absence of Cx32 (Fig. 7D–F). Cx29 was normally localized along thinly myelinated fibers in the spinal cord gray matter, in the cerebellum and in the cerebrum in all three genotypes without apparent differences. Cx32 was expressed along medium and large myelinated fibers mostly without colocalization with Cx29 in TG$^+$Cx32/Cx47dKO and Cx47KO mice, while it was absent in Cx32/Cx47dKO (Fig. 7G–I).

Counts of GJ plaques surrounding oligodendrocytes in confocal images of spinal cord gray matter revealed similar numbers of Cx30 GJ plaques in all genotypes, while Cx32 GJ plaques were increased in TG$^+$Cx32/Cx47dKO compared with Cx47KO mice and showed higher overlap ratios with Cx30 GJ plaques (Fig. 7J). Counts of Cx43 plaques were significantly increased in Cx32/Cx47dKO compared with TG$^+$Cx32/Cx47dKO or Cx47KO mice, likely reflecting astrogliosis. Also with this double labeling Cx32 GJ plaques showed higher counts in transgenic compared with Cx47KO mice, as well as increasing overlap with Cx43 (Fig. 7K). However, Cx32 GJ plaques around TG$^+$Cx32/Cx47dKO oligodendrocytes showed significantly lower overlap levels with Cx43 than with Cx30 ($P < 0.0001$), indicating that transgenically expressed Cx32 forms O/A GJs mainly through coupling with Cx30.

Transgenic expression of Cx32 was also examined in different WM areas of TG$^+$Cx32/Cx47dKO compared with Cx32/Cx47dKO and Cx47KO mice, including the spinal cord WM, cerebellum, optic nerve and cerebrum at the CC level. In the spinal cord and cerebellar WM of TG$^+$Cx32/Cx47dKO and Cx47KO mice Cx32 was expressed along large diameter myelinated fibers, but TG$^+$Cx32/Cx47dKO mice additionally showed Cx32 GJ plaques at oligodendrocyte cell bodies. Cx32 did not colocalize with Cx43 GJ plaques that were diffusely present in all WM areas (Supplementary Material, Fig. S1A–C). While Cx47KO mice showed the expected mutually exclusive expression of Cx29 along thin fibers and of Cx32 along large fibers (8), in TG$^+$Cx32/Cx47dKO there was some expression of Cx32 also along thin fibers colocalizing with Cx29 (Supplementary Material, Fig. S1D–F). Similar expression pattern was found in cerebellum, in which Cx32 formed GJ plaques in WM fibers in both Cx47KO and TG$^+$Cx32/Cx47dKO mice, but in addition there was expression along thin fibers of the molecular layer only in the TG+ (Supplementary Material, Fig. S1G–L). In WM areas were Cx32 is not physiologically expressed, including the optic nerve and CC (11), Cx47KO showed no Cx32 expression, while TG$^+$Cx32/Cx47dKO showed Cx32 forming GJ plaques at oligodendrocyte cell bodies with partial colocalization with Cx43, as well as along thinly myelinated fibers colocalizing with Cx29. In Cx47KO and Cx32/Cx47dKO optic nerve and CC Cx32 was absent (Supplementary Material, Fig. S1M–R; and data not shown).

In conclusion, these findings suggest that transgenic expression of hCx32 in GJ-deficient oligodendrocytes of Cx32/Cx47dKO leads to strong GJ formation along the myelinated fibers, with some ectopic expression along thin fibers as well, as well as re-establishment of O/A heterotypic connections mainly between Cx32 and Cx30 in the GM, and in the WM also by homotypic O/O GJs, similar to the connectivity in Cx47KO CNS. However, Cx32 does not appear to be able to replace Cx47 in O/A connections with Cx43.

Discussion

Phenotypic and pathological rescue of the Cx32/Cx47dKO mice

We have successfully generated transgenic lines strongly expressing hCx32 specifically in oligodendrocytes throughout the CNS, as confirmed by our expression analysis on Cx32KO background. Reestablishment of GJ connectivity in oligodendrocytes rescued the severe phenotype of early CNS demyelination and death in Cx32/Cx47dKO mice. Furthermore, expression of Cx32 in Schwann cells prevented the peripheral neuropathy in Cx32KO mice, confirming that connexin loss in both central and peripheral myelinating cells causes disease through cell autonomous effects.

The Plp promoter has been shown to drive expression specifically in oligodendrocytes (23–25). Interestingly, our results confirm that the Plp promoter is also active in Schwann cells, although at lower levels compared with oligodendrocytes, as also reported in previous studies. Our transgene expression levels in the CNS were overall higher, up to 3-fold, compared with WT Cx32 expression. This is both due to higher expression in each oligodendrocyte, as shown by the increased number of Cx32 GJ plaques per cell compared with the Cx47KO (Fig. 7), as well as due to the extra-physiological expression in all oligodendrocytes, such as those in the CC and optic nerves, in contrast to restricted Cx32 expression in specific subpopulations in WT CNS (11). Plp-driven expression levels were higher compared with CNP-driven expression in previously generated mutants, reflecting the higher expression per cell, since CNP promoter also provided expression in all subsets of oligodendrocytes (7).

There was no obvious adverse effect of Cx32 expression beyond the known subsets of oligodendrocytes, and these

and oligodendrocyte marker CC-1 confirms that many oligodendrocytes undergo apoptosis in Cx32/Cx47dKO (arrowheads) but none in TG$^+$Cx32/Cx47dKO. Nuclei are labeled with DAPI (blue). (**I**) Quantification of optic nerve GFAP and Iba1 immunoreactivity in groups of mice ($n = 4$ per genotype) confirms significant improvement of astrogliosis and inflammation in TG$^+$Cx32/Cx47dKO compared with Cx32/Cx47dKO. (**J**) Counts of caspase-3 positive apoptotic oligodendrocytes are significantly reduced in TG$^+$Cx32/Cx47dKO compared with Cx32/Cx47dKO. (**K**) Quantitative immunoblot analysis of MBP and MOG in spinal cord lysates of Cx32/Cx47dKO and TG$^+$Cx32/Cx47dKO mice ($n = 3$ per genotype) at 1 month of age shows that the levels of both myelin proteins normalized for loading are significantly increased in transgenic tissues. GAPDH blots are shown as loading control. Scale bars: (A–B) 200 μm; (C–H) 20 μm; in insets: 10 μm.

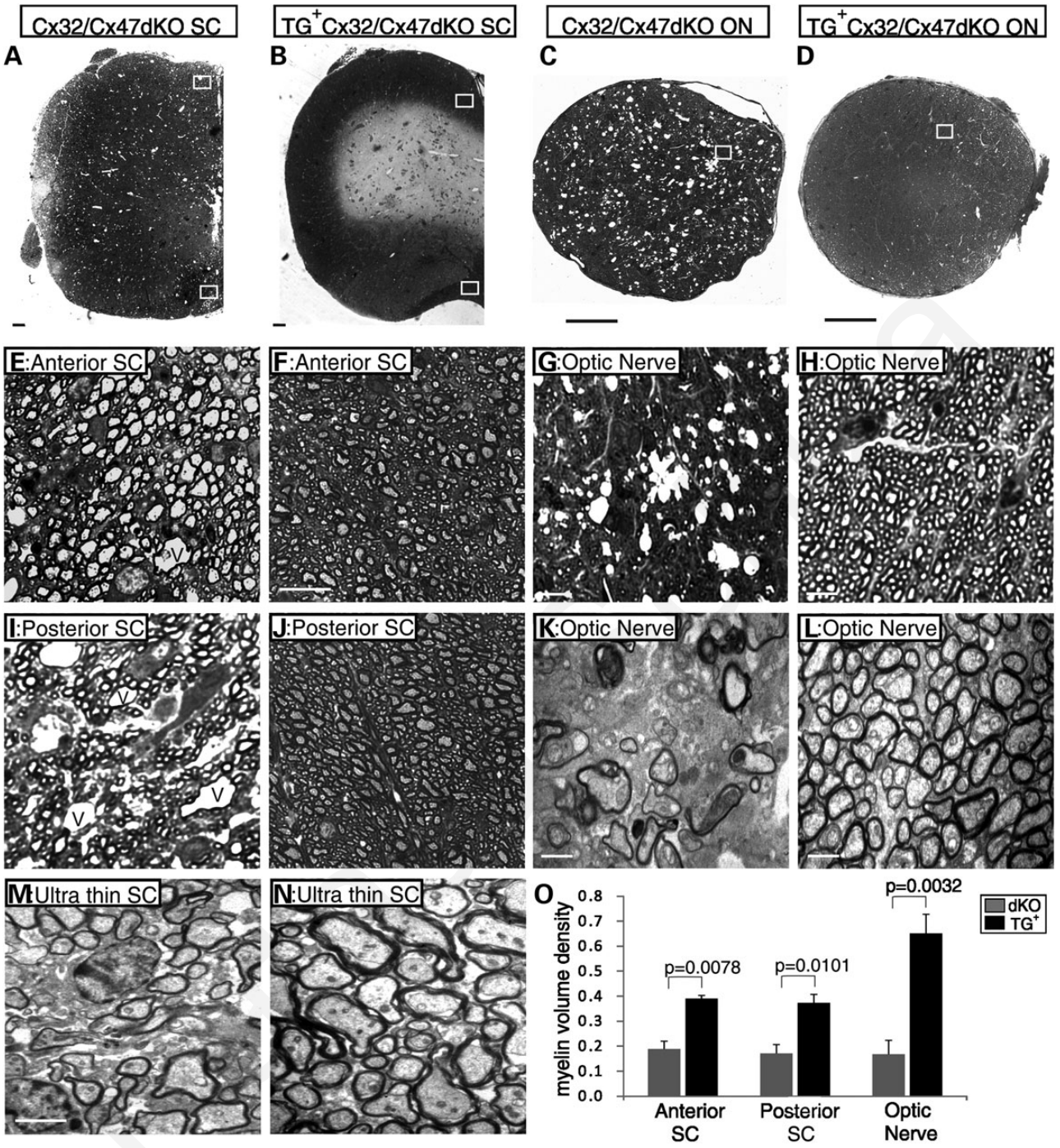

Figure 6. Prevention of CNS demyelination in TG$^+$Cx32/Cx47dKO mice. Photomicrographs of semithin (**A–J**) and ultrathin (**K–N**) sections from spinal cord and optic nerves from 1-month-old mice. Overview of transverse sections from Cx32/Cx47dKO and TG$^+$Cx32/Cx47dKO spinal cords (A and B) and optic nerves (C and D), as indicated as well higher magnification images of Cx32/Cx47dKO anterior and posterior spinal cord (E, I and M) reveal that many axons appear thinly myelinated and some demyelinated with extensive vacuolation (V) whereas in TG$^+$Cx32/Cx47dKO mice (F, J and N) axons appear normally myelinated. A marked loss of myelinated axons and vacuole formation in the myelin sheaths are also noticed in Cx32/Cx47dKO optic nerves whereas in TG$^+$Cx32/Cx47dKO most optic nerve axons are normally myelinated (C–D, G–H, K–L). Scale bars: (A and B) 200 μm; (C–F, I, J) 10 μm; (G, H, K, L) 2 μm; (M and N) 2.5 μm. (**O**) Myelin volume density measured in semithin sections from anterior and posterior spinal cord funiculus as well as optic nerves ($n = 4$ mice in each group) reveals that myelin density is significantly increased in TG$^+$Cx32/Cx47dKO compared with Cx32/Cx47dKO in both spinal cord and optic nerve.

expression levels were sufficient to rescue the CNS phenotype of Cx32/Cx47dKO mice, similar to what has been achieved in the PNS using the P0 promoter transgene (20). Interestingly, peripheral neuropathy was also rescued in this model, even with expression levels slightly below the WT levels, while P0 promoter-driven transgenic Cx32 expression levels in Schwann cells were much higher than WT levels (20).

The main goal of this project was to rescue the Cx32/Cx47dKO leukodystrophy model by replacing one of the two missing oligodendrocyte connexins, in this case hCx32. Cx32/

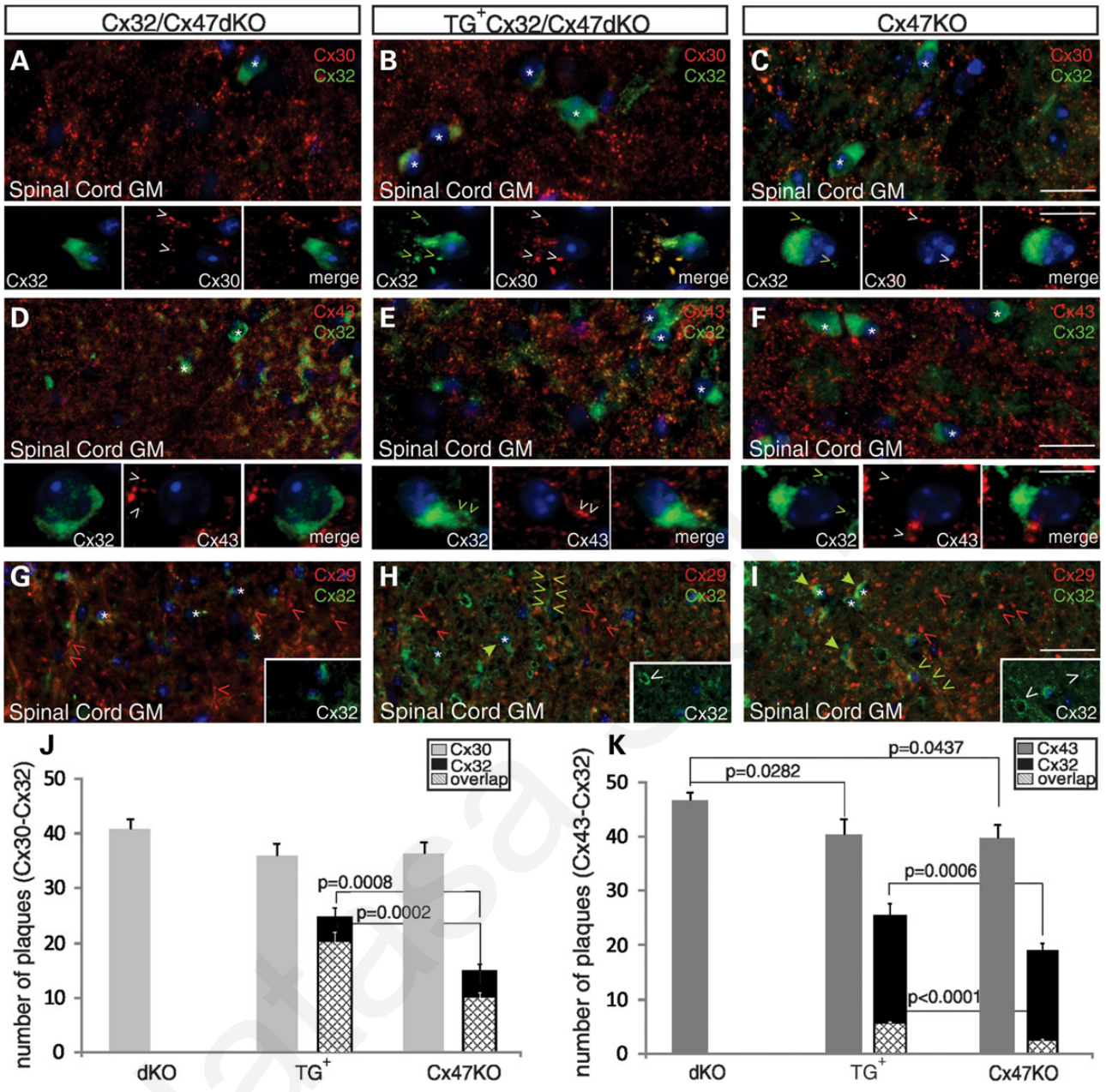

Figure 7. Gap junction formation by hCx32 in TG$^+$Cx32/Cx47dKO gray matter oligodendrocytes. These are images of transverse sections from the indicated CNS gray matter (GM) regions of Cx32/Cx47dKO, TG$^+$Cx32/Cx47dKO and Cx47KO mice. Sections were double labeled with anti-Cx32 (green) and either anti-Cx30 (**A–C**), anti-Cx43 (**D–F**) or anti-Cx29 (**G–I**) antibodies (red). Cell nuclei are visualized with DAPI (blue). Note that due to the replacement of Cx47 ORF with EGFP in Cx47KO mice oligodendrocyte cell bodies are green fluorescent in all three genotypes (asterisks). (A–C) Cx30 forms GJ plaques (open arrowheads) diffusely in the gray matter in all genotypes, but shows colocalization with Cx32 GJ plaques around oligodendrocytes only in TG$^+$Cx32/Cx47dKO and Cx47KO mice indicating the formation of O/A channels, but not in Cx32/Cx47dKO mice in which Cx32 is absent. In TG$^+$Cx32/Cx47dKO and Cx47KO mice, Cx32 forms GJ plaques also along medium size myelinated fibers (green open arrowheads). (D–F) Cx43 forms diffusely GJ plaques that appear increased in Cx32/Cx47dKO in which Cx32 is absent, compared with TG$^+$Cx32/Cx47dKO and Cx47KO. Some Cx43 GJ plaques colocalize with Cx32 around oligodendrocytes in TG$^+$Cx32/Cx47dKO and Cx47KO mice but less than Cx30. (G–I) Cx29 shows expression along thin myelinated fibers in all three genotypes (red open arrowheads), while Cx32 is expressed along larger fibers (green open arrowheads) only in Cx47KO and TG$^+$Cx32/Cx47dKO mice without colocalization with Cx29. Scale bars, 20 μm; in insets, 10 μm. Counts of GJ plaques formed by Cx30 and Cx32 (J) or by Cx43 and Cx32 (K) around individual spinal cord GM oligodendrocytes show that Cx32 GJs are significantly increased in TG$^+$Cx32/Cx47dKO compared with Cx47KO mice and are absent from Cx32/Cx47dKO. Moreover, the percentage of Cx32 GJ plaques overlapping with Cx30 as well as with Cx43 is increased in TG$^+$Cx32/Cx47dKO compared with Cx47KO. Cx30 GJ plaque counts do not differ between genotypes, while Cx43 GJ plaque counts are significantly increased in Cx32/Cx47dKO mice.

Cx47dKO mice have been characterized in detail (12,13) and provide a relevant model of hypomyelinating leukodystrophy offering an opportunity to study possible therapeutic interventions. In our hands, Cx32/Cx47dKO mice presented the previously reported phenotype of action tremor followed by tonic seizures during the fourth to fifth postnatal week, which increased in frequency and severity leading to death by the sixth postnatal week. Pathological analysis at 1 month of age showed the

expected severe demyelination, axonal degeneration and apoptosis of oligodendrocytes in the spinal cord funiculi and in the optic nerve. Both the behavioral as well as the pathological comparison of Cx32/Cx47dKO with TG$^+$Cx32/Cx47dKO mice clearly demonstrated that Plp-driven Cx32 replacement rescued the Cx32/Cx47dKO phenotype.

TG$^+$Cx32/Cx47dKO mice outperformed Cx32/Cx47dKO mice in all tests of motor performance reaching the performance level of Cx47KO and WT mice. Only in the rotarod test, although clearly improved compared with Cx32/Cx47dKO littermates, TG$^+$Cx32/Cx47dKO mice remained below the performance of Cx47KO and WT mice. The reason for this discrepancy is unclear. In contrast to Cx47KO or WT mice with normal Cx32 expression in Schwann cells, lower than physiological Cx32 expression in TG$^+$Cx32/Cx47dKO Schwann cells could have caused a degree of peripheral neuropathy at 1 month of age, contributing to the lower rotarod performance. Finally, examining the survival rates between the two groups confirmed that transgenic Cx32 expression rescued the early mortality in Cx32/Cx47dKO mice and allowed a normal life span.

The behavioral correction of TG$^+$Cx32/Cx47dKO mice was accompanied by a complete rescue of the pathological changes that are typical for Cx32/Cx47dKO mice (12,13). Immunostaining and immunoblot analysis of myelin proteins, as well as electron microscopy with morphometric analysis demonstrated that the severe demyelination and vacuole formation in spinal cord gray and WM, cerebrum, cerebellum and optic nerve were prevented, while oligodendrocyte apoptosis was significantly reduced. Furthermore, secondary inflammatory changes that have been described in PMLD models with GJ-deficient oligodendrocytes (5), including activation of microglial cells and recruitment of macrophages, as well as astrogliosis, reflected in increased GFAP and Cx43 immunoreactivity, were prevented in our TG$^+$Cx32/Cx47KO mice. These inflammatory changes are likely to play a role in disease progression similar to what has been shown for Cx32KO mice in the PNS (26,27), as well as in experimental models of CNS myelin gene defects (28–30).

Oligodendrocyte GJs in TG$^+$Cx32/Cx47dKO mice

Our analysis of GJ formation in oligodendrocytes in TG$^+$Cx32/Cx47dKO mice revealed that Cx32 was extensively expressed along myelinated fibers, forming the homotypic intracellular channels, and also along fibers that normally express only Cx29, such as the CC and optic nerves (11,14). Furthermore, numerous Cx32 GJ plaques were formed around the cell bodies and were overall increased compared with Cx47KO mice, colocalizing mostly with Cx30 and to a much lesser degree with Cx43. Thus, transgenic replacement of Cx32 in the Cx32/Cx47dKO mouse appears to reestablish in part oligodendrocyte GJ connectivity, but does not replace Cx47 in O/A GJs, the majority of which are formed by Cx47 paired with Cx43 (10,14,17,31). Therefore, the TG$^+$Cx32/Cx47dKO phenotype resembles that of Cx47KO mice. Even with the high levels of Cx32 expression achieved in all oligodendrocytes, Cx32 is likely to form only heterotypic O/A GJs with astrocytic Cx30, and homotypic O/O GJs with itself. This is in keeping with previous studies showing lack of coupling between transfected cells where one expresses Cx32 and the other Cx47 (15,32). Furthermore, Cx32 is unlikely to replace Cx47 in pairing with Cx43, since the available literature indicates that no functional Cx32/Cx43 channels can be formed (15,32,33).

Mice that lack Cx32 or express Cx32 mutants on Cx32KO background, such as T55I and R75W develop a progressive demyelinating peripheral neuropathy after 3 month of age (21) with subtle changes in the CNS myelin (7,34). Cx47KO mice show sporadic vacuolation of CNS myelinated fibers starting from the optic nerve. Myelination of the peripheral nerves is not affected by the deletion of Cx47 (12,13). In humans, unlike mice, loss of Cx47 function leads to PMLD or spastic paraparesis (1,16), while loss of Cx32 only rarely (35), suggesting that Cx47 is more crucial for oligodendrocyte function and survival. Cx47 may play more important roles during development and oligodendrocyte differentiation and myelination (13): its expression in developing oligodendrocytes precedes those of Cx32 and Cx29 (36). Moreover, oligodendrocytes throughout the CNS express Cx47 but only certain subpopulations express Cx32 (11,14).

Supporting these findings from rodent models, oligodendrocyte precursor cells in postmortem human brain studies were shown to express Cx47 but not Cx32, while mature oligodendrocytes express Cx47 throughout the human brain, similar to the expression pattern in rodents (37,38). Taken together, while our study provides the proof of principle for amelioration of phenotype by replacing—at least in part—GJ connectivity in oligodendrocytes in this PMLD model, it may be necessary to replace Cx47 in future clinical studies, since the presence of Cx32 in PMLD patients does not prevent the disease. Interestingly, a *GJC2* mutation affecting O/O but not O/A GJ connectivity was found in a subclinical leukodystrophy patient (39), indicating that even partial restoration of oligodendrocyte connectivity as described in our model may be sufficient to ameliorate the clinical phenotype, also in the human disease.

Why the loss of Cx47 is more detrimental for humans with PMLD as opposed to Cx47 KO mice is not clear, but may be related to several factors operating in humans that are not present in mice. Greater life span and brain size is a consideration, as well as stressful conditions that increase metabolic demand and requirements on GJ connectivity in oligodendrocytes, as also recognized for the CNS phenotypes resulting from Cx32 mutations (3,35). This metabolic stress occurs only under experimental conditions in laboratory mice and has indeed caused increased myelin vacuolation flowing increased axonal activity in Cx47 KO mice (40). Another consideration is that Cx32/Cx30 channels can compensate for the loss of Cx47/Cx43 channels in mice more effectively than in humans, although the overall distribution of glial connexin expression appears to be similar between human and rodent brain (11,19,37,38).

Oligodendrocyte connectivity to panglial network

Oligodendrocytes are closely connected to astrocytes via GJs. Both human disorders such as occulodental digital dysplasia syndrome resulting from *GJA1*/Cx43 mutations (41), as well as mouse models with astrocyte connexin deletions may cause demyelination, highlighting the importance of the panglial network connectivity for oligodendrocytes. Besides the Cx32/Cx47dKO model, various other double connexin mutants including astrocytic connexins have sown similar phenotypes: The deletion of two astrocytic connexins in Cx30/Cx43$_{Astro}$dKO resulted in early onset vacuolation, edema, astrogliosis and oligodendrocyte apoptosis in the brain, as well as multiple behavioral deficits, although life span was normal (31,42). Overall, the WM abnormalities in these mutants resembled the ones in Cx32/Cx47dKO mice, but their milder phenotype highlighted the importance of O/O GJs (43,44) that were preserved as opposed to the Cx32/Cx47dKO.

Deletion of one astrocytic and one oligodendrocytic connexin proved to be more pathogenic than the loss of two astrocytic connexins, and resembled more the loss of two oligodendrocyte connexins. Cx32/Cx43$_{Astro}$KO mice (with mGFAP-cre driven deletion of Cx43) developed WM vacuolation by the fifth week and seizures by the eighth week with early mortality by 20 weeks (45). However, mGFAP-cre driven Cx43$_{Astro}$KO might have been incomplete and subsequent generation of another Cx32/Cx43$_{Astro}$dKO (with nestin-cre driven deletion of Cx43) resulting in complete deletion of Cx43 in astrocytes demonstrated loss of oligodendrocytes with demyelination and more phenotypic similarities to Cx32/Cx47dKO (46). Furthermore, Cx47 expression in oligodendrocytes and stability on the cell membrane was shown to depend in the presence of Cx43 in astrocytes, indicating that in the Cx32/Cx43dKO Cx47:Cx30 O/A are also lost, and only homotypic O/O Cx47 GJs may be preserved, explaining the severity of the phenotype resembling Cx32/Cx47dKO. Likewise, Cx30/Cx47dKO mice showed early onset myelin pathology, severe vacuolation in the WM and activation of microglia and astrocytes, leading to early mortality (47). As described in our study, this double mutant demonstrates that Cx32 cannot replace Cx47 in O/A GJs, but can only form channels with Cx30 in astrocytes. Overall, the results of glial connexin mutants highlight the importance of both O/O and O/A GJs for CNS myelination and homeostasis.

In conclusion, we show that the severe phenotype of the hypomyelinating leukodystrophy model with GJ-deficient oligodendrocytes can be rescued by replacement of one, in this case Cx32, oligodendrocyte connexins, by reestablishing, at least in part, the O/O and O/A connectivity. This study has implications for future therapeutic trials targeting CNS and PNS disorders resulting from connexin mutations, including PMLD and CMT1X.

Materials and Methods

Cloning of the transgenic construct

The transgenic construct was generated using the ~11 kb mouse Plp promoter cloned in pBluescript SK+ vector (a gift from Prof. Karagogeos laboratory, University of Crete) previously used successfully to generate transgenic mice driving expression specifically in oligodendrocytes (24,48–50) and downstream cloning of the human *GJB1*/Cx32 open reading frame (ORF) obtained from the pSLN1180 vector (7). To have compatible sites with the MCS of the pBluescript SK+ vector, two new restriction sites, *Asc*I and *Pac*I, were introduced in pSLN1180 vector by PCR amplification using the following primers: *Asc*I-F1 (5-′TACGCGTACG GCGCGCCCGCGGACA-3′) and *Pac*I-R (5′CCTTAATTAAGGGGCG GATCCTCAGCAGGCCGAGCA-3′). The hCx32 ORF was isolated from pSLN1180 vector using *Asc*I and *Pac*I restriction enzymes, purified and ligated downstream of the PLP promoter in pBluescript SK+. Colonies were screened by PCR using two primer sets: Plp-F1 (5′-TGGGTGTTGGTTTTTGGAGA-3′) and Cx32-R (5-CGCTFTTGCAGCCAGGCTGG-3′) resulting in a 824 bp PCR product (94°C for 5 min 40 cycles of 94°C × 30 s, 60°C × 30 s, 72°C × 30 s and then 72°C for 7 min), as well as withPlp-F2 (5′CTGAG-TATTGTAGGCAAGGG-3′) and Cx32-R resulting in a 528 bp product. The transgenic cassette (PLP promoter with hCx32) (Fig. 1A) was then released from pBluescript SK+ by double digestion with *Apa*I and *Not*I. The ~12 kb band was isolated and purified using Qiagen Gel extraction kit and finally eluted in microinjection buffer (Millipore, MR-095-F). The orientation and the in-frame positioning of the transgenic construct was further confirmed by direct sequencing analysis, including the entire ORF.

Animal strains and procedures

For this study we used C57BL/6 mice (Harlan Laboratories) for generation of transgenic lines, as well as *Gjb1*-null/Cx32 knockout (KO) mice (C57BL/6_129) (51) and *Gjc2*/Cx47 KO mice (C57BL/6;129P2/OlaHsd) (13), both obtained from the European Mouse Mutant Archieve Monterotondo, Italy (originally generated by Prof. Klaus Willecke, University of Bonn). For all studies mice received anesthesia with intraperitoneal Avertin injection and then were either transcardially perfused and tissues were fixed for immunostaining analysis or electron microscopy, or tissues were removed unfixed for immunoblot and RNA analysis. All experimental procedures were conducted in accordance with the animal care protocols approved by the Cyprus Government's Chief Veterinary Officer according to EU guidelines (EC Directive 86/609/EEC).

Generation of transgenic mice expressing the WT human Cx32

The purified fragment was microinjected into the male pronucleus of fertilized oocytes obtained from C57BL/6 mice according to standard protocols at the Mouse Facility of the Cyprus Institute of Neurology and Genetics. After successful pregnancies and offspring delivery, founders were PCR screened by genomic tail DNA with specific primer sets for Plp promoter and Cx32 gene. Two primer sets were used for the promoter region (proximal ligation site) and one for the distal ligation site to the multiple cloning site: (i) Plp-F1 and Cx32-R (as above) (ii) PlpF2 and Cx32-R (as above) and (iii) PlpMCS-F (5′-AGGTTTAAACAGTC GACTCTAG-3′) and Cx32-F2 (5′-GGCTCACCAGCAACACATAG-3′) resulting a 600 bp product (Fig. 1B). Founders (TG$^+$) were bred with *Gjb1*-null/Cx32 KO mice in order to obtain mice expressing the transgene on a Cx32KO background (TG$^+$Cx32KO).

Generation of TG$^+$Cx32/Cx47dKO and Cx32/Cx47dKO mice

Cx47KO mice were crossed with transgenic mice on a Cx32KO background (TG$^+$Cx32KO). The mouse Cx47 coding region has been replaced with enhanced green fluorescent protein (EGFP) reporter gene in these mice. The Cx32 gene is located on the X chromosome and Cx47 gene is autosomal. F1 offspring was then crossed again to obtain males TG$^+$Cx32KO/Cx47Het and Cx32KO/Cx47Het. Offspring of F2 generation were breed again to obtain TG$^+$Cx32KO/Cx47dKO and Cx32KO/Cx47dKO. Cx32 genotype was tested by PCR screening using primers mentioned above. Cx47 genotype was screened by multiplex-PCR using simultaneously three primers. One primer is Cx47 intron-specific (P1-5′-CAGGATCAATGGAAGATTCTCGGTCCC-3′), the second is exon-specific (P3-5′-GCCAAGCGGTGGACTGCSTSGCCCAGG-3′) and the last EGFP-specific (P4) under conditions 95°C for 5 min 40 cycles of 94°C × 45 s, 64°C × 45 s, 72°C × 1 min and then 72°C for 7 min. A band at 530 bp represents the WT allele and at 340 bp the Cx47KO allele (13) (Fig. 1B).

Reverse transcription PCR

Snap-frozen brain and spinal cord tissue from TG$^+$Cx32KO, Cx32KO and WT mice were collected. RNA was isolated with the RNeasy Lipid Tissue Mini Kit (QIAGEN) following manufacturer's protocol. DNase treatment was performed and RNA was quantified by spectrophotometry. Of note, 0.5 μg of RNA was used to synthesize cDNA using Taqman Reverse transcription reagents (Applied Biosystems). cDNA was amplified using Cx32-F (5′-TGAGGCAGGATGAACTGGACAGGT-3′) and Cx32-R (5′-CAC

GAAGCAGTCCACTGT-3′) primers. cDNA was then digested with *Msc*I or *Hha*I as well as with both enzymes. *Msc*I cuts the human cDNA into two fragments (280 and 273 bp); *Hha*I cuts the mouse cDNA product into two fragments (230 and 323 bp). Digestions were run on 1.5% agarose gel to estimate the relative levels of transgene/human and endogenous/mouse mRNAs (Fig. 1C).

Immunoblot analysis

Fresh mouse tissues were collected and lysed in ice cold RIPA buffer (10 mM sodium phosphate, pH 7.0, 150 mM NaCl, 2 mM EDTA, 50 mM sodium fluoride, 1% NP-40, 1% sodium deoxycholate and 0.1% SDS) containing a cocktail protease inhibitors (Roche, Basel, Switzerland). Tissues were sonicated and protein concentrations were measured on NanoDrop. Fifty micrograms of protein from each tissue lysate were loaded into each well and fractioned by 12% SDS-PAGE gel. Then proteins were transferred to a Hybond-C extra membrane (GE Healthcare Bio-Sciences), using semidry transfer unit. Nonspecific sites on the membrane were blocked with 5% non-fat milk in Tris-buffered saline containing 0.1% Tween 20 (TBS-T) for 1 h (h) at room temperature (RT). Immunoblots were then incubated with rabbit antiserum against Cx32 (Clone 918, 1 : 5000; (18) in 5% milk and TBS-T, at 4°C overnight. After washing away excess primary antibody, immunoblots were incubated with anti-rabbit or anti-mouse horseradish peroxidase-conjugated secondary antiserum (Jackson ImmunoResearch Laboratories, 1 : 3000) in 5% milk-TBS-T, for 1 h. GAPDH antibody (Santa Cruz, 1 : 4000) was then incubated on the same membranes and used as a loading control. The bound antibody was visualized by enhanced chemiluminescence system (ECL Plus, GE Healthcare Bio-Sciences, Amersham). Band intensity was measured and quantified using TinaScan software version 2.07d.

Immunohistochemistry

Following transcardial perfusion with 4% paraformaldehyde, brain, spinal cord, optic and sciatic nerves were post fixed for 30 min in the same fixative and then cryoprotected in 20% sucrose in 0.1 M PB buffer overnight. Tissues were then embedded in OCT and placed in ice cold-acetone and stored in −80°C. Ten micrograms of thick sections were thaw-mounted onto glass slides. Tissues were permeabilized in cold acetone (−20°C) for 10 min and incubated at RT with blocking solution of 5% bovine serum albumin containing 0.5% Triton X-100 for 1 h followed by incubation overnight at 4°C with various combinations of primary antibodies: mouse anti-Cx32 (Zymed, 1 : 50), rabbit Cx32 (Zymed, 1 : 50), Cx29 (Zymed, 1 : 300), Cx30 (Invitrogen 1 : 500), Cx43 (Cell signaling, 1 : 50), CC-1 (Calbiochem, 1 : 50), *Glial fibrillary acidic protein* (GFAP) (Invitrogen, 1 : 400), NeuN (Chemicon, 1 : 400), MBP (Abcam, 1 : 50), CD68 (Serotec, 1 : 100), Caspase-3 (Millipore, 1 : 20), Iba-1 (Biocare medical, 1 : 300), MOG (UK, 1 : 50). Sections were washed in PBS and incubated with rhodamine (TRITC) conjugated Affinity Pure Goat Anti-rabbit IgG and Fluorescin (FITC) conjugated AffiniPure Goat Anti-Mouse IgG secondary antibodies (Jackson ImmunoResearch Laboratories, 1 : 500) for 1 h at RT. Cell nuclei were visualized with 4′,6′-diamidino-2-phenylindole (DAPI) (Sigma-Aldrich). Slides were mounted Fluorescent Mounting Medium (Dako). Images were photographed under a Zeiss fluorescence microscope with a digital camera using the Zeiss Axiovision software (Carl Zeiss MicroImaging) at magnifications ×50, ×100, ×200 and ×400. Images with comparable exposure times were obtained to allow better comparison between different tissues. Selected images for GJ plaque counts were captured on a TCSL confocal microscope (Leica, Germany).

Quantitative analysis of pathology and GJ plaque formation

The fluorescent intensity of positive GFAP and IbaI from microscope pictures was calculated using *ImageJ* software. For quantification of GJ formation by oligodendrocytes, we randomly captured at least 20 individual oligodendrocytes within an area of 20 × 20 μm from spinal cord gray matter from three different mice per genotype. Pictures from the three genotypes were captured at ×400 magnification. The total number of Cx32, Cx30 and Cx43 GJ plaques in each image were counted using Adobe photoshop 6. In addition, we counted the number of GJ plaques in which Cx32 colocalized with either Cx30 or with Cx43 immunoreactivity and the overlap ratio was calculated in Microsoft Excel.

Electron microscopy and morphometric analysis

For electron microscopy, 1-month-old litters of G^+Cx32/Cx47dKO and Cx32/Cx47dKO mice ($n = 4$ per genotype) were transcardially perfused with 2.5% glutaraldehyde in 0.1 M PB. Brain, spinal cord, optic nerve and sciatic nerve were dissected and further fixed overnight at 4°C, then osmicated, dehydrated and embedded in Araldite resin. Transverse semithin sections (1 μm) were obtained and stained with alkaline toluidine blue. Ultrathin sections (80–100 nm) were counterstained with lead citrate and uranyl acetate before being examined in a JEOL JEM-1010 transmission electron microscope.

The CNS myelin fraction was calculated in semithin sections of the spinal cord dorsal and ventral funiculus and the optic nerve using a modified method to estimate the density of myelinated fibers and myelin sheaths (34,52,53). Images of semithin sections captured at ×630 final magnification following the same processing and microscopy settings were imported into Photoshop (Adobe Systems) and a transparent counting grid was placed on the image. All intersections of the grid lines hitting WM, myelinated fibers and myelin sheaths were counted separately. The volume density of the myelinated fibers in the WM was calculated by the total number of points hitting myelinated fibers in the WM over the total number of points hitting WM.

Behavioral analysis

Foot slip test

To explore the motor behavior of mice a modified method of Britt (54) was used, which is considered sensitive for CNS demyelination models. One-month-old mice were placed in a 15 × 15 × 15 cm clear plexiglass box with a floor consisting of a metal wire grid with 1.25 cm spacing with a 1.25 cm grid suspended 1.25 cm above the floor. Mice were acclimated in the box for 1 h before each session. The trial consisted of 50 steps. If a misstep results in the hindlimb or forelimb falling through the grid but the limb is withdrawn prior to touching the floor is scored 1; if the limb touches the floor it is scored 2. A video camera was used to film the mice to ensure accurate counts, and video recordings were evaluated in slow motion. TG^+ Cx32/Cx47dKO mice were compared with Cx32/Cx47dKO littermates using the Student's *t*-test. Significance was defined as $P < 0.05$ in all comparisons.

Rotarod analysis

This apparatus consists of a computer-controlled, motor-driven rotating spindle and four lanes for four mice. One-month-old

mice were habituated to the apparatus the first day for 180 s sessions twice at constant speeds of 12 and 20 rpm. The second day mice exert four trials with accelerating speed from 4 to 40 rpm. The mean latency to fall off the rotarod is calculated.

Foot print analysis

Footprints were obtained by painting the paws with nontoxic colored inks and the mouse was allowed to walk down a narrow, open-top runway covered with white paper. The runway length was 22 cm long 10 cm wide. Furthermore, the open-top runway was flanked by two walls at each side that were 11 cm high. The mice were acclimatized to the environment for at least 60 min, and were allowed two practice runs before coloring the paws. To facilitate subsequent analysis, forelimbs and hindlimbs were colored with different colors: blue for the front and red for the hindlimbs. Each mouse was subjected to a total of nine trials (three trials per day for 3 days). Once the footprints had dried, the following parameters were measured: overlap width, forelimb stride length, and hindlimb stride length for the left and right limbs separately.

Survival rates

The Kaplan–Meier survival curve was used to compare the survival rates of TG^{+}Cx32/Cx47dKO with those of Cx32/Cx47dKO littermates. Two groups of 10 mice were used for this analysis and followed until they became severely ill and preterminal, but before they died of seizures. A graph was plotted for the percentage of surviving animals over time in weeks.

Supplementary Material

Supplementary Material is available at *HMG* online.

Acknowledgements

We thank Prof. Domna Karagogeos and Dr Maria Savvaki for the gift of the Plp promoter construct.

Conflict of Interest statement. None declared.

Funding

This work is funded by a Cyprus Telethon Grant (2010-14 to K.A.K.) and by European Leukodystrophy Association (ELA) Research Foundation (ELA 2011-025I2 to K.A.K.).

References

1. Uhlenberg, B., Schuelke, M., Ruschendorf, F., Ruf, N., Kaindl, A.M., Henneke, M., Thiele, H., Stoltenburg-Didinger, G., Aksu, F., Topaloglu, H. *et al.* (2004) Mutations in the gene encoding gap junction protein alpha 12 (Connexin 46.6) cause Pelizaeus–Merzbacher-like disease. *Am. J. Hum. Genet.*, **75**, 251–260.
2. Kleopa, K.A. and Scherer, S.S. (2002) Inherited Neuropathies. *Neurol. Clin. N. Am.*, **20**, 679–709.
3. Paulson, H.L., Garbern, J.Y., Hoban, T.F., Krajewski, K.M., Lewis, R.A., Fischbeck, K.H., Grossman, R.I., Lenkinski, R., Kamholz, J.A. and Shy, M.E. (2002) Transient central nervous system white matter abnormality in X-linked Charcot–Marie-Tooth disease. *Ann. Neurol.*, **52**, 429–434.
4. Taylor, R.A., Simon, E.M., Marks, H.G. and Scherer, S.S. (2003) The CNS phenotype of X-linked Charcot–Marie-Tooth disease: more than a peripheral problem. *Neurology*, **61**, 1475–1478.
5. Tress, O., Maglione, M., Zlomuzica, A., May, D., Dicke, N., Degen, J., Dere, E., Kettenmann, H., Hartmann, D. and Willecke, K. (2011) Pathologic and phenotypic alterations in a mouse expressing a connexin47 missense mutation that causes Pelizaeus–Merzbacher-like disease in humans. *PLoS Genet.*, **7**, e1002146.
6. Shy, M.E., Siskind, C., Swan, E.R., Krajewski, K.M., Doherty, T., Fuerst, D.R., Ainsworth, P.J., Lewis, R.A., Scherer, S.S. and Hahn, A.F. (2007) CMT1X phenotypes represent loss of GJB1 gene function. *Neurology*, **68**, 849–855.
7. Sargiannidou, I., Vavlitou, N., Aristodemou, S., Hadjisavvas, A., Kyriacou, K., Scherer, S.S. and Kleopa, K.A. (2009) Connexin32 mutations cause loss of function in Schwann cells and oligodendrocytes leading to PNS and CNS myelination defects. *J. Neurosci.*, **29**, 4748–4761.
8. Altevogt, B.M., Kleopa, K.A., Postma, F.R., Scherer, S.S. and Paul, D.L. (2002) Connexin29 is uniquely distributed within myelinating glial cells of the central and peripheral nervous systems. *J. Neurosci.*, **22**, 6458–6470.
9. Rash, J.E., Yasumura, T., Dudek, F.E. and Nagy, J.I. (2001) Cell-specific expression of connexins and evidence of restricted gap junctional coupling between glial cells and between neurons. *J. Neurosci.*, **21**, 1983–2000.
10. Altevogt, B.M. and Paul, D.L. (2004) Four classes of intercellular channels between glial cells in the CNS. *J. Neurosci.*, **24**, 4313–4323.
11. Kleopa, K.A., Orthmann, J.L., Enriquez, A., Paul, D.L. and Scherer, S.S. (2004) Unique distribution of gap junction proteins connexin29, connexin32, and connexin47 in oligodendrocytes. *Glia*, **47**, 346–357.
12. Menichella, D.M., Goodenough, D.A., Sirkowski, E., Scherer, S. S. and Paul, D.L. (2003) Connexins are critical for normal myelination in the CNS. *J. Neurosci.*, **23**, 5963–5973.
13. Odermatt, B., Wellershaus, K., Wallraff, A., Seifert, G., Degen, J., Euwens, C., Fuss, B., Bussow, H., Schilling, K., Steinhauser, C. *et al.* (2003) Connexin 47 (Cx47)-deficient mice with enhanced green fluorescent protein reporter gene reveal predominant oligodendrocytic expression of Cx47 and display vacuolized myelin in the CNS. *J. Neurosci.*, **23**, 4549–4559.
14. Kamasawa, N., Sik, A., Morita, M., Yasumura, T., Davidson, K., Nagy, J. and Rash, J. (2005) Connexin-47 and connexin-32 in gap junctions of oligodendrocyte somata, myelin sheaths, paranodal loops and Schmidt-Lanterman incisures: implications for ionic homeostasis and potassium siphoning. *Neuroscience*, **136**, 65–86.
15. Orthmann-Murphy, J.L., Freidin, M., Fischer, E., Scherer, S.S. and Abrams, C.K. (2007) Two distinct heterotypic channels mediate gap junction coupling between astrocyte and oligodendrocyte connexins. *J. Neurosci.*, **27**, 13949–13957.
16. Orthmann-Murphy, J.L., Salsano, E., Abrams, C.K., Bizzi, A., Uziel, G., Freidin, M.M., Lamantea, E., Zeviani, M., Scherer, S.S. and Pareyson, D. (2009) Hereditary spastic paraplegia is a novel phenotype for GJA12/GJC2 mutations. *Brain*, **132**, 426–438.
17. Nagy, J.I., Ionescu, A.V., Lynn, B.D. and Rash, J.E. (2003) Coupling of astrocyte connexins Cx26, Cx30, Cx43 to oligodendrocyte Cx29, Cx32, Cx47: implications from normal and connexin32 knockout mice. *Glia*, **44**, 205–218.
18. Ahn, M., Lee, J., Gustafsson, A., Enriquez, A., Lancaster, E., Sul, J., Haydon, P., Paul, D., Huang, Y., Abrams, C. *et al.* (2008) Cx29 and Cx32, two connexins expressed by myelinating glia, do

not interact and are functionally distinct. *J. Neurosci. Res.*, **86**, 992–1006.
19. Sargiannidou, I., Ahn, M., Enriquez, A.D., Peinado, A., Reynolds, R., Abrams, C.K., Scherer, S.S. and Kleopa, K.A. (2008) Human oligodendrocytes express Cx31.3: function and interactions with Cx32 mutants. *Neurobiol. Dis.*, **30**, 221–233.
20. Scherer, S.S., Xu, Y.T., Messing, A., Willecke, K., Fischbeck, K. H. and Jeng, L.J. (2005) Transgenic expression of human connexin32 in myelinating Schwann cells prevents demyelination in connexin32-null mice. *J. Neurosci.*, **25**, 1550–1559.
21. Anzini, P., Neuberg, D.H.-H., Schachner, M., Nelles, E., Willecke, K., Zielasek, J., Toyka, K., Suter, U. and Martini, R. (1997) Structural abnormalities and deficient maintenance of peripheral nerve myelin in mice lacking the gap junction protein connexin32. *J. Neurosci.*, **17**, 4545–4561.
22. Scherer, S.S., Xu, Y.-T., Nelles, E., Fischbeck, K., Willecke, K. and Bone, L.J. (1998) Connexin32-null mice develop a demyelinating peripheral neuropathy. *Glia*, **24**, 8–20.
23. Anderson, T.J., Montague, P., Nadon, N., Nave, K.A. and Griffiths, I.R. (1997) Modification of Schwann cell phenotype with Plp transgenes: evidence that the PLP and DM20 isoproteins are targeted to different cellular domains. *J. Neurosci. Res.*, **50**, 13–22.
24. Savvaki, M., Theodorakis, K., Zoupi, L., Stamatakis, A., Tivodar, S., Kyriacou, K., Stylianopoulou, F. and Karagogeos, D. (2010) The expression of TAG-1 in glial cells is sufficient for the formation of the juxtaparanodal complex and the phenotypic rescue of tag-1 homozygous mutants in the CNS. *J. Neurosci.*, **30**, 13943–13954.
25. Jiang, H.Y., Duchala, C.S., Awatramani, R., Shumas, S., Carlock, L., Kamholz, J., Garbern, J., Scherer, S.S., Shy, M.E. and Macklin, W.B. (2000) Proteolipid protein mRNA stability is regulated by axonal contact in the rodent peripheral nervous system. *J. Neurobiol.*, **44**, 7–19.
26. Kobsar, I., Berghoff, M., Samsam, M., Wessig, C., Maurer, M., Toyka, K.V. and Martini, R. (2003) Preserved myelin integrity and reduced axonopathy in connexin32-deficient mice lacking the recombination activating gene-1. *Brain*, **126**, 804–813.
27. Groh, J., Heinl, K., Kohl, B., Wessig, C., Greeske, J., Fischer, S. and Martini, R. (2010) Attenuation of MCP-1/CCL2 expression ameliorates neuropathy in a mouse model for Charcot–Marie-Tooth 1X. *Hum. Mol. Genet.*, **19**, 3530–3543.
28. Ip, C.W., Kroner, A., Fischer, S., Berghoff, M., Kobsar, I., Mäurer, M. and Martini, R. (2006) Role of immune cells in animal models for inherited peripheral neuropathies. *Neuromol. Med.*, **8**, 175–190.
29. Ip, C.W., Kroner, A., Crocker, P.R., Nave, K.A. and Martini, R. (2007) Sialoadhesin deficiency ameliorates myelin degeneration and axonopathic changes in the CNS of PLP overexpressing mice. *Neurobiol. Dis.*, **25**, 105–111.
30. Ip, C.W., Kroner, A., Groh, J., Huber, M., Klein, D., Spahn, I., Diem, R., Williams, S.K., Nave, K.A., Edgar, J.M. *et al.* (2012) Neuroinflammation by cytotoxic T-lymphocytes impairs retrograde axonal transport in an oligodendrocyte mutant mouse. *PLoS ONE*, **7**, e42554.
31. Wallraff, A., Kohling, R., Heinemann, U., Theis, M., Willecke, K. and Steinhauser, C. (2006) The impact of astrocytic gap junctional coupling on potassium buffering in the hippocampus. *J. Neurosci.*, **26**, 5438–5447.
32. Magnotti, L.M., Goodenough, D.A. and Paul, D.L. (2011) Functional heterotypic interactions between astrocyte and oligodendrocyte connexins. *Glia*, **59**, 26–34.
33. Bruzzone, R., White, T.W., Scherer, S.S., Fischbeck, K.H. and Paul, D.L. (1994) Null mutations of connexin32 in patients with X-linked Charcot–Marie-Tooth disease. *Neuron*, **13**, 1253–1260.
34. Sutor, B., Schmolke, C., Teubner, B., Schirmer, C. and Willecke, K. (2000) Myelination defects and neuronal hyperexcitability in the neocortex of connexin 32-deficient mice. *Cereb. Cortex*, **10**, 684–697.
35. Al-Mateen, M., Craig, A.K. and Chance, P.F. (2013) The central nervous system phenotype of X-Linked Charcot–Marie-Tooth Disease: a transient disorder of children and young adults. *J. Child Neurol.*, **29**, 342–348.
36. Parenti, R., Cicirata, F., Zappalà, A., Catania, A., La Delia, F., Cicirata, V., Tress, O. and Willecke, K. (2010) Dynamic expression of Cx47 in mouse brain development and in the cuprizone model of myelin plasticity. *Glia*, **58**, 1594–1609.
37. Markoullis, K., Sargiannidou, I., Schiza, N., Hadjisavvas, A., Roncaroli, F., Reynolds, R. and Kleopa, K.A. (2012) Gap junction pathology in multiple sclerosis lesions and in normal appearing white matter. *Acta Neuropathol.*, **123**, 873–886.
38. Markoullis, K., Sargiannidou, I., Schiza, N., Roncaroli, F., Reynolds, R. and Kleopa, K.A. (2014) Oligodendrocyte gap junction loss and disconnection from reactive astrocytes in multiple sclerosis gray matter. *J. Neuropathol. Exp. Neurol.*, **73**, 865–879.
39. Abrams, C.K., Scherer, S.S., Flores-Obando, R., Freidin, M.M., Wong, S., Lamantea, E., Farina, L., Scaioli, V., Pareyson, D. and Salsano, E. (2014) A new mutation in GJC2 associated with subclinical leukodystrophy. *J. Neurol.*, **261**, 1929–1938.
40. Menichella, D.M., Majdan, M., Awatramani, R., Goodenough, D.A., Sirkowski, E., Scherer, S.S. and Paul, D.L. (2006) Genetic and physiological evidence that oligodendrocyte gap junctions contribute to spatial buffering of potassium released during neuronal activity. *J. Neurosci.*, **26**, 10984–10991.
41. Paznekas, W.A., Boyadjiev, S.A., Shapiro, R., Daniels, O., Wollnik, B., Keegan, C.E., Innis, J.W., Dinulos, M.B., Christian, C., Hannibal, M.C. *et al.* (2003) Connexin 43 (GJA1) mutations cause the pleiotropic phenotype of oculodentodigital dysplasia. *Am. J. Hum. Genet.*, **72**, 408–418.
42. Lutz, S.E., Zhao, Y., Gulinello, M., Lee, S.C., Raine, C.S. and Brosnan, C.F. (2009) Deletion of astrocyte connexins 43 and 30 leads to a dysmyelinating phenotype and hippocampal CA1 vacuolation. *J. Neurosci.*, **29**, 7743–7752.
43. Maglione, M., Tress, O., Haas, B., Karram, K., Trotter, J., Willecke, K. and Kettenmann, H. (2010) Oligodendrocytes in mouse corpus callosum are coupled via gap junction channels formed by connexin47 and connexin32. *Glia*, **58**, 1104–1117.
44. Wasseff, S.K. and Scherer, S.S. (2011) Cx32 and Cx47 mediate oligodendrocyte:astrocyte and oligodendrocyte:oligodendrocyte gap junction coupling. *Neurobiol. Dis.*, **42**, 506–513.
45. Magnotti, L.M., Goodenough, D.A. and Paul, D.L. (2011) Deletion of oligodendrocyte Cx32 and astrocyte Cx43 causes white matter vacuolation, astrocyte loss and early mortality. *Glia*, **59**, 1064–1074.
46. May, D., Tress, O., Seifert, G. and Willecke, K. (2013) Connexin47 protein phosphorylation and stability in oligodendrocytes depend on expression of Connexin43 protein in astrocytes. *J. Neurosci.*, **33**, 7985–7996.
47. Tress, O., Maglione, M., May, D., Pivneva, T., Richter, N., Seyfarth, J., Binder, S., Zlomuzica, A., Seifert, G., Theis, M. *et al.* (2012) Panglial gap junctional communication is essential for maintenance of myelin in the CNS. *J. Neurosci.*, **32**, 7499–7518.
48. Fuss, B., Mallon, B., Phan, T., Ohlemyer, C., Kirchoff, F., Nishiyama, A. and Macklin, W.B. (2000) Purification and

analysis of in vivo-differentiated oligodendrocytes expressing the green fluorescent protein. *Dev. Biol.*, **218**, 259–274.
49. Michalski, J.P., Anderson, C., Beauvais, A., De Repentigny, Y. and Kothary, R. (2011) The proteolipid protein promoter drives expression outside of the oligodendrocyte lineage during embryonic and early postnatal development. *PLoS ONE*, **6**, e19772.
50. Wight, P.A., Duchala, C.S., Readhead, C. and Macklin, W.B. (1993) A myelin proteolipid protein-lacZ fusion protein is developmentally regulated and targeted to the myelin membrane in transgenic mice. *J. Cell Biol.*, **123**, 443–454.
51. Nelles, E., Butzler, C., Jung, D., Temme, A., Gabriel, H.-D., Dahl, U., Traub, O., Stumpel, F., Jungermann, K., Zielasek, J. *et al.* (1996) Defective propagation of signals generated by sympathetic nerve stimulation in the liver of connexin32-deficient mice. *Proc. Natl Acad. Sci. USA*, **93**, 9565–9570.
52. Tang, Y. and Nyengaard, J.R. (1997) A stereological method for estimating the total length and size of myelin fibers in human brain white matter. *J. Neurosci. Methods*, **73**, 193–200.
53. Vavlitou, N., Sargiannidou, I., Markoullis, K., Kyriacou, K., Scherer, S.S. and Kleopa, K.A. (2010) Axonal pathology precedes demyelination in a mouse model of X-linked demyelinating/type I Charcot–Marie Tooth neuropathy. *J. Neuropathol. Exp. Neurol.*, **69**, 945–958.
54. Britt, J.M., Kane, J.R., Spaeth, C.S., Zuzek, A., Robinson, G.L., Gbanaglo, M.Y., Estler, C.J., Boydston, E.A., Schallert, T. and Bittner, G.D. (2010) Polyethylene glycol rapidly restores axonal integrity and improves the rate of motor behavior recovery after sciatic nerve crush injury. *J. Neurophysiol.*, **104**, 695–703.